Dissertation

submitted to the

Combined Faculties for the Natural Sciences and for Mathematics

of the Ruperto-Carola University of Heidelberg, Germany

for the degree of

Doctor of Natural Sciences

presented by

Sajo Kaduthanam, M.Sc. in Molecular Biosciences

born in Düsseldorf, Germany

Oral examination date: 08th April 2016

The role of microRNAs in prognosis and therapy resistance of lung adenocarcinoma

Referees: **Prof. Dr. Peter Angel**

                 Prof. Dr. Holger Sültmann

Abstract

The diagnosis of non-small cell lung cancer (NSCLC) usually occurs when the disease has locally advanced or spread into distant sites. Patients with early-stage NSCLC have a better overall rate of survival than those patients with advanced stages. Assessment of tumor progression is therefore critical for treatment options. For this purpose, this study used two approaches to analyze the development of NSCLC. First, circulating microRNAs (miRNAs) were examined as prognostic markers from serum samples of early-stage lung adenocarcinoma patients. Secondly, this study investigated the role of miRNAs in the progression of lung adenocarcinoma cells after treatment with the tyrosine-kinase inhibitor (TKI) gefitinib and subsequent resistance.

Genome-wide circulating miRNA expression profiling revealed miRNAs out of which *miR-142-3p* was validated to be associated with poor prognosis in patients with lung adenocarcinoma. In order to improve the prognostic value of circulating miRNAs, a miRNA panel was searched to predict the overall survival and the relapse-free survival. Since no stable set of miRNAs was found, pre-analytical variables were identified as critical for miRNA analysis. In this case, the impact of blood collection and hemolysis were shown to have an influence on the expression level. The miRNAs, which were selected based on their prognostic relevance, showed a tendency to be lesser expressed in arterial blood than miRNAs derived from venipuncture. Moreover, *miR-20b-5p* and *miR-486-5p* were affected by hemolysis.

In order to further investigate the progression of the tumor, the role of miRNAs and mRNAs in the development of resistance to EGFR-TKI gefitinib was studied. Therefore, a gefitinib resistance model was used by co-culturing lung fibroblasts (MRC-5) with the two different gefitinib-sensitive NSCLC cell lines HCC827 and PC-9. Global miRNA analysis revealed expression changes associated with EGFR-TKI resistance. A total of eleven miRNAs were selected, from which *miR-503-5p* was validated in both EGFR-TKI NSCLC cell lines. Subsequently, global gene expression profiling revealed 211 differentially expressed mRNAs in the resistant HCC827 and PC-9 cells. Putative target genes of *miR-503-5p* were determined by comparing global gene expression profiling with miRNA prediction databases. The autophagy gene *GABARAPL1* was validated at both the mRNA and protein level. Ectopic overexpression of *miR-503-5p* resulted in significant reduction of *GABARAPL1*. Moreover, luciferase reporter assays showed the direct interaction between *miR-503-5p* and the 3'UTR of *GABARAPL1*. Different autophagy markers were analyzed in co-cultured HCC827 cells after gefitinib treatment. Thereby, the accumulation of the SQSTM1, as well as a decrease of LC3B-II and GABARAPL1 levels were observed. In accordance with this finding, siRNA-mediated knockdown of *GABARAPL1* resulted in an accumulation of SQSTM1 (p62). In conclusion, these data suggest that inhibiting *GABARAPL1* through *miR-503-5p* modulates autophagic activity in gefitinib resistant *EGFR*-mutant lung adenocarcinoma cells.

Zusammenfassung

Die Diagnose des nicht-kleinzelligen Bronchialkarzinoms (NSCLC) erfolgt meistens, wenn die Krankheit lokal fortgeschritten ist oder schon Metastasen gebildet hat. Patienten im Frühstadium von NSCLC haben eine bessere Überlebensrate als jene mit fortgeschrittenen Tumorstadien. Daher ist die Einschätzung der Tumorprogression von entscheidender Bedeutung für die Abwägung von Therapieoptionen. Zu diesem Zweck wurden in dieser Arbeit zwei Ansätze verfolgt, um die Entwicklung von NSCLC zu studieren. Zunächst wurden zirkulierende microRNAs (miRNAs) als prognostische Marker von Serumproben von NSCLC-Patienten im Frühstadium untersucht. Zweitens wurde im *in-vitro* Modell die Rolle von miRNAs in der Progression von Adenokarzinomzellen der Lunge nach einer Resistenz gegenüber dem Tyrosinkinase-Inhibitor (TKI) Gefitinib untersucht.

In einem genomweiten Screening-Ansatz wurden zirkulierende miRNAs in Serumproben von NSCLC-Patienten im Frühstadium identifiziert und *miR-142-3p* wurde mit einer schlechten Prognose assoziiert. Um den prognostischen Wert von zirkulierenden miRNAs zu verbessern, wurde nach einem miRNA Panel gesucht. Es konnte jedoch keine stabile Gruppe von miRNAs für das Gesamtüberleben oder Rezidiv-freie Überleben gefunden werden. Daher wurde der potentielle Einfluss verschiedener prä-analytischer Variablen untersucht, die entscheidend für die Analyse von zirkulierenden miRNAs aus dem Serum sind. Es konnte gezeigt werden, dass die Art der Blutentnahme und das Auftreten von Hämolyse Auswirkungen auf die Abundanz verschiedener miRNAs hat. Die vorher wegen ihrer prognostischen Aussagekraft selektieren zirkulierenden miRNAs zeigten eine niedrigere Expression im arteriellem- im Vergleich zum venösen Blut. Darüber hinaus waren *miR-20b-5p* und *miR-486-5p* durch Hämolyse beeinflusst.

Bei den Untersuchungen zur Progression von NSCLC Tumoren wurde die Rolle von miRNAs und mRNAs bei der Resistenzentwicklung gegenüber dem EGFR-TKI Gefitinib im *in-vitro* Modell erforscht. Mittels Ko-kultur von Lungenfibroblasten (MRC-5) mit den Gefitinib-sensitiven NSCLC Zelllinien HCC827 und PC-9 konnte eine Resistenz gegenüber Gefitinib entwickelt werden. Aus einer globalen miRNA-Analyse von ko-kultivierten Zellen wurden elf Kandidaten selektiert, wobei die *miR-503-5p* in beiden NSCLC-Zelllinien validiert werden konnte. Bei der Analyse des globalen Genexpressionsprofils wurden 211 differentiell exprimierte mRNAs in den resistenten HCC827 und PC-9 Zellen identifiziert. Durch den Vergleich des Genexpressionsprofils mit miRNA-Vorhersage-Datenbanken konnten putative Zielgene von *miR-503-5p* ermittelt werden. Dabei wurde das Autophagie-Gen *GABARAPL1* auf mRNA und Protein-Ebene validiert. Die transiente Überexpression von *miR-503-5p* führte zu einer signifikanten Reduktion von *GABARAPL1*. Luziferase-Reporter Assays zeigten eine direkte Interaktion zwischen *miR-503-5p* und dem 3'UTR von *GABARAPL1*. Weiterhin wurden verschiedene Marker der Autophagie nach Ko-Kultur von Gefitinib behandelten HCC827-Zellen gemessen. Dabei konnte ein Anstieg von SQSTM1 (p62) und eine Senkung des LC3B-II und GABARAPL1 Proteingehalts beobachtet werden. Entsprechend führte ein siRNA-vermittelte Knockdown von *GABARAPL1* zu einer Akkumulation von SQSTM1. Zusammenfassend deuten diese Daten darauf hin, dass die Inhibition von *GABARAPL1* durch *miR-503-5p* die autophagische Aktivität in Gefitinib resistenten *EGFR*-mutierten Adenokarzinomzellen der Lunge reguliert.

Table of contents

Abbreviations

4IPBA	4-iodophenylboronic acid
5-PL	Fifth Party Logistik Model
ADc	Adenocarcinoma
AKT	Protein kinase B
ATP	Adenosine-5'-triphosphate
AUC	Area under the curve
BCA	Bicinchoninic acid
bp	base pair
BRAF	Murine sarcoma viral oncogene homolog B1
BSA	bovine serum albumin
CDK	Cyclin-dependend kinase
cDNA	complementary DNA
cel	Caenorhabditis elegans
cMYC	Avian myelocytomatosis viral oncogene homolog
Cp	crossing point
Ct	cycle threshold
DAPI	4',6-Diamidin-2-phenylindol
DAVID	Database for Annotation, Visualization and Integrated Discovery
del	deletion
DFS	disease-free surival
DMEM	Dulbecco's modified eagle medium
DMSO	Dimethylsulfoxid
DNA	deoxyribonucleic acid
DNase	deoxyribonuclease
dNTP	deoxynucleoside triphosphate
DPBS	Dulbecco's phosphate buffered saline
E. coli	Escherichia coli
ECL	enhanced chemiluminescence
ECM	extracellular matrix
EDTA	ethylenediaminetetraacetic acid
EGF	Epidermal growth factor
EGFP	enhanced green fluorescent protein
EGFR	Epidermal growth factor receptor
ELISA	enzyme-linked immunosorbent assay
EMEM	Eagle's modified eagle medium
EMT	epithelial-mesenchymal transition
ERBB	Erythroblastic leukemia viral oncogene
ERK	Extracellular signal-regulated kinase
EtOH	ethanol
FACS	fluorescence activated cell sorting
FBS	fetal bovine serum
FC	fold change
FDA	Food and Drug Administration
FFPE	formalin fixed paraffin embedding
FISH	fluorescence in-situ hybridization
GABARAP L1	Gamma-aminobutyric acid receptor-Associated protein like 1
GRB2	Growth factor receptor-bound protein 2
GSK3α/β	Glycogen synthase kinase 3 alpha/beta
HGF	hepatocyte growth factor
HR	hazard ratio
HSA	Homo sapiens
IC50	Half maximal inhibitory concentration
ID	Identity
IGF	Insulin-like growth factor
IGF-1R	Insulin-like growth factor 1 receptor
IgG	Immunoglobulin G
INS	Insulin
IPA	Ingenuity Pathway Analysis
IR	Insulin receptor
IRS	Insulin receptor substrate
KEGG	Kyoto Encyclopedia of Genes and Genomes
KRAS	V-Ki-Ras2 kirsten rat sarcoma viral oncogene homolog
LC3B	Light chain 3B
LNA	locked nucleic acid
mAb	Monoclonal antibody
MAPK	Mitogen-activated kinase
MEK	Mitogen-activated kinase kinase
MEM	Minimum essential media
MeOH	methanol
Met	Mesenchymal epithelial transition factor
MFI	mean fluorescent intensity
miR	micro RNA
mRNA	messenger RNA
MTOR	Mammalian target or rampamycin
NA	not available
ND	not detected
NF-κB	Nuclear factor of kappa light polypeptide gene enhancer in B-cells
NSCLC	Non-small-cell lung carcinoma
NT	non targeting
ORF	open reading frame
OS	overall-survival
p53	Tumor protein p53
p62/ SQSTM1	ubiquitin-binding protein p62, Sequestosome-1
p70 S6K	Ribosomal protein S6 kinase, 70kDa, polypeptide
PAGE	polyacrylamide gel electrophoresis
PBS	Phosphate buffered saline
PCR	polymerase chain reaction
PE	Phycoerythrin
PI	propidium iodide
PI3K	Phosphatidylinositol 3-kinase
pre	precursor
pri	primary
PTEN	Posphatase and tensin homolog
PVDF	Polyvinylidenfluorid
qRT-PCR	quantitative RT-PCR
RAF	Rapidly growing fibrosarcoma protein
RAS	Rat sarcoma protein
RFS	recurrence-free survival
RIN	*RNA* integrity number
RIPA	Radioimmunoprecipitation assay
RISC	RNA induced silencing complex
RNA	ribonucleic acid
RNase	ribonuclease
RPMI	Rosell park memorial institute medium
RT	room temperature/reverse transcription
RTK	Receptor tyrosine kinase
SCLC	small-cell lung cancer
SD	standard deviation
SDS	sodium dodecyl sulfate
sh	small-hairpin
SHC	Src homology 2 domain-containing transforming protein
siRNA	small intefering RNA
TBST	Tris-buffered saline Tween-20
TGF α	transforming growth factor α
TKI	Tyrosine-kinase inhibitor

TNM	Tumor, Nodes, Metastases Classification of Malignant Tumours
Tris	Tris(hydroxymethyl)aminomethane
TSC2	Tuberous sclerosis 2 protein
Tyr	Tyrosine
U	Unit
UPL	universal probe library
UTR	untranslated region
UV	ultraviolet
VEGF	Vascular endothelial growth factor
VIS	visible
WT	wild-type

1 Introduction

1.1 Lung cancer biology

Lung cancer is one of the most common cancers and the leading cause of cancer-related death worldwide, with 1.6 million deaths per year [1]. The main types of lung cancer are non-small-cell lung cancer (NSCLC) and small-cell lung cancer (SCLC) (Figure 1). NSCLC accounts for most cases of lung cancer with about 85% and SCLC follows with 15%. The three types of NSCLC are (I) adenocarcinoma (acinar, papillar, bronchioalveolar, and solid), which mainly develops from the peripheral airway compartment from secreting cells of bronchioles or alveoli with a glandular shape (Biomarkers: TTF1; KRT7). (II) Squamous cell carcinoma develops from the epithelial cells of the bronchi and is diagnosed by the squamous differentiation (Biomarkers: KRT6/7; SOX2; p63). (III) Large cell lung cancer can be diagnosed if glandular or squamous histology as well as biomarkers can be excluded. The small cell lung carcinoma, conversely, develops from the epithelial cells of the main bronchi [2-4].
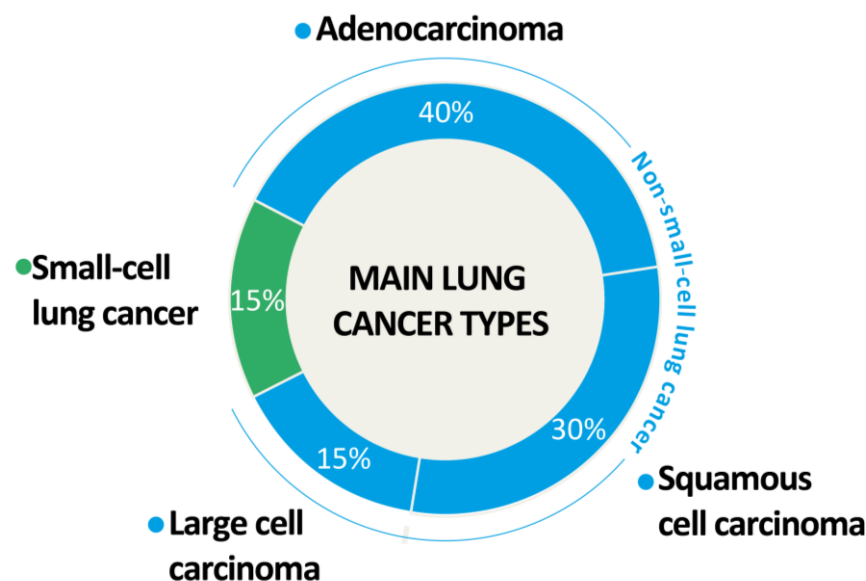
Figure 1 Main types of lung cancer. Lung cancer is generally divided into small-cell lung cancer (SCLC) (green) and non-small cell lung cancer (NSCLC) (blue). NSCLC is further subdivided into adenocarcinoma, squamous cell carcinoma and large cell carcinoma. This graphic is adapted and modified from Bender [5].

Lung cancer patients are diagnosed according to the international TNM staging system [6]. At the time of diagnosis, lung cancer is most often found at a locally advanced stage and has already spread to distant sites. Survival rates are low (13% at stage IV). The detection of NSCLC at early stages and the subsequent surgical resection increases the 5-year survival rate

(about 30-70% at stage I-II) [6]. However, 20-40% of patients at an early stage (I-IIIa) encounter a recurrence after surgery. Depending on the stage of the disease, different approaches such as surgery, radiotherapy, or chemotherapy are applied [7]. The identification of NSCLC subsets is critical for further patient care. For example, low-dose computed tomographic (CT) screening was shown to reduce lung cancer mortality by 20% [8]. Lung cancer patients at high-risk, such as smokers, were the main target group to be screened [9]. However, false positive results, radiation-induced cancers and over-diagnosis cannot be excluded [10]. Therefore, the identification of NSCLC subsets requires innovative cancer-related biomarker signatures with high sensitivity and specificity that use state-of-the-art technologies [11].

1.2 Aberrant signaling pathways in NSCLC

Smoking is the primary risk factor for lung cancer [12]. Lung tumors from never-smokers show a markedly different tumor genomic landscape in comparison to those developed in smokers. Smokers have a 10-fold higher mutation frequency than never-smokers, in which C:G > A:T transversions are more common in smokers. On the other hand, C:G > T:A transitions are predominant in never-smokers. Molecular profiling from 230 lung adenocarcinomas using a comprehensive multiplatform analysis (mRNA, microRNA (miRNA), DNA sequencing, copy number analysis, methylation and proteomic analysis) revealed a mean of 8.9 somatic mutations per megabase. *TP53* was the most commonly mutated gene. Various critical pathways were affected in lung adenocarcinoma, for instance, the activation of receptor tyrosine kinase (RTK)/RAS/RAF pathway, or alternatively, the activation of the PI(3)K-MTOR pathway (Figure 2). Oncogenes such as *KRAS*, *EGFR*, *BRAF*, *PIK3CA*, *MET*, and *RIT1* were found to be frequently mutated. On the other hand, tumor suppressors such as *STK11* as well as *KEAP1*, *NF1*, *RB1*, *CDKN2A* in the cell cycle regulation and oxidative stress pathway were found to be mutated. Moreover, chromatin modifying genes such as *SETD2*, *ARID1A*, and *SMARCA4,* the RNA slicing genes *RBM10* and *U2AF1* and as well as the *MGA* gene that regulates the MYC pathway were commonly mutated [13].

KRAS mutations have been frequently described to be involved in the pathogenesis of lung cancer and are associated with poor prognosis [14]. *KRAS* mutations and epidermal growth factor receptor (*EGFR*) mutations have been found to be mutually exclusive of one another [15]. Mutations in the *EGFR* and anaplastic lymphoma kinase (*ALK*) fusions were predominantly found in patients that were never-smokers rather than smokers. On the other hand, *KRAS* and *TP53* mutations were mainly found in smokers [16]. An inversion of the

short arm of chromosome 2, where the genes *ALK* and *EML4* are located, has been shown to result in a fusion protein. This protein has been identified in a NSCLC subset to confer constitutive tyrosine kinase activity [17].
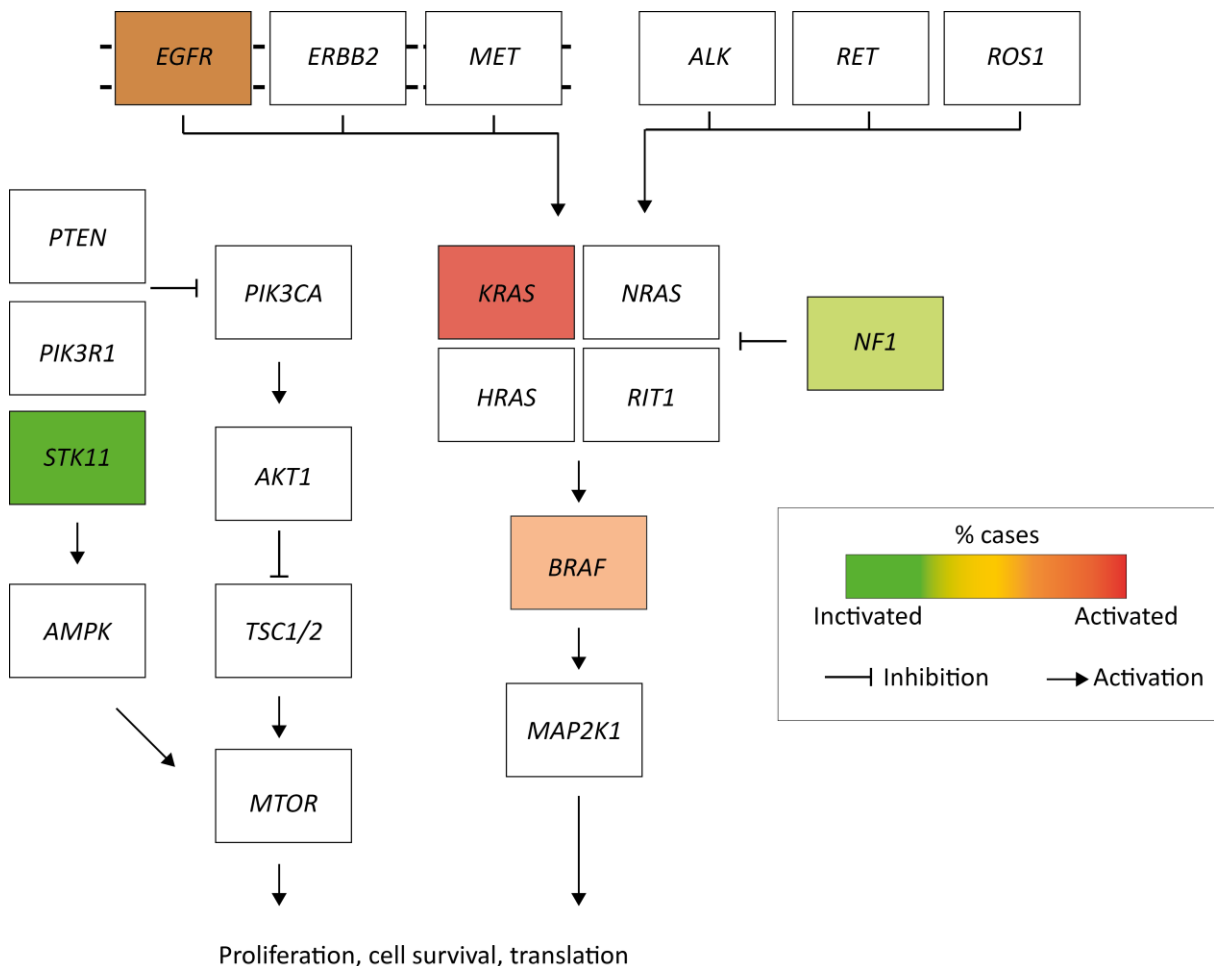
Figure 2 Receptor tyrosine kinase (RTK) signaling in lung adenocarcinomas. Molecular alterations of key pathways such as RTK/RAS/RAF pathway and PI(3)K-MTOR pathway including the percent of cases with activating and inhibiting mutations. The graphic has been adapted and modified from Cancer Genome Atlas Research Network [13].

1.3 The EGFR family

The EGFR belongs to the ERBB family of proteins, which includes four type 1 transmembrane tyrosine kinase receptors: EGFR (ERBB1), ERBB2 (HER2), ERBB3 (HER3), and ERBB4 (HER4). The pairing between the receptors that form homo- or heterodimers enables the activation of a variety of different downstream signaling pathways [18]. The EGFR protein is composed of an extracellular domain for ligand binding, a transmembrane domain, and a cytoplasmic domain. The receptors occur as inactive monomers, i.e. they are folded in a closed conformation. EGF can bind to the extracellular region of EGFR and

thereby rearranges the conformation and thus induces dimerization [19]. Several ligands can bind to EGFR including EGF, transforming growth factor α (TGF α), amphiregulin (AR), epithelial mitogen (EPGN), betacellulin (BTC), HB-EGF, and epiregulin (EPR) [20]. Ligand binding stabilizes the dimerization of EGFR, which results in the transactivation through the phosphorylation of key tyrosine residues in the activation loop of the catalytic tyrosine kinase domain [21-23]. Molecules such as growth-factor-receptor bound-2 (GRB2) and Src-homology-2-containing (Shc) can bind to the phosphorylated tyrosine residues, recruit RAS and subsequently activate the downstream RAS/RAF/MAPK signaling pathway cascade. Phosphoinositide 3-kinase (PI3K) is indirectly recruited to the phosphorylated tyrosine residue and can induce the PI3K-AKT signaling (Figure 2). Moreover, the calcium signaling pathway via the phospholipase C pathway leads to the activation of protein kinase C (PKC) [24].

1.3.1 EGFR-targeted therapy for NSCLC

Clinical benefits in subsets of NSCLC tumors with *EGFR* activating mutations were observed after treatment with reversible tyrosine kinase inhibitors (TKI) such as gefitinib (Iressa; Astra Zeneca) or erlotinib (Tarceva; Roche) and irreversible TKI such as afatinib (Giotrif; Boehringer-Ingelheim) [25-29]. Gefitinib is a 4-anilinoquinazoline compound that targets the intracellular tyrosine kinase domain of EGFR. It competes with ATP for the ATP binding site within the tyrosine kinase domain of EGFR, and thereby prevents the receptor autophosphorylation [30].

The overexpression of EGFR has been reported and associated with poor prognosis in NSCLC [31]. About 10% of NSCLC cases in North America and Western Europe and about 30-50% of cases in patients in East Asia have shown *EGFR* mutations. Female patients with adenocarcinomas and bronchioalveolar morphology were identified as a subset that clinically benefit from targeted therapy with the EGFR-TKI gefitinib or erlotinib [32, 33]. *EGFR* mutations are found in four exons (18-21) of the tyrosine kinase domain. The most common mutations were found in exon 19 (45%) with the E746-A750 in-frame deletion and in exon 21 (40-45%) with the L858R point mutation. These mutations are commonly clustered around the active site of kinase and denoted as activating mutations since they lead to increased ligand-independent kinase activity of the receptor [28, 34]. *KRAS* mutations have been suggested as predictive markers for EGFR-TKI insensitivity [35]. Up until now, however, there exists no FDA-approved drug to target *KRAS* mutated NSCLC subsets.

1.3.2 EGFR-TKI resistance in NSCLC

Although 70-75% of patients with activating mutations of *EGFR* respond well to the EGFR-TKI treatment, 25-30% have intrinsic resistance to EGFR-TKI, and almost all NSCLC patients ultimately develop resistance to these agents of 8 to 16 months on average [25, 36, 37]. Most patients (~ 60%) acquire a secondary mutation (T790M) leading to the resistance to EGFR-TKI [38-40]. Furthermore, a small subset of patients developed acquired resistance by transforming from NSCLC into SCLC histology [41, 42]. In about 20% of resistance cases, amplification of the *MET* oncogene has been observed [43, 44]. In addition to this amplification and the secondary T790M mutation, hepatocyte growth factor (HGF) conferred short-term EGFR-TKI resistance in two *EGFR*-mutant lung cancer cell lines (PC-9 and HCC827) [45, 46]. HGF was first described as a mitogenic protein for hepatocytes [47]. Its receptor is MET, a tyrosine kinase that is overexpressed in various types of cancer cells. The binding of HGF to MET induces pleiotropic biological effects in many cell types such as mitogenic, morphogenic, and antiapoptotic characteristics [48]. It has been found that HGF-activated MET restored the phosphoinositide 3-kinase (PI3K)/AKT pathway [44]. Tumor-stroma interaction between tumor cells and fibroblasts is widely accepted to influence tumor progression after therapy and known to compensate for blocked pathways targeted by specific inhibitors [49]. For example, HGF has been described as a mediator of tumor-stroma interactions that mediate invasiveness and metastasis by activating the MET pathway [45, 46].

1.4 Transcriptional regulation by miRNAs

Mammalian miRNAs are small non-coding RNA molecules (~ 22 nt) (Figure 3). They play important roles in physiological processes such as development and the pathogenesis of cancer. miRNA genes in the human genome are located in intronic or exonic regions of protein- or non-protein-coding transcripts [50-52]. Nearly half of the human miRNAs appear in clusters and are expressed polycistronically [53]. According to the miRBase21 database, a total of 1881 precursor and 2588 mature human miRNA sequences are known to date [54]. The transcription of miRNA genes by RNA polymerase II (Pol II) results in capped, polyadenylated primary miRNAs (pri-miRNA) that can be as large as several kilobases (kb), comprised of hairpin-stems and a terminal loop [55, 56]. A microprocessor complex, composed of the RNase III endonuclease DROSHA and the ds-RNA binding protein DGCR8 (DiGeorge critical region 8) cleaves the pri-miRNAs in the nucleus [57-59]. The resulting precursor miRNA (pre-miRNA), which contains a 2 nucleotide (nt) overhang at the 3'-end,

comprises a stem with a size of about 22 nt and a terminal loop [59]. The transport of the pre-miRNA is then mediated by exportin-5, a Ran-GTP dependent ds-RNA-binding protein, into the cytoplasm [60, 61]. A ternary complex composed of the RNase endonuclease III DICER, the ds-RNA binding proteins TRBP (Tar RNA binding protein) and PACT (protein activator of PKR) cleaves the terminal loop of the pre-miRNA. This process results in a miRNA duplex with a size of about 22 nt and a 2 nt overhang at the 3'-end [62-64]. After DICER cleavage, the ternary complex dissociates and the duplex miRNA unwinds into a functional guide strand, which is loaded into the RNA-inducing silencing complex (RISC) [65], whereas the passenger strand is degraded [66]. RISC is a multi-protein complex composed of the ternary complex described above and the Argonaute-2 (AGO2), which mediates its effector functions on mRNA targets [67]. Although there are different AGO proteins, only the human AGO2 has been described to guide RNA cleavage [68]. The functionally active RISC complex can mediate independent mechanisms to silence mRNAs, such as through mRNA target cleavage, translational repression, and mRNA deadenylation [69-73]. The target recognition and perfect matching of the 'seed sequence' at the 5' region of miRNAs to the 3'-untranslated region (UTR) of mRNAs has been described [74, 75]. Apart from perfect matching, miRNAs also imperfectly base pair to their mRNA targets. Moreover, a single miRNA can target several sites at the 3'-UTR of mRNAs. Vice versa, research has also shown that the 3'-UTR of mRNAs contain several target sites for different miRNAs [76].

1.4.1 miRNA deregulation in cancer

miRNAs have emerged as important players in many cellular processes including cell division, differentiation and apoptosis [77]. They have been suggested as promising cancer biomarkers, as they appear to be cell-type and tissue specific [78]. miRNAs have been shown to be more accurate in the classification of human cancers in comparison to mRNA [79].

Several important factors have been associated with the deregulation of miRNAs, such as aberrant methylation of promoter regions [80], the rearrangement of chromosomal regions [81], and changes in the expression of transcription factors [82, 83]. Moreover, the aberrant expression of different factors at posttranscriptional levels in the miRNA processing pathway has also been shown in cancer [84].
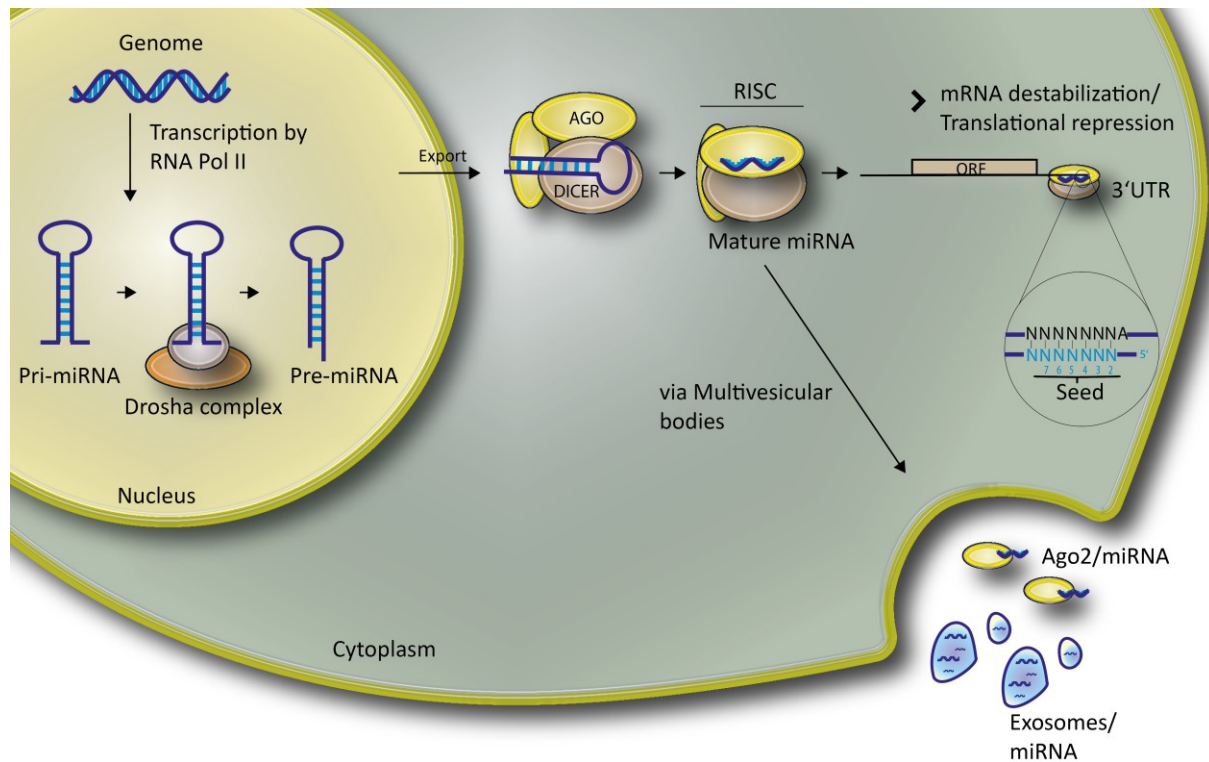
Figure 3 miRNA biogenesis and function. This graphic has been adapted and modified from Schwarzenbach *et al.* [85].

1.4.2 Deregulation of miRNAs in lung cancer pathogenesis

Several miRNAs have been described as aberrantly expressed in lung cancer tissues. Members of the *let-7* cluster are frequently reported as tumor suppressors, whereas members of the *miR-17-92* cluster are reported as oncogenes. The *let-7* family of miRNAs suppresses the expression of *RAS* and also inversely correlates with the RAS protein. Moreover, it is lower expressed in lung tumors compared to normal samples, and thus has a tumor suppressive role [86]. Early-stage NSCLC patients were classified into two clusters, depending on the expression of the *let-7* cluster, while the cluster with reduced expression of the *let-7* members significantly correlates with a shorter survival time after tumor resection [87]. Moreover, low levels of *let-7a-2* have also been shown to correlate with poor prognosis in lung cancer [88].

In contrast, members of *miR-17-92* cluster are frequently overexpressed in lung cancer. The cluster is located within the *C13orf25* gene, which has been found to be amplified in SCLC. Interestingly, the overexpression of the *miR-17-92* cluster, rather than the overexpression of the *C13orf25* transcript, resulted in increased cell growth [89]. The oncogene *MYC* encodes a transcription factor that binds E-box sequences about 1.5 kb upstream of the *miR-17-92* cluster and induces its expression [90]. Moreover, the *miR-17-92* cluster has been linked with

oncogenic potential, as its overexpression augments the perfusion of tumors with blood vessels in mouse models. The knockdown of the *miR-17-92* cluster has been shown to restore, for example, the expression of the anti-angiogenic protein thrombospondin-1 (THBS1) [82].

The analysis of miRNAs as biomarkers derived from tumor tissue can provide information about tumor-specific miRNAs. A study using formalin-fixed and paraffin-embedded tissues (FFPE) has provided evidence for a miRNA panel that is associated with the prognosis of early-stage NSCLC patients after surgery [91]. However, access to tumor tissues is limited because it requires an invasive procedure.

1.4.3 Circulating miRNAs as biomarkers in cancer

Blood-based biomarkers offer the ability to monitor the disease after surgery as well as a minimally invasive testing procedure. Biomarkers derived from blood or other body fluids can indirectly be associated with the disease, e.g. via secreted factors from the growing tumor and the tumor's microenvironment [92]. Circulating miRNAs have been shown as valuable prognostic and diagnostic tools as a result of their stability in body fluids such as serum. miRNA levels have been robustly measured after the exposure of plasma to extreme conditions such storage at room temperature for 24 h, several freeze-thawing cycles, and RNase activity [93]. Circulating miRNAs in serum have been found to be associated with cancer pathogenesis [93-95] and were reported to be much more robust than serum mRNAs [96]. Several studies have addressed the stability of circulating miRNAs in the blood, and these studies have shown their association not only with exosomes [97], but also with proteins such as AGO2 [98]. Exosomes are small membrane vesicles (50-90 nm) of endocytic origin and are released from cells into the extracellular environment upon the fusion of multivesicular bodies (MVB) with the plasma membrane [99]. Moreover, miRNA leakage from cells during tissue damage or apoptosis is also known [100].

One of the first studies on disease-specific circulating miRNAs was conducted by Lawrie and colleagues, who observed that high levels of *miR-21* in serum is associated with poor prognosis of patients with diffuse large B-cell lymphoma [95]. The concordance between serum miRNAs and blood cell miRNAs in cancer patients is considerably lower than in healthy patients that appear to have similar expression profiles. Moreover, miRNAs detected in serum from healthy and cancer patients also show low concordance [94]. Therefore, it has been suggested that specific miRNA signatures can be identified in cancer patients. However, the origin of these specific miRNA signatures is not clear and is still under investigation.

1.4.3.1 Circulating miRNAs as biomarkers in NSCLC

Besides their cost-effective analysis, circulating miRNAs enable the risk assessment of operable or unresectable NSCLC tumors in a minimally invasive sampling procedure and may be monitored before and after surgery or therapy. However, there is a lack of robust blood-based biomarkers for both the diagnosis and prognosis of NSCLC.

A panel of 34 miRNAs has been able to identify asymptomatic high-risk individuals with early-stage lung adenocarcinoma through the categorization of the individuals into two groups: one with malignant and the other with benign cancer [101]. miRNA signatures have also been associated with aggressive lung cancer cases [102]. In a combinatorial study with low-dose CT, these miRNA signatures have been shown to improve the benefit of low-dose CT through the reduction of the false-positive rate [103]. A panel consisting of four serum miRNAs (*miR-486*, *miR-1*, *miR-499*, *miR-30d*) has been identified to be associated with poor prognosis in early stages of NSCLC [104]. Cui *et al.* have also reported increased levels of *miR-125b* in inoperable advanced NSCLC, which is associated with poor prognosis [105, 106]. The high expression of *miR-21* in the serum of NSCLC patients has been associated with poor prognosis [107]. Furthermore, a 10-miRNA signature has been used for diagnosis, including 400 NSCLC and 220 control cases, which resulted in a high sensitivity ROC of 0.96 in the training or 0.97 in the validation set [108].

As the analysis of circulating miRNAs as diagnostic and prognostic biomarkers progresses, it may improve patient care. The risk assessment of operable NSCLC disease is critical to reduce the high mortality rate. Different technologies that measure miRNA levels are available, whereby qRT-PCR has been shown to generate robust results in contrast to different microarray platforms [109, 110]. The identification of disease-relevant circulating miRNAs can be challenging due to their minute amounts in serum and because there is no consensus about the normalization of miRNAs. Moreover, pre-analytical parameters must be considered in order to select the best possible set of miRNAs. As hemolysis has been shown to affect miRNA expression levels [111], it is critical to use a hemolysis-based miRNA indicator to determine the degree of potential hemolysis in serum samples [111, 112].

1.4.4 miRNAs in EGFR-TKI-resistant lung cancer

Recurrence of lung adenocarcinoma after surgery is commonly treated with chemotherapy, radiotherapy, or if an actionable driver mutation is found, targeted therapy [113]. Considerable progress has been made in the discovery of druggable targets in NSCLC patients, such as EGFR [25-29]. However, the functional relevance of miRNAs in tumor progression, particularly in EGFR-TKI resistant NSCLC tumors, remains poorly understood.

Weiss *et al*. reported that *miR-128b* downregulates EGFR expression and the loss of heterozygosity of this miRNA was commonly found in lung cancer [114]. Gefitinib treatment of NSCLC patients with loss of *miR-128b* showed a better overall rate of survival in comparison to patients with no loss of miRNA. In addition, Wang *et al*. demonstrated an upregulation of *miR-214* in gefitinib resistant NSCLC cells and a depletion of this miRNA resulted in increased sensitivity towards gefitinib, perhaps through the upregulation of PTEN [115]. Through a 13-miRNA signature, Bryant *et al*. were able to predict the response to EGFR-therapy [116]. Garofalo *et al*. reported the regulation of miRNAs through EGF and MET receptors. They developed cell lines with stable knockdowns of *MET* and *EGFR* using shRNA lentiviral particles. The knockdown of *EGFR* and *MET* resulted in the downregulation of *miR-30b/c* and *miR-221/222* expression. *miR-30b/c* and *miR-221/222* were found to target the apoptotic factors *BIM* and *APAF-1*, respectively. Gefitinib treatment also resulted in the downregulation of these miRNAs. These miRNAs, however, were not deregulated in gefitinib resistant lung cancer cell lines. Their study suggested that modulating specific miRNAs in EGFR-TKI resistant NSCLC could enable novel treatment options [117].

It is widely accepted that the tumor-stroma is critical for the progression of the tumor, for example after treatment with inhibitors such as the EGFR-TKI gefitinib [49]. Therefore, the crosstalk of tumor cells with stromal fibroblasts, and their underlying miRNA signaling network in NSCLCs may modulate gefitinib resistance, which was investigated through an *in-vitro* co-culture model [46]. The model enabled the development of "short-term" resistant cells towards gefitinib through the induction of paracrine factors from the tumor-stroma interaction, as in comparison to time-consuming stably established resistant cells. Moreover, the reduction of EGFR activity through gefitinib treatment mimics a more physiologic analysis of miRNA regulation in comparison to the use of shRNA-mediated knockdown of *EGFR*, as reported by Garofalo *et al*. [117]. The screening approach that uses miRNA qPCR-based arrays has been described as very accurate and efficient and can be achieved by simple computational analysis [118].

1.5 Aim of the present study

To investigate the role of miRNAs in the development of lung adenocarcinoma, two approaches were used, i.e. by studying their prognostic potential in the serum of early-stage tumors and their functional role in therapy resistance *in-vitro*.

The aim of the first study was to identify circulating miRNAs that are clinically relevant for NSCLC prognosis. Circulating miRNAs were isolated from serum samples of patients with early stages of NSCLC. The miRNAs from these samples were analyzed using expression profiling such as qRT-PCR based arrays. Specific miRNAs with prognostic potential were selected to find a suitable miRNA signature that can significantly predict recurrence-free and the overall survival of early-stage lung adenocarcinoma patients. This study may help to improve the identification of clinically relevant patient subsets. Furthermore, different pre-analytical factors, such as blood collection and hemolysis that may contribute to sample bias between the cohorts were analyzed.

The study's second aim was to further evaluate the role of miRNAs after therapy resistance of NSCLC. Therefore, the study used and evaluated a co-culture system, which enabled the identification of transcriptomic changes associated with therapy resistance. The study applied global miRNA and mRNA analysis using high-throughput expression profiling techniques to identify putative miRNA and mRNA candidates that are involved in resistance towards gefitinib. *In-silico* analysis using miRNA target prediction algorithms were used to search for interactions between miRNAs and target genes. The miRNA-mRNA interaction should be validated by overexpression, inhibition and luciferase assays. The knockdown of the miRNA targets using siRNA-mediated knockdown was used to identify relevant biological pathways and the underlying miRNA signaling network in NSCLCs that may modulate gefitinib resistance.

2 Materials and Methods

2.1 Materials

Table 1: Equipment

Item	Supplier
Agarose gel electrophoresis chamber	Renner
Bacterial shaker/incubator, Ecotron	Infors HAT
Camera, AxioCam MRm	Carl Zeiss
Cell counter, CASY Cell Counter & Analyzer System Model TT	Innovatis/Roche
Centrifuges	Heraeus, Eppendorf
ChemiDoc XRS+,	Bio-Rad
CO2 incubator, CB 150	Heraeus
Flow cytometer, FACSCanto II	BD Biosciences
Freezing container cell culture, Mr Frosty	Nalgene
Heating block, Thermomixer comfort	Eppendorf
Micropipette manual, Pipetman	Gilson
Micropiptette electronic multichannel, Xplorer	Eppendorf
Microplate reader, Infinite M200	Tecan
Microscope, Axiovert 40 CFL	Carl Zeiss
Pipettor, Pipetboy Integra	Biosciences
Power supply, E835	Consort
Protein electrophoresis/blotting, Mini Protean	Biorad
Real time PCR, Light Cycler 480	Roche
Sterile cell culture hood, HERA Safe	Thermo Scientific, MJ Research
Trans-Blot® Turbo Transfer System	BioRad
UV imager, QUANTUM	Vilber Lourmat
Vacuum manifold, QIAvac 24 Plus	Qiagen
Vortexer, Vortex Genie	Scientific Industries

Table 2: Chemicals

Item	Supplier
4IPBA (4-Iodophenylboronic acid)	Sigma
acetic acid	Riedel de Haen
agar agar	Roth
agarose (for gel electrophoresis)	Roth
ampicillin	Sigma
bovine serum albumin	PAA Laboratorien
chloroform	Roth
DAPI dihydrochloride	Invitrogen
EDTA	Sigma

ethanol	Sigma
ethidium bromide	Sigma
glycine	Gerbu
hydrochloric acide	Sigma
hydrogen peroxide	Sigma
isopropyl alcohol	Sigma
luminol	Sigma
methanol	Sigma
non fat dry milk	Roth
peptone	Roth
Ponceau S	Sigma
propidium Iodide solution, 1 mg/mL in water	Sigma
sodium chloride	AnalaR NORMAPUR
sodium deoxycholate	Sigma
sodium dodecyl sulfate	Roth
sodium hydroxide	Fluka
tris base	Sigma
TRI Reagent	Sigma
tris HCl	Sigma
triton X-100	Sigma
tween 20	Sigma
yeast extract	Gerbu

Table 3: Molecular biology reagents

Item	Supplier
Absolute qPCR Mastermix	Thermo Scientific
AmpliTaq DNA polymerase	Applied Biosystems
CellTiter blue cell viability assay	Promega
cOmplete, Mini,EDTA-free Protease Inhibitor Cocktail Tablet	Roche
DNA ladder mix, Generuler	Fermentas
dNTPs	Genaxxon
ExiLENT SYBR Green master mix	Exiqon
CSF2	Sigma
Gel Loading Dye, Orange (6x)	New England Biolabs
HGF human	Sigma
HotStar Taq DNA polymerase	Qiagen
KAPA Hifi Hot Start PCR Kit	Peqlab
Lipofectamine RNAiMAX	Invitrogen
Lipofectamine 2000	Invitrogen
Mini Complete Protease Inhibitor Cocktail	Roche
Nuclease free water	Ambion
PhosSTOP Phosphatase Inhibitor Cocktail Tablets	Roche
pmirGLO plasmid vector	Promega
Precision Plus Protein Kaleidoscope Prestained Standards	BioRad
Probes 480 Master Enzyme Mastermix	Roche

Restriction enzymes	NEB, Roche
RNAse A	Applichem
SOC medium	Invitrogen
Universal Probe Library (UPL)	Roche

Table 4: Kits

Item	Supplier
BCA Protein Assay Kit	Thermo Scientific
HU HGF ELISA	Invitrogen
microRNA Ready-to-Use PCR, Human panel I+II, V2	Exiqon
MILLIPLEX MAP Phospho Mitogenesis RTK Magnetic Bead 7-Plex Kit	EMD Millipore
MILLIPLEX® MAP AKT/MTOR Phosphoprotein Magnetic Bead 11-Plex Kit	EMD Millipore
Mini-PROTEAN TGX Stain-Free Precast Gels (10%, 4-20%)	BioRad
miRCURY LNA™ Universal cDNA synthesis Kit II	Exiqon
miRNeasy Kit	Qiagen
Plasmid Midi Kit	Qiagen
Plasmid Mini Kit	Qiagen
QIAquick Gel extraction Kit	Qiagen
RevertAid H-Minus First Strand cDNA Synthesis Kit	Fermentas
RNeasy Mini Kit	Qiagen
Taqman MicroRNA Reverse Transcription Kit	Applied Biosystems
TOPO TA Cloning Kit	Invitrogen
Trans-Blot Turbo RTA Mini LF PVDF Transfer Kit	BioRad

Table 5: Cell culture item

Item	Supplier
0.25% Trypsin-EDTA	Gibco
CASYton	Innovatis/Roche
DMSO, cell culture grade	AppliChem
DPBS (- CaCl2, - MgCl2)	Gibco
EMEM	ATCC
F-12K with glutamine	ATCC
FBS	Gibco
Opti-MEM I	Gibco
RPMI Medium 1640	Gibco

Table 6: Consumables

Item	Supplier
0.5 ml, 1.5 ml, 2 ml microcentrifuge tubes	Eppendorf
384-well plate, white, for Light Cycler 480	Roche
6-well, 96-well plates, flat bottom, transparent	BD Falcon
adhesive optically clear plate seal	Thermo Scientific
bacterial culture tube, 12mL	Greiner
CASY cups	Innovatis/Roche

cell culture flasks, T-25, T-75, T-150	TPP
cell culture plate, flat bottom, transparent, 96-, 48-, 12- and 6-well	BD Falcon
cell culture plate, flat bottom, white, black, 96 well	Perkin Elmer
cell scraper	Corning
cell spatula	TPP
conical tubes, 15mL, 50mL	BD Falcon
cryovials 1.8 ml	Nunc
FACS tube, 5mL Polystyren Round Bottom Tube	BD Falcon
filter tips, 10μL, 20μL, 100μL, 200μL, 1000μL	Neptune
LightCycler 480 PCR plate, white, 384 well	Roche
LightCycler 480 Sealing Foil	Roche
pasteur pipettes	WU
PCR strips 0.2mL	Steinbrenner
Petri dish, 10cm	TPP
Petri dish, 6cm Greiner	Bio one
reagent reservoirs	Roth
scalpels	PFM medical AG
serological pipettes 2.5 ml, 5 ml, 10 ml, 25 ml	BD Falcon
Thincert 24 well cell culture insert, 1 μM pore size	Greiner Bio one

Table 7: Drugs

Item	Supplier
Bafilomycin A1	Sigma
Erlotinib	NEB
Gefitinib	Biocat

Table 8: Software and Online tools

Item	Supplier
AxioVision	Carl Zeiss MicroImaging
Bio-Plex Manager 6.1	Bio-Rad
Excel 2010	Mircrosoft
DAVID v6.7	NIAID, NIH
FACSDiva 6.1.2	BD Biosciences
GraphPad Prism 5.01	GraphPad Software, Inc
Image Lab Software Version 5.2.1	Bio-Rad
Ingenuity pathway analysis	Ingenuity systems
LightCycler 480 Software release 1.5.0	Roche
TargetScan 6.2	Whitehead Institute

Table 9: Cell lines (TM Name)

Item	Subtype	Supplier
A549 (CCL-185)	Lung cancer	ATCC
CCD-19Lu (CCL-210)	Normal lung fibroblast	ATCC
HCC827 (CRL-2868)	Lung adenocarcinoma	ATCC
MRC-5 (CCL-171)	Normal lung fibroblast	ATCC
PC-9	Lung adenocarcinoma	PHE
H1650	Lung adenocarcinoma	ATCC
H1975	Lung adenocarcinoma	ATCC
H2030	Lung adenocarcinoma	ATCC

Table 10: Antibodies

Item	Catalog-No	Supplier
anti-c-MET	sc-161	Santa Cruz
anti-EGFR	sc-03	Santa Cruz
anti-ERBB2	#2165	Cell Signaling
anti-ERBB3	#4754	Cell signaling
anti-GABARAPL1	ab86497	Abcam
anti-GAPDH	#2118	Cell Signaling
anti-LC3B	#3868	Cell signaling
anti-mouse-HRP	#7076	Cell Signaling
anti- SQSTM1 (p62)	610832	BD Bioscience
anti-rabbit HRP	#7074	Cell Signaling
anti-ß-ACTIN	#13E5	Cell Signaling

Table 11: siRNAs

Item	Sequence	Supplier
AllStars	Proprietary information	Qiagen
siRNA-*GABARAPL1*_#6	cagctgctagttagaaaggtt	Qiagen
siRNA-*GABARAPL1*_#7	cagctgcaagttcttgtataa	Qiagen
siRNA-*GABARAPL1*_#8	tacagtgatgagagtgtctat	Qiagen
siRNA-*GABARAPL1*_#9	gcggtgcatcatgaagttcca	Qiagen

Table 12: Primer

Item	Sequence	Supplier
GABARAPL1-NheI fw	ggtaagctagcattgtggcctacagtgatgagagtg	Sigma
GABARAPL1-SalI rev	agcttgtcgactcgatttatttccttggcctgatgg	Sigma
GABARAPL1-trc_UTR-NheI	agcttgtcgactcgatggccatcatgtagcattcct	Sigma

miRNA primers

TaqMan-based real-time quantification of miRNAs was done according to Chen *et al.* [109] in the serum study. SYBR Green real-time quantification of miRNA was done according to [119] in the co-culture study. All PCR reactions included a "–RT" control without cDNA to detect genomic DNA contamination. If not otherwise stated, all miRNAs in this study are human miRNAs, usually denoted with a hsa for human (Homo sapiens).

Table 13: miRNA TaqMan Primers

miRNA-ID	Mature miRNA sequence	Supplier
miR-20b-5p	caaagugcucauagugcagguag	Life Technologies
miR-21-5p	uagcuuaucagacugauguuga	Life Technologies
miR-23a-3p	aucacauugccagggauuucc	Life Technologies
miR-29b-3p	uagcaccauuugaaaucaguguu	Life Technologies
miR-30d-5p	uguaaacauccccgacuggaag	Life Technologies
miR-125b-5p	ucccugagacccuaacuuuguga	Life Technologies
miR-142-3p	uguaguguuuccuacuuuaugga	Life Technologies
miR-331-3p	gccccugggccuauccuagaa	Life Technologies
miR-451a	aaaccguuaccauuacugaguu	Life Technologies
miR-486-5p	uccuguacugagcugccccgag	Life Technologies

Table 14: miRNA mimics & inhibitors

miRNA-Name	Catalogue number	Supplier
miRIDIAN microRNA Hairpin Inhibitor Negative Control #1	IN-001005-01	Dharmacon, GE
miRIDIAN microRNA *miR-503-5p* hairpin inhibitor	IH-300841-07-0005 5	Dharmacon, GE
miRIDIAN microRNA *miR-503-5p* mimic	C-300841-05-0005 5	Dharmacon, GE
miRIDIAN microRNA Mimic Housekeeping Positive Control #2 (GAPDH)	CP-001000-02	Dharmacon, GE
mIRIDIAN microRNA Mimic Negative Control #2	CN-002000-01	Dharmacon, GE
miRIDIAN microRNA Mimic Transfection Control with Dy547	CP-004500-01	Dharmacon, GE

Table 15: miRNA primers

miRNA-ID	Sequence	Supplier
let-7a-2-3p	cguuacagccuccuagcuuucc	Exiqon
miR-103-3p	agcagcauuguacagggcuauga	Exiqon
miR-1296-5p	uuagggcccuggcuccaucucc	Exiqon
miR-181a-2-3p	accacugaccguugacuguacc	Exiqon
miR-181a-3p	accaucgaccguugauuguacc	Exiqon
miR-181a-5p	aacauucaacgcugucggugagu	Exiqon
miR-181b-5p	aacauucauugcugucgguggau	Exiqon
miR-191	caacggaaucccaaaagcagcug	Exiqon
miR-205-5p	uccuucauuccaccggagucug	Exiqon
miR-222-5p	cucaguagccaguguagauccu	Exiqon
miR-29b-1-5p	gcugguuucauauggugguuaga	Exiqon
miR-423-5p	ugaggggcagagagcgagacuuu	Exiqon
miR-503-5p	uagcagcgggaacaguucugcag	Exiqon
miR-941	cacccggcugugugcacaugugc	Exiqon

mRNA primer design

Primer pairs for mRNA real time PCR were designed using the Roche UPL assay design center software (http://qpcr.probefinder.com/organism.jsp). Primer pairs were designed with the Taqman or MGB-Probe module. Primer pairs spanned exon-intron boundaries whenever possible. Primer pairs were assessed for secondary structure. Total amplicon length was checked via agarose gel electrophoresis. Assay efficiency was tested by measuring cDNA dilution curves. Only specific assays with efficiencies of > 1.70 were used.

Table 16: UPL primers

UPL (#probe)	Primers forward	Primers reverse	Supplier
ACTB (#64)	ccaaccgcgagaagatga	ccagaggcgtacagggatag	Roche
c-MET (#31)	tgaaattcatccaaccaaatctt	aatagaaaactgacaatgttgagagg	Roche
DCKL1 (#34)	caaccaggaatgtattggataaga	cctggttgcgtcttcgtc	Roche
FLT-1 (#85)	ccactcccttgaacacgag	gtcgccttacggaagctct	Roche
GABARAPL1 (#3)	tgggccaactgtatgagga	ctacccccaagtccaggtg	Roche
GMCSFR (#12)	agtctccgagagaagaaaagca	cggattttcctgctgtaaacc	Roche
HGF (#49)	gattggatcaggaccatgtga	ccattctcattttatgttgctca	Roche
KDR (#18)	ccccaaattccattatgacaa	cggctctttcgcttactgtt	Roche
OSBPL7 (#77)	gaggcttccgcttcatca	catggcaggccgagatag	Roche
ZMAT3 (#2)	ccaggaaagaagggaatgagt	gcggggattgaagtaaggac	Roche

Buffers

TAE buffer:
40mM Tris base
40mM acetic acid
1mM EDTA0.05%

LB medium:
10g peptone
5g yeast extract
10g/L NaCl
fill to 1L with water
adjust pH to 7, autoclave

RIPA protein lysis buffer:
150 mM sodium chloride
1.0% Triton X-100
0.5% sodium deoxycholate
0.1% SDS
50 mM Tris base, pH 8.0

ECL solution:
100mM Tris-HCl pH 8.8
1.25mM luminol

2mM 4IPBA
store dark at 4 °C
add 5 µL hydrogen peroxide per 15mL ECL solution
freshly

LB agar:
1L LB medium
15g agar
autoclave, cool to 50 °C
add ampicillin (100 µg/mL)

PBS-T:
DPBS
0.05% Tween-20

Transfer Buffer:
200ml 5x Transfer Buffer (BioRad)
200ml Ethanol (100%)
fill to 1l with water

SDS running buffer:
25mM Tris base
192mM glycine
0.1% SDS

Serum samples and patient characteristics

Collection and use of serum samples from different patient cohorts was done at the Thoraxklinik at Heidelberg University following written patient consent and the approval by the local ethics committee (27/2001).

Serum samples were obtained from 275 lung adenocarcinoma patients (stage I-III, Union for International Cancer Control (UICC) 7th edition) on the day of surgery. Patients were only included that had a complete tumor resection (local R0 status). This cohort is independent of a previous study [120]. Detailed patient cohort description and follow-up data are listed in Table 18. Additional thirteen serum samples were obtained from patients by three sequential blood-sampling methods as described by Kahn *et al*. [121].

2.2 Methods

2.2.1 Molecular biology methods

RNA and miRNA isolation from serum

All following steps described in this section were carried out at room temperature (RT). A combination of phenol-guanidine-based lysis and silicamembrane- based purification was used for the isolation of cell-free RNA from serum samples. A total volume of 100 µL of human serum was thawed on ice and mixed with 300 µl Tri Reagent BD (Sigma). To ensure complete dissociation of nucleoprotein complexes, the mixtures were incubated for 5 min at RT. For serum samples there is no consensus about the normalization and a lack of robust endogenous miRNA, therefore synthetic miRNAs from *C.elegans* were used for normalization of sample-to-sample variation in RNA isolation [93]. A pool of miRNA mimics from *C.elegans* (*cel-miR-39*, *cel-miR-54*) (Qiagen) with a concentration of 20 nM in a volume of 5 µL were added as spike-in control. Additionally, 3 µg of glycogen from a 20 µg/µL glycogen stock was added to enhance the recovery of RNA. A total of 80 µl pure chloroform was added; the mix was shaken vigorously and allowed to stand for 5 min at RT. After 15 min of centrifugation (12,000 x g; 4 °C), the upper aqueous phase was transferred to a fresh tube. Purification of extracted total RNA was performed with the RNeasy kit (Qiagen) according to the manufacturer's instructions. Briefly, the aqueous phase was mixed with 1.5 x volume 100% ethanol to enable small RNA binding to the silica-membrane-based spin-columns. All following centrifugation steps were performed at 8,000 x g if not otherwise stated. The mix was immediately transferred on an RNA spin-column and centrifuged for 15 sec. Then, 700 µL RWT buffer was added, mixed, and subsequently centrifuged for 15 sec. Next, 500 µl RPE buffer was added and centrifuged for 15 sec. The step was repeated but the centrifugation lasted for 1 min and finally the RNA was eluted in a final volume of 35 µl nuclease-free water at 8,000 x g. Hemolysis grade of each serum was visually rated. *miR-23a-3p/ miR-451a* ratios were used as hemolysis indicator as previously reported [112].

RNA and miRNA isolation from cells

All steps described in this section were carried out at RT. 700 µl of Qiazol (Qiagen) was added for up to 1×10^7 cells, mixed and incubated for 5 min. A total of 140 µl pure chloroform was added; the mix was shaken vigorously and allowed to stand for 5 min at RT. After 15 min of centrifugation (12,000 x g; 4 °C), all of the upper aqueous phase was transferred to a fresh tube. Purification of extracted total RNA was performed with the RNeasy kit (Qiagen) according to the manufacturer's instructions as described earlier.

Quantification of nucleic acids

Nanodrop spectrophotometry

Nucleic acid concentration was measured by UV/VIS spectrophotometry using the Nanodrop ND-1000. The absorption maximum of nucleic acids is 260 nm and proteins have the maximum absorption at 280 nm. The purity of the nucleic acids was determined by calculating the ratio of the absorption values at 260 nm/280 nm and 260 nm/230 nm. H_2O or TE buffer was used as the blank reference measurement for unknown sample measurements.

Bioanalyzer

The RNA integrity number (RIN) is a metric for the quality of RNA by the Agilent 2100 Bioanalyzer (Agilent Technologies, Santa Clara, US). In this study, RNA integrity was assessed using the Agilent RNA 6000 Pico Kit for the screening of miRNAs and mRNA from the HCC827 co-culture according to the manufacturer's instructions (Agilent Technologies). The RNA in all samples was observed to have good quality (RIN > 9).

Reverse transcription and quantitative real-time PCR of serum miRNA using TaqMan technology

For the measurement of single miRNA assays in the serum study, the following components were mixed for each well of a 96-well plate: A volume of 1.5 µL total RNA including miRNA was reverse transcribed with 0.038 µL dNTP's (100 mM), 0.38 µL 10 x RT Buffer, 0.75 µL 5 x RT primers, 0.048 µL RNase Inhibitor (20 U/µL), 0.25 µL Multiscribe Reverse Transcriptase (50 U/µL), and 0.54 µL nuclease-free water. The reaction mix was incubated on ice for 5 min. Finally, RNA was reverse transcribed in three sequential steps. The first incubation was performed at 16 °C for 30 min followed by the strand synthesis at 42 °C for 30 min and the inactivation of the enzyme at 85 °C for 5 min.

For each reaction mix, a volume of 2.5 µL of cDNA was mixed with 0.25 µL TaqMan miRNA assay (20 x) and 2.75 µL ABsolute PCR Mix that comprises a Thermo-Start DNA Polymerase and a proprietary reaction buffer, and quantified using a LightCycler 480 (Roche). The cycle started with an initial temperature of 95 °C for 15 min to denature DNA and activate the enzyme and was followed by a total number of 40 cycles including 95 °C incubation for 15 sec and a 60 °C step for 1 min. Three technical replicates were measured for each sample.

Reverse transcription and quantitative real-time PCR of miRNA from cell culture samples using low density based arrays

In order to determine differentially regulated miRNAs in resistant cells, a qRT-PCR miRNA expression profiling was performed. Here, more than 700 miRNAs were analyzed following the recommended protocol (Exiqon miRCURY LNA Universal RT microRNA PCR, A and B- Human microRNA PCR panels V2). Amplification reactions were performed in a 384-well plate containing lyophilized primers.

Reverse transcription for panel I+II was done by mixing 5 x reaction buffer (8 µl), nuclease-free water (18 µl), 10 x enzyme mix (4 µl), synthetic UniSp6RNA spike ins (2 µl) and total RNA (8 µl) (5 ng/µl), equivalent to 40 ng, for each sample. The reaction mix was centrifuged and incubated on ice for 5 min, reverse transcribed by incubating for 60 min at 42 °C and heat inactivated at RT for 5 min at 95 °C. Afterwards, the cDNA was diluted by combining cDNA (20 µl) with nuclease-free water (1,980 µl) and 2 x ExiLENT SYBR Green master mix (2000 µl) for each panel. For each reaction, 10 µl of the cDNA:PCR Master mix was added to each well, centrifuged, and measured on the LightCycler480. Thermal cycling was performed in the LightCycler480 (Roche) according to the recommended conditions by the supplier of the enzyme mix.

Reverse transcription and quantitative real-time PCR of miRNA using SYBR Green

For the measurement of single miRNA assays, total RNA isolated from cells were mixed with the following components for each well of a 96-well plate: A volume of 2 µL (5 ng/µl) total RNA including miRNA (equivalent to 10ng) was reverse transcribed with 5 x reaction buffer (2 µl), nuclease-free water (4.5 µl), 10x enzyme mix (1 µl), and synthetic UniSp6RNA spike ins (0.5 µl). The reaction mix was reverse transcribed as described in the previous section.

Each cDNA sample was diluted 1:80 in water and 4 µl of diluted cDNA was mixed with 5 µl 2 x ExiLENT SYBR Green master mix and 1 µl PCR primer mix and measured on a LightCycler480. To exclude variability between plates, an assay (UniSp3) was premixed in three wells of each plate to evaluate qPCR performance. The UniSP3 showed low SD (SD = 0.14) between all plates suggesting good overall quality for comparing samples between each other.

Reverse transcription and quantitative real-time PCR of mRNA using UPL from cell culture samples

To amplify mRNAs by PCR or measure mRNA levels by quantitative RT-PCR, mRNA was

reverse transcribed to cDNA. For this, the RevertAid H-Minus First Strand cDNA Synthesis Kit (Fermentas) was used. The following components were mixed in a PCR tube on ice: total RNA (0.5 µg-3 µg), random hexamer primer (1 µL), water (ad 11.5 µL), 5 x reaction buffer (4 µL), RiboLock RNase Inhibitor (0.5 µL), 10 mM dNTP mix (2 µL), 200 U/µL RevertAid H Minus M-MuLV Reverse Transcriptase (1 µL). The reaction was mixed and incubated for 5 min at 25 °C followed by 60 min at 42 °C in a thermal cycler. Enzymes were inactivated by heating at 70 °C for 5 min. cDNA was either frozen at -80 °C or kept on ice for use on the same day.

The mRNA levels were quantified by quantitative RT-PCR using the LightCycler480 (Roche) and Universal Probe Library (UPL) (Roche). For UPL assays, the following components were mixed per well of a 384 well qPCR plate: cDNA equivalent of 5-10 ng total RNA (5 µL), probes 480 Master Enzyme Mastermix (Roche) (5.5 µL), forward and reverse primer mix (each 20 µM) (0.11 µL), UPL probe (0.11 µL), nuclease free water (0.28 µL). Cycling conditions were used as recommended by the manufacturers. Three technical replicates were measured for each sample.

Microarray

Total RNA (50 ng/µl) was analyzed using HumanHT-12 v4 Expression BeadChip Kit from Illumina comprising 31,000 annotated genes and 48,107 probe IDs derived from the NCBI RefSeq Release 38 (Nov 7, 2009). The labeling and hybridization were performed by the Expression Profiling Service of the DKFZ Microarray Core Facility.

Bacterial cultures

For amplification of vector DNA, the bacterial *E.coli* strain TOPO Top10 was used and cultured in LB-medium. Bacterial cells were grown under selection pressure using ampicillin (100 µg/mL).

3'-UTR-cloning PCR

To isolate the 3'UTR of *GABARAPL1*, primers (listed in Table 12) were designed for the specific region of interest and a PCR was performed as described in the following: For each reaction the following reagents were added to a PCR tube on ice as described from the manufacturer's recommendation (Protocol: KAPA Hifi protocol): DNA (max. 40 ng), 5 x Buffer (5 µl), 10 mM dNTPs (0.75 µl), 10 µM GABARAPL1-NheI fw and GABARAPL1-SalI rev (for full length 3'UTR of GABARAPL1) or GABARAPL1-trc_UTR-NheI (for

truncated version without binding site for *miR-503-5p*) (0.75 µL each), water (ad 25 µL) and 0.5 µl KAPA Hifi DNA Polymerase (0.02 U/µl). The following temperature cycling was performed in a thermal cycler: initial denaturation (5 min at 95 °C), denaturation (20 sec at 98 °C), annealing (15 sec at Tm +/- 10 °C), and extension (1 min/kb expected PCR product size at 72 °C). Steps from denaturation to extension were repeated 40 times followed by a final extension step for 10 min at 72 °C and cooling to 4 °C.

Restriction digest and manipulation of DNA

Restriction digests were conducted with enzymes from New England Biolabs (NEB) following the manufacturer's instructions.

Agarose gel electrophoresis and isolation of PCR fragments

After amplification of DNA fragments by PCR, the PCR products were run with 6 x Gel Loading Dye, Orange (NEB) and separated by agarose gel electrophoresis. Agarose was mixed with 1 x TAE buffer to 1.0% concentration and boiled until the agarose dissolved. Gels were poured with the liquid agarose after cooling down to about 50 °C. For visualization of DNA bands, 10 µl of 0.5 mg/L ethidium bromide solution was added to 100 ml agarose solution, solidified and run in 1 x TAE buffer at 10 V/cm length of the gel until the loading dye had migrated for the desired distance. Bands were visualized using a UV transilluminator and the desired bands were cut from the gel and purified with the Qiaquick PCR purification kit (Qiagen) according to manufacturer's protocol.

T4 DNA ligation

The double digested PCR fragment and the double digested pmirGLO (7350 bp) were ligated according to the protocol from NEB. DNA was extracted from 1% agarose gel. 10 x T4 DNA Ligase Buffer (2 µl), PCR insert fragment and the plasmid vector were used in a molecular ratio of 3:1 and 5:1. T4 DNA Ligase (1 µl) was incubated with the reaction at 16 °C, overnight. 5 µl of the ligation were used for the transformation of TOP10 chemically competent bacteria (see below). After incubation of the plated bacteria, a colony PCR was performed using the KAPA Hifi protocol. Six clones per plate were analyzed.

Transformation of bacteria

To transform chemically competent TOP10 *E. coli* cells (Invitrogen) with plasmids, the heat shock method was used. For this purpose, a bacterial suspension of 50 µl competent cells was

thawed on ice and mixed with 5-15 µl of DNA and incubated for 20 min on ice. Then, the cells were heat shocked for 30 sec at 42 °C in a water bath and immediately incubated once for 2 min. For the growth of the bacteria, 800 µl of SOC medium (Invitrogen) was added and incubated for at least 45 min at 37 °C by gentle mixing. Thereafter, cells were transferred to a selective agar plate and incubated at 37 °C bottom-up in an incubator overnight.

Colony PCR

Colony PCR was used to screen for successfully recombined vectors with the target of interest. For this purpose, only single bacterial colonies were used. A sterile pipet was used to pick up one single colony from the agar plates. Each pipet was transferred to PCR tubes containing 25 µl of the prepared PCR mixture. The remaining bacterial colony at the sterile pipet was transferred into 2 ml LB medium for later bacterial growth and plasmid DNA extraction after the correct recombinant plasmid had been identified by PCR. The KAPA Hifi protocol was performed as previously described to identify the insertion of 3'UTR of *GABARAPL1* in the pmirGLO vector. PCR products were analyzed by agarose gel electrophoresis.

DNA extraction from bacterial lysates

To obtain vector constructs from transformed bacteria, the bacteria were prepared using the QIAprep Miniprep protocol (Qiagen), which is based on alkaline lysis. In brief, bacteria on a selective media were transferred into 2 ml of LB medium containing a selection pressure and incubated for at least 8 h or overnight. Afterwards, the bacteria were transferred into a 1.5ml microcentrifuge tube and centrifuged at 800 x g for 3 min. The cells were harvested, resuspended and lysed under NaOH/SDS conditions and in the presence of RNase A. The lysate was neutralized with a buffer containing guanidine hydrochloride and acetic acid thereby adjusting the lysate to high-salt binding conditions. The suspension was centrifuged in the following always at 17,900 x g. First, the suspension was centrifuged for 10 min at RT. The supernatant was transferred on a QIAprep spin column, whereby DNA is adsorped onto a silica membrane, washed with 70% EtOH and centrifuged twice for 1 min. The DNA adsorped on the silica membrane was eluted by low-salt liquids such as Tris-Chloride (10 mM Tris-Cl, pH 8.5) or water. A fresh 1.5 ml microcentrifuge tube was used and low-salt liquids were added to the center of the QIAprep column and incubated for 1 min. To obtain the DNA, the microcentrifuge tube was spun for 1 min.

DNA gel extraction

Analytical agarose gels (1%) were used to identify and purify DNA fragments such as PCR products for cloning. The QIAquick Gel Extraction Kit (Qiagen) was used for purification of excised gel following the manufacturer's instructions.

Sanger Sequencing

For verification of the inserted PCR fragment (for example *GABARAPL1*) inside the pmirGLO vector, Sanger sequencing was used. The sequencing reactions were performed using DNA and primers, which were submitted at GATC Biotech (Konstanz).

2.2.2 Cell culture

The human lung cancer cell lines HCC827, PC-9, H1650, H1975, and H2030 were maintained in RPMI 1640, MRC-5 and CCD-19LU (CCL-210) in EMEM medium, and A549 in F-12K medium supplemented with 10% fetal calf serum (FCS).

Cells were passaged every 2 to 3 days during their exponential phase in a ratio of 1:3 or 1:5, whereas the confluence of cells was lower than 80%. In order to split cells, the medium was completely aspirated and cells were washed in 10 mL DPBS. To remove cells from the bottom of the plate, cells were incubated with 2.5 mL 0.25% Trypsin-EDTA at 37 °C. After 3-5 min, 10 mL complete medium was added in order to inhibit the function of trypsin. Subsequently, cells were transferred into a new culture flask and maintained in an incubator at 37 C, 5% CO_2 and 95% humidity.

Testing for Mycoplasma contamination and cell line authentication

Cells were regularly tested for mycoplasma following the manufacturer's instructions (Multiplexion). Cell lines were authenticated before use, once every year and after completion of the project. DNA was extracted following the manufacturer's instructions (Multiplexion).

Cell counting

The CASY Cell Counter & Analyzer System Model TT (Innovatis) is a cell counting system based on the electric recording of cells as they pass a measuring capillary. Cells with intact cell membrane act as electric insulators. The electric current cannot go through the membrane of intact cells (electric current exclusion). A signal is generated depending on the volume of the cells. Dead cells cannot act as electric insulators as their membrane is porous and are recorded by the volume of their nucleus. Cells were counted after trypsinization from the cell

culture dish. After resuspension of detached cells, 50 µl of the cell suspension was diluted in 10 mL of isotonic salt solution (CASY-Ton). Only cells with viability > 85% and an aggregation rate lower than 1.5 were used in the experiments.

Cryopreservation of cell lines

Freshly obtained cells were propagated and frozen to establish cell banks for each cell line. At least 20 aliquots of each cell line at an early passage were frozen in the vapour phase of liquid nitrogen. A minimum of 1×10^6 cells in 1.5 mL "freezing medium" were frozen. The freezing medium contains the appropriate complete cell culture medium supplemented with 5% (v/v) DMSO. For freezing cells, the cells were first counted and a desired cell number was centrifuged at 300 x g for 5 min. The pellet was resuspended in freezing medium, and the appropriate cell number was transferred in freezing medium to 1.8 mL CryoTubes (Nunc). CryoTubes were transferred into an isopropyl alcohol isolated freezing container (Nalgene) and frozen at -80 °C. On the next day, the cells were transferred to the vapor phase of liquid nitrogen.

Co-culture

In each well of a 24 well plate, 2×10^4 HCC827 or PC-9 cells were seeded overnight. In parallel 6×10^4 MRC-5 or CCD-19LU cells were seeded in each transwell insert of a 24-well plate. On the next day, the medium was aspirated and the cells were treated with gefitinib (0.5 µM) in EMEM medium supplemented with 10% FCS for at least 1 h in the incubator. After 1 h incubation, the medium was aspirated and fresh medium was added to the NSCLC cells. For each well of a 24-well plate, a transwell insert containing the lung fibroblasts was placed inside and incubated for 48 h. As a result, "short-term" resistant HCC827 and PC-9 towards gefitinib were generated. In the following text, the term "resistance" instead of "short-term resistance" for HCC827 and PC-9 was used.

Cell viability assay

Cell viability assays were performed using CellTiter-Blue cell viability assay (Promega). The CellTiter-Blue solution contains Resazurin, which gives the blue color in the solution. If cells are metabolically active, they can convert Resazurin into Resofurin, which is observed by a color change from blue to pink. For fluorescence measurements, black 96-well plates were used. Since cell culture medium evaporates over time at the outer wells of the plate, they were filled with 100 µl DPBS. This reduces the loss of cell culture medium from the inner wells.

3000 HCC827 and PC-9 cells were seeded in 150 μL of the appropriate medium. Wells containing only medium served as blank controls. The first cell viability measurement was carried out immediately after the treatment. One fifth medium volume of CellTiter-Blue reagent was added to the cells. The solution was then incubated for three hours after addition of CellTiter-Blue. The fluorescence intensity (excitation 579 nm, emission 584 nm) was measured in each well using the Infinite M200 plate reader (Tecan).

All reagents such as the volume of medium, treatment solution and CellTiter-Blue reagent and the number of cells were upscaled when culture dishes other than 96-well plates were used. At least three technical replicate measurements were performed for each measurement.

Impedance measurement

For quantifying cell impedance of HCC827 cells after gefitinib treatment, the real-time electrical impedance based cell based assay system xCELLigence RTCA DP with E-plates 16 (Roche) [122] was used. 100 μl media containing 10% FCS was added into each well of an E-plate and incubated at RT for 30 min to ensure equilibration of media and E-plate. Thereafter, the E-plate was placed into the RTCA-DP in an incubator for background measurement. After background measurement, 3000 HCC827 cells were placed into each well of an E-plate and the measurements were started. Impedance was measured every 15 min for 72 h. After 24 h the E-plate was taken out and the medium was aspirated without touching the bottom of the well. Medium containing HGF (20 ng/μl) or only media containing 10% FCS was added to each well. The changes in impedance were measured as raw cell index, which was normalized to the 24 h value.

Transient transfection of cell lines with miRNAs or siRNAs

Transfection of synthetic miRNA mimics or siRNA into cells provides a technique to elucidate the functional role of miRNAs in cells. Overexpression of siRNAs or miRNAs can reduce the levels of specific mRNAs in cell lines. All siRNAs and miRNAs mimics were purchased from Dharmacon. Lyophilized siRNAs and miRNAs were spun down, dissolved in nuclease-free water and vortexed. After an incubation of 30 min at RT, the siRNAs and miRNAs were resuspended. All siRNAs and miRNAs were initially diluted to 10 μM or 20 μM, respectively, and stored at -20 °C.

In this study, the HCC827 lung cancer cell line was transfected using RNAiMAX Transfection Reagent (Invitrogen). Cells were initially seeded at a density of 1.5×10^5 cells in a volume of 2 ml per well of a 6-well plate and incubated for two days to achieve a cell

confluence of 60-80%. When culture dishes other than 6-well plates were used, numbers of cells, volumes of medium, RNAiMax were scaled accordingly. The medium was replaced after 24 h. First, separate tubes containing Opti-MEM serum free medium (Gibco) were used for the siRNAs or miRNAs and RNAiMAX reagent. All diluted reagents were incubated for 5 min at RT. To enable the formation of transfection complexes, the solution of both tubes were mixed and incubated for 20 min at RT. The siRNA/miRNA:RNAiMAX transfection solution was then added to the cell culture medium in a dropwise manner. After the transfection for 24 h, the old medium was aspirated and fresh medium was added. For each reaction, a concentration of 0.16% (v/v) of RNAiMAX in the medium was used. siRNAs were used at a final concentration of 10 nM. miRNAs were used at a final concentration of 5 nM to 40 nM.

Transient co-transfection of cell lines with plasmid DNA and miRNA

To verify direct interaction of miRNA with the 3'UTR sequence of the miRNA target, a luciferase assay was performed.

1.5×10^4 HCC827 cells were seeded in each well of a white 96 well plate (Perkin-Elmer) and incubated overnight in a volume of 75 µl. On the next day, empty pmirGLO (pmirGLO_empty vector) (12.5 ng) was co-transfected with mimic *miR-503-5p* or negative mimic ctrl#2 (40 nM). In parallel, the 3'UTR *GABARAPL1* cloned into pmirGLO (pmirGLO_*GABARAPL1* vector) (12.5 ng) and a truncated 3'UTR *GABARAPL1* (without the binding site for *miR-503-5p*) were co-transfected with mimic *miR-503-5p* or negative mimic ctrl#2 (40 nM) using Lipofectamine 2000 (0.5 µl) following the manufacturer's instructions (Invitrogen).

Cell cycle analysis

Propidium iodide (PI), a fluorescent agent intercalates with DNA, and can be used to stain cells to analyze the cell cycle. This was done by measuring the DNA content of single cells by staining with the DNA intercalating fluorophore and subsequent FACS analysis.

1×10^5 HCC827 or PC-9 cells were seeded in each well of a 6-well plate and cultured overnight. In parallel, 6×10^4 fibroblast cells (MRC-5 or CCD-19LU) cells were cultured in transwell inserts. On the next day, the tumor cells were treated with gefitinib (0.5 µM) and incubated for 48 h. Cells were detached from the dish by trypsinization. After centrifugation at 300 x g for 5 min, the pellet was resuspended in 1 mL of ice-cold PBS. For fixation of cells, ethanol was used. Cells were fixed by adding 2.5 mL ice-cold 100% ethanol dropwise to the cell suspension while vortexing. Fixed cells were stored at -20 °C until analysis. On the day of

measurement, the cells were centrifuged at 300 x g rpm for 5 min, the supernatant was decanted. Cells were stained and permeabilized when the pellet was resuspended in 0.5 mL PI staining solution (PBS containing 50 µg/ml PI, 0.1 mg/ml RNase A, 0.05% (v/v) Triton X-100) and incubated for 40 min at 37 °C. RNase A was used to prevent background staining by degrading cellular RNA. The staining solution was diluted by adding 4 mL of PBS was added. The cells were centrifuged at 300 x g for 5 min and resuspended in 0.4 mL of PBS and transferred to a FACS tube. All samples were stored on ice until analysis. A FACSCanto II flow cytometer (BD) in the PE channel was used for PI stained cells. Data were analyzed using the software FACS DIVA.

Luciferase assay

All reagents were thawed to RT using a water-bath. Cells were equilibrated to room temperature in the cell culture hood. Medium was aspirated from cells so that a 50 µl volume remained. Cells were lysed by addition of 50 µl of luciferase substrate buffer and incubated at room temperature for at least 10 min. Firefly luciferase activities were measured by luminescence using Tecan M200. Following the firefly measurement 50 µl of Stop & Glo solution was added and incubated for 10 min. Luminescence was measured after 10 min. Firefly luciferase activities were normalized against the subsequently measured Renilla luciferase activity (Promega Dual Luciferase Reporter Assay System). Here, six replicates were performed for each transfection condition. For statistical analysis, the firefly luciferase activity of pmirGlo_GABARAPL1/pmirGLO_empty vector co-transfected with negative mimic ctrl#2 was defined at 100% and compared to the co-transfection with mimic *miR-503-5p*.

2.2.3 Immunochemical methods

Protein isolation

RIPA lysis buffer was used to harvest proteins from cells. The final RIPA buffer (10 ml) was prepared by mixing 1 tablet cOmplete, Mini, EDTA-free (Roche), 1 tablet PhosSTOP (Roche) and 100 µl 0.5 M EDTA (5 mM), which were always added freshly before use. During the protein isolation the cells were always placed on ice after washing the cells once with ice-cold PBS. For a confluent well of a 6-well plate 100 µL RIPA lysis buffer was added. The lysate was collected with a cell spatula and transferred to a 1.5 mL tube. The lysates were incubated on ice at 4 °C for 30 min by slowly shaking on a Thermomixer. Then, the tubes were centrifuged at 12,000 x g at 4 °C for 30 min. The protein lysate was then isolated by

transferring the supernatant to an ice-cold microcentrifuge tube. All protein samples were stored at -80 °C.

BCA assay

To determine the concentration of protein lysates, the BCA Protein Assay Kit (Thermo Scientific) was used. Samples were diluted 1:10 in appropriate lysis buffer. 10 μL of sample and standards were added to a 96-well plate in duplicate. After addition of 200 μL BCA working reagent, the plate was incubated for 30 min at 37 °C. In the presence of proteins, the BCA reagent form complexes with proteins resulting in a color change, from light blue to violet. The Infinite M200 plate reader (Tecan) was used to measure absorbance at 562 nM using. Using a dilution curve with dose-dependent concentrations of BSA, the protein concentrations were calculated.

SDS polyacrylamide gel electrophoresis and Western Blot

Proteins in the cell lysates were quantified by Western blotting. To detect specific proteins in the cell lysate, SDS-PAGE was used to separate proteins based on their molecular weight. This is achieved due to their differential rates of migration through a gel under an electric current. SDS-PAGE was carried out using a 4-20% gradient gel (BioRad), SDS running buffers and protein ladders (BioRad). The samples were mixed with appropriate volumes of lysis buffer and the proteins were reduced and their tertiary structure was denatured by 4 x Roti-Load (Roth). The samples were vortexed, shortly centrifuged and incubated at 95 C for 5 min on a Thermomixer. Finally, the samples were loaded onto the gels (20 μl, 30 μg per lane) and the gels were run using the Mini Protean gel chamber system (BioRad) for about 45 min at 120 V, 60 mA. Due to their negative charge, the proteins move from the negative cathode to the positive anode.

Transfer of separated proteins from the gel onto a PVDF membrane was carried out using the Trans-Blot Turbo Transfer System (BioRad). The PVDF membrane was activated in methanol for 5 min then equilibrated with transfer stacks in 1 x transfer buffer (BioRad). Low-molecular weight proteins ($<$ 30kDa) were transferred for 5 min, mixed-molecular weight proteins (5-150) for 7 min, and high-molecular weight proteins for 10 min at 1.3 A for up to 25 V. After the transfer, the membrane was blocked with either 5% non-fat dry milk or 5% BSA in 1 x PBS-T buffer depending on the primary antibody used. Transfer of proteins was checked by PonceauS solution by incubating the membrane for 5 min at RT. The membrane was cleared by rinsing the membrane for 5 min in water and destained by washing

with PBS-T (0.05%) for 5 min. Then, the blocking solution was exchanged for the primary antibody solution which was prepared in the respective blocking buffer recommended for the antibody. The membrane was incubated with the primary antibody solution over night at 4 °C while shaking slightly. On the next day, the membrane was washed 3 times for 5 min with PBS-T before incubation with the secondary, horseradish peroxidase (HRP)-conjugated antibody in PBS-T for 1 h at RT. After another 3 washes for 5 min in PBS-T, bands were recorded using a non-commercial ECL solution [123] and the ChemiDoc XRS+ system (BioRad).

Luminex-based protein quantification

The Luminex xMAP technology allows to analyze total and phosphoproteins based on fluorescently labeled beads. Proteins were quantified using the BCA protein assay kit after lysing the cellular samples in Milliplex lysis buffer. After the lysis, the samples were incubated with the fluorescently labeled beads coated with specific primary antibodies. For detection of the primary antibodies certain secondary antibodies, Streptavidin PE conjugates and Biotin detection antibodies were used. Signal detection was done by exciting the fluorescent dye of the primary (635 nm) and Streptavidin PE coupled to the secondary (532 nm) antibodies. The signals were detected by a Bio-Plex 200 System. Quantification of signals was reported in mean fluorescent intensities (MFI). This was achieved by detecting the signal of each individual microsphere by digital-signal processors and quantifying the fluorescent reporter signals [124]. The protocol was performed according to the manufacturer's instructions. The Luminex analysis was carried out in two independent experiments. In this study, the MILLIPLEX MAP Phospho Mitogenesis RTK Magnetic Bead 7-Plex Kit (20 µg protein per well) or the MILLIPLEX MAP 11-Plex AKT/MTOR Panel-Phosphoprotein kit (20 µg protein per well) were used. Luminex analysis was done using a Bio-Plex 200 system (BioRad) and data were exported from the Bio-Plex Manager software 6.1.

Luminex-based cytokine quantification

For cytokine measurement, the supernatant of cells was taken and directly placed on ice. A total of 41 analytes was tested. A standard curve and quality control samples were included for the screening. 25 µl supernatant of each sample was used for analysis according to manufacturer's instructions (Millipore). After equilibrating the 96-well plate with 200 µl washing buffer, 25 µl standard or control, and 25 µl matrix solution was added. For the

samples of interest, 25 µl of samples and 25 µl assay buffer were added to each well. Next, 25 µl beads were added and incubated overnight at 4°C under constant agitation (350 rpm). On the next day, and after a 1x washing step, 25 µl PE-conjugated streptavidin was added, which can bind to biotinylated detection antibodies and bound to the protein of interest. Incubation was for 1h at room temperature. Here, the human cytokine/chemokine magnetic bead panel (HCYTMAG-60K-PX41) was used. Standard curves were performed using the 5-PL method. Luminex analysis was done using a Bio-Plex 200 system (BioRad) and data were exported from the Bio-Plex Manager software 6.1.

ELISA

Extracellular levels of human hepatocyte growth factor (Hu HGF) were quantitatively determined in cell culture supernatant of HCC827/MRC-5 co-culture cells or single cultures. Here, the ELISA kit measuring Hu HGF (Invitrogen) was applied. For this, 2×10^4 HCC827 cells were seeded in a well of a 24-well plate and 6×10^4 MRC-5 cells into a transwell insert of a 24-well plate and treated with gefitinib and co-cultured as described earlier. The cells were treated with gefitinib (0.5 µM) and co-cultured for 48 h. The supernatant of the cells was thereafter taken from each well, centrifuged at 300 x g and the remaining supernatant was transferred into a fresh 1.5 ml microcentrifuge and directly stored at -80 °C. The extracellular concentration of Hu HGF in the supernatant of the co-culture was measured at an absorbance wavelength at 450 nm (Tecan) according to the manufacturer's instructions using a diluted standard curve of Hu HGF with predefined concentrations.

2.2.4 Computational analysis

Statistical data analysis

Statistical analysis for the serum study was performed using R. The raw data were read in and normalized against the mean of two spike-ins (*cel-miR-39* and *cel-miR-54)*. The following formula was used in the serum study for calculating delta-delta (ΔΔ) Cp values:

$$\Delta\Delta Cp = -\left(Cp_i - mean\left(Cp\right)\right)$$

Recurrence-free and overall survival were used as clinical endpoint. Second tumors were censored. Univariable and multivariable Cox models were used to assess hazard-ratio and p-value for each miRNA or altogether. In the univariable case, only one miRNA entered the model at a time. In the multivariable case, all miRNAs were used as predictors. Maximization of the concordance index was used to test different miRNA combinations in a prognostic

model. Analysis was done using 5-time repeated 10-fold cross-validation to prevent over-fitting. The additional value of a miRNA marker panel to standard clinical parameters was tested in a likelihood-ratio test. The hazard ratio (HR) indicates the risk to relapse. For example, an HR with a fold change of 2 is calculated by the change of a miRNA by 1 Cp value.

Statistical analysis for the co-culture study was performed using GraphPad Prism 5.01 or Qlucore Omics software 3.0 (Two-group comparison). P-values if not derived from a two-tailed test (inequality) are described in each figure legend. P-values are depicted as asterisks where * $p < 0.05$, ** $p < 0.01$ and *** $p < 0.001$.

The Cp values from the quantitative real-time PCR in the miRNA screening of the co-culture study were calculated and normalized by overall median. Relative expression fold changes were calculated using the $2^{(-\Delta\Delta Cp)}$ method [125, 126]. To determine appropriate miRNA normalizing genes, the stability of expression was calculated by the overall average expression of all genes in all samples and compared with the individual gene using the NormFinder software [127]. Here, miRNAs from one plate (n = 384) were used to assess potential housekeeping genes.

Assessment of hemolysis

In order to evaluate the impact of hemolysis in this patient cohort, a miRNA-based hemolysis indicator measuring *miR-23a-3p*/*miR-451a* ratios was used [111, 112]. The ratio between *miR-451a*, which is known to be affected by hemolysis and *miR-23a-3p*, which is known to be unaffected by hemolysis, was calculated. Samples with a ΔCp value (*miR-23a-3p-miR-451a*) lower than seven were categorized as not hemolytic and samples that had a higher ΔCp value of seven as affected by hemolysis.

Pathway analysis using DAVID

To find canonical pathways enriched in genes differentially regulated between co-cultured treated and only treated cells, a pathway analysis was performed using the online software tool Database for Annotation, Visualization and Integrated Discovery (DAVID) [128]. Genes were determined for upregulation and downregulated in co-cultured treated in comparison to single treated NSCLC tumor cells through microarray expression profiling by Qlucore Omics software 3.0 analysis using p-value < 0.05 and linear fold change (FC) ≥ 1.5. The data was uploaded on to the DAVID server and a functional analysis was performed with default settings.

Ingenuity pathway analysis

To find miRNA/mRNA interactions within co-cultured treated and only treated cells, a microRNA Target Filter analysis was performed using the online software tool Ingenuity Pathway Analysis (IPA®, QIAGEN Redwood City, www.qiagen.com/ingenuity). The data from the microarray experiment was uploaded to the IPA server and correlated using the Ingenuity microRNA target filter with putative targets of *miR-503-5p* with default settings.

3 Results

3.1 Serum miRNAs of early-stage lung adenocarcinoma patients

Circulating miRNAs have been found to be promising biomarkers for prognosis and diagnosis in a plethora of cancer diseases [85]. In an initial work, serum miRNAs were screened in early-stage (I-IIIa) lung adenocarcinoma patients with early recurrence after surgery within 24 months (n = 20) against patients that did not develop a recurrence within 24 months (n = 20). Serum miRNAs including *miR-142-3p* and *miR-29b-3p* were validated in a cohort of 114 patients. Combinatorial analysis of *miR-142-3p* expression levels with tumor stage information improved stratification of patients with high and low-risk to develop a recurrence (AUC: 0.78) [120].

3.1.1 miRNA selection

In this study, the prognostic potential of eight selected miRNAs was evaluated (Table 17). The eight miRNAs were included here as they were reported as prognostic marker candidates in previous studies. Five of them were found to be promising candidates in the study by Kaduthanam *et al.* [120]. The miRNAs *miR-21-5p*, *miR-142-3p*, *miR-331-3p* and *miR-486-5p* were also included in miRNA signatures as prognostic or diagnostic markers [101, 102]. To search for the best miRNA panel that can significantly predict progression-free and overall survival in early-stage lung adenocarcinoma patients the prognostic potential of the selected miRNAs was evaluated.

Table 17: Promising prognostic or diagnostic circulating miRNAs in lung cancer

miRNA-ID	References
miR-20b-5p	[120, 129]
miR-21-5p	[102, 107, 130, 131]
miR-29b-3p	[120]
miR-30d-5p	[104]
miR-125b-5p	[105, 106]
miR-142-3p	[101, 102, 120]
miR-331-3p	[101, 120]
miR-486-5p	[101, 102, 104, 120, 132]

3.1.2 Pre-analytical consideration of blood-sampling collection

In a previous study, increased levels of circulating *miR-142-3p* were identified and validated in early relapsed lung adenocarcinoma patients in comparison to patients with no relapse

within 24 months [120]. To further validate these results in a new cohort of NSCLC patients, a total of 275 serum samples were collected. Of these, 65 samples (in the following defined as cohort 1) were collected after induction of anesthesia via an arterial catheter. Samples from cohort 1 were collected in the same manner as in the previous study [120]. The remaining 210 samples were collected before anesthesia via venipuncture, which is the routine sampling procedure in the clinics (internal discussion) and in the following defined as cohort 2. Samples from cohort 1 (n = 65) and the previous study (n = 154) were studied in a retrospective manner. Patient samples from cohort 2 (n = 210) were studied in a prospective manner by updating patient data each year. The follow-up time of the patients from cohort 1 was longer (about 10 months) in comparison to samples from cohort 2 (Table 18). Patients with stage Ib tumors in cohort 1 were not observed. Moreover, a significantly higher fraction of patients was observed to have stage IIa tumors in cohort 1 in comparison to cohort 2. All tumors in cohort 1 were initially classified according to UICC TNM 6th edition. In contrast to tumors from cohort 2, which were already classified according to TNM 7th edition. The main changes from the revision of TNM 6th ed. to TNM 7th ed. included the staging classification (T staging) [6]. Upon revision to TNM 7th ed. most tumors with T 2b N0 M0 were re-classified from stage Ib (TNM 6th ed.) to stage IIa (TNM 7th ed.).

After extracting RNA from the serum samples, the spike-in miRNAs (*cel-miR-39* and *cel-miR-54*) were measured among all serum samples (Figure 4). Since none of the measurements showed a drop-out, all samples were included in this study. *cel-miR-39* showed slightly lower variance (0.36) among the samples than *cel-miR-54* (0.47). The two miRNAs were highly correlating to each other (Pearson: 0.9) indicating that both external spike-in miRNA controls were suitable for normalization.

Table 18: Patient characteristics of lung adenocarcinoma patients

Patient characteristics	Cohort 1 n=65	Cohort 2 n=210	Test statistic (p-value)
Primary tumors UICC TNM 7th			
IA	9 (14%)	42 (20%)	0.2438
Ib	0 (0%)	43 (20%)	NA
IIa	33 (51%)	25 (12%)	*< 0.0001*
IIb	6 (9%)	35 (17%)	0.1425
IIIa	17 (26%)	65 (31%)	0.4614
Adjuvant therapy			
Chemotherapy	14 (22%)	74 (35%)	*0.0390*
Radiotherapy	9 (14%)	30 (14%)	0.9306
Median time DFS, m (n=81; n=27)	10.8	14.3	0.1709
Median time RFS, m (n=66; n=22)	7.3	13.4	0.1231
Metastatic site			
Local recurrence	4 (6%)	9 (4%)	0.5375
Distant metastasis	18 (28%)	57 (27%)	0.9318
Second tumor	5 (8%)	15 (7%)	0.8833
Unknown	0	1	NA
Disease-free (no second tumor)	38 (58%)	128 (61%)	0.6898
Deaths	18 (28%)	50 (24%)	0.5276
Time to death, m (n=50; n=18)	18	19	0.9059
Follow-Up, m	46.9	36.3	*< 0.0001*
Epidemiology			
Age, y	63	65	0.8632
Sex			
M	37 (57%)	122 (58%)	0.8683
F	28 (43%)	88 (42%)	0.9689
Smoking, pack year	30	35	0.6350

Numbers are presented as median; abbreviations: m, months; y, years; DFS (Disease-free survival, including second tumor); RFS (recurrence-free survival, without second tumor); Test statistic (p-value): Mann-Whitney
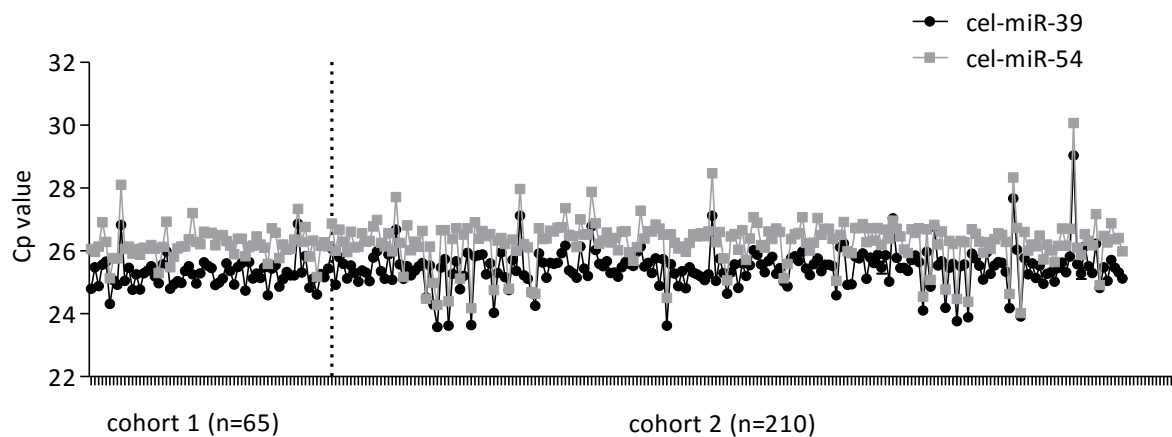
Figure 4 *cel-miR-39* and *cel-miR-54* expression among cohort 1 (n = 65) and cohort 2 (n = 210).

3.1.2.1 Increased miRNA levels detected in serum samples from venipuncture in comparison to serum samples from arterial catheter

First, the miRNA levels between the two cohorts were compared. Each of the selected miRNA was compared between the cohort 1 and the cohort 2 to identify if the different blood drawings have an impact on the miRNA expression level. All eight miRNAs measured from cohort 1 samples drawn from arterial catheter were significantly downregulated ($p < 0.001$) with a median fold change (FC) of 0.6 in comparison to cohort 2 (Figure 5).
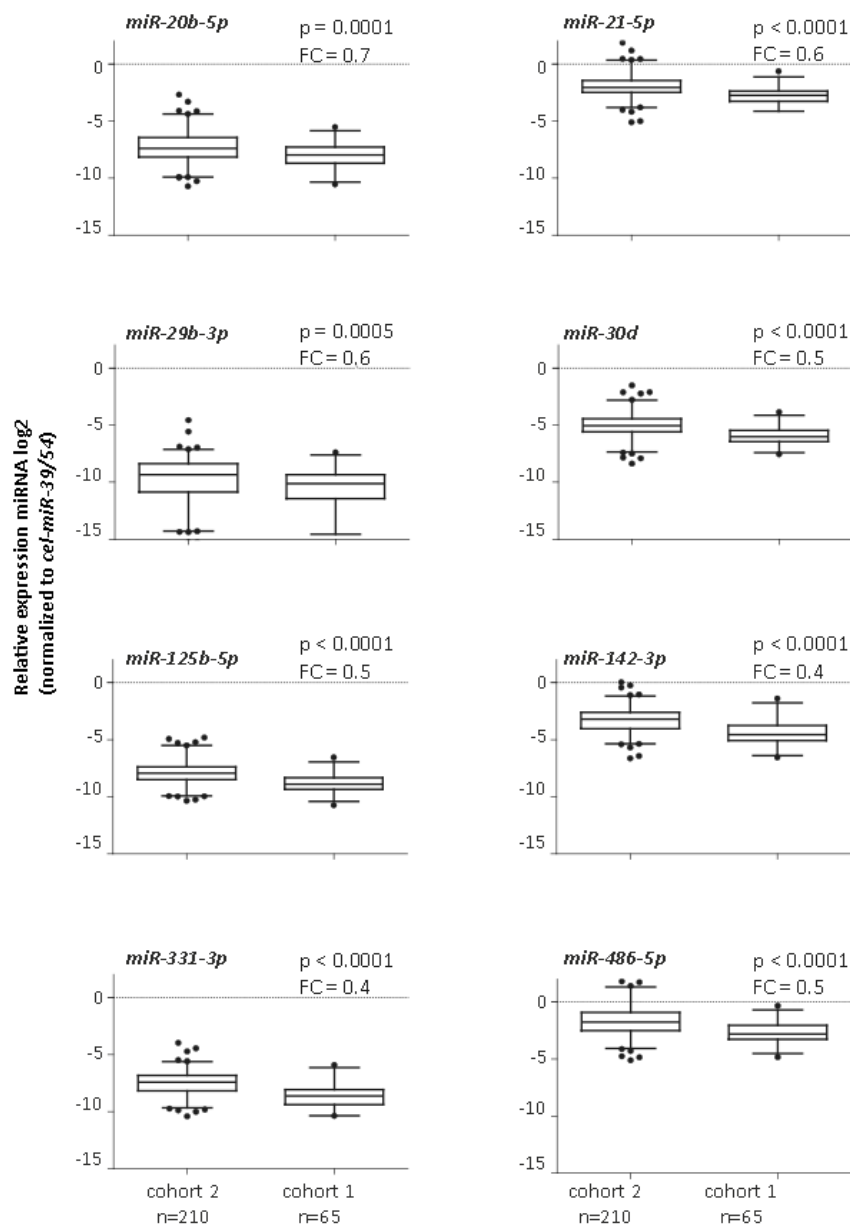
Figure 5 miRNA expression between cohort 1 vs cohort 2. n = 275 serum samples were collected from early-stage lung adenocarcinoma patients. A fraction of patients n = 210 (cohort 2) was collected via venipuncture without anesthesia and n = 65 (cohort 1) were collected via an arterial catheter after induction of anesthesia. The miRNA values were normalized using the mean of *cel-miR39/54*. Box and Whiskers: 2.5-97.5% percentile. p-values were tested using Mann-Whitney test.

In order to test whether the differences between cohort 1 and cohort 2 can be traced back to the blood drawings, three different blood samples from each patient (n = 13) were collected. The three blood samples were sequentially drawn

      a) via venipuncture one to two days before surgery,

      b) via venipuncture on the same day but prior to surgery with a sedative and

      c) via arterial catheter including induction with anesthetics prior to surgery.

For each sample, ten miRNAs were tested. Here, miRNAs in serum drawn via venipuncture (a) (FC = 1.3) or venipuncture with sedative (b) (FC = 1.4) showed a tendency to be increased in comparison to blood drawn from arterial catheter (c) (Figure 6). In particular, *miR-20b-5p* (p = 0.011) and *miR-29b-3p* (p = 0.025) showed significant differences between the sampling methods a/b in comparison to c (Table 19). The sampling methods (a) and (b) were comparable (FC = 0.98). Only *miR-125b-5p* did not show the same tendency, which might be due to its low expression. Whether the reduction of miRNAs in serum drawn via arterial catheter is derived from the anesthetics or from the blood drawing from the artery could not be determined. In conclusion, pre-analytical consideration must take place at the stage when blood is drawn from the patients as this has an impact on serum miRNA expression levels.
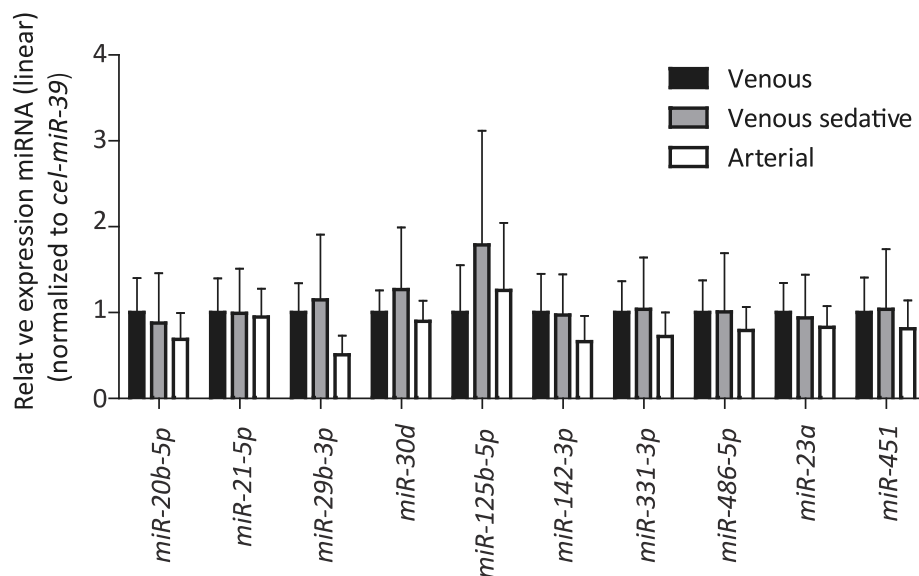
Figure 6 miRNA expression from sequentially drawn blood samples. Three serum samples were drawn from each of the 13 patients via (a) venipuncture (n = 13), 2) via (b) venipuncture with sedative (n = 13), and via (c) an arterial catheter (n = 13). The miRNA values were normalized using *cel-miR39*. p-values were determined using Wilcoxon matched pairs test.

Table 19 miRNA expression from different blood drawings in comparison to miRNAs derived from serum via venipuncture

miRNA-ID	Venous (FC)	Venous sedative (FC)	Arterial (FC)
miR-20b-5p	1.00	0.88	0.69*
miR-21-5p	1.00	0.99	0.95
miR-29b-3p	1.00	1.15	0.51*
miR-30d-5p	1.00	1.27	0.90
miR-125b-5p	1.00	1.79	1.26
miR-142-3p	1.00	0.97	0.66
miR-331-3p	1.00	1.04	0.72
miR-486-5p	1.00	1.01	0.79
miR-23a-3p	1.00	0.94	0.83
miR-451a	1.00	1.04	0.81

*pVal < 0.05; FC: fold change

3.1.3 *miR-142-3p* levels associated with early relapse in cohort 1

After having shown that miRNA expression levels differ in serum samples when derived from venous or arterial blood, miRNA expression levels derived via venipuncture or via arterial catheter were separately analyzed. For example, the *miR-142-3p* expression level was analyzed using a binary endpoint such as relapse within 24 months (n = 11) in comparison to no relapse within 24 months (n = 19) within cohort 1 (serum samples via arterial catheter (data not shown) The remaining 35 samples either did not meet the inclusion criteria, or were excluded due to a miRNA-hemolysis indicator above seven Cp. *miR-142-3p* was found to be elevated (FC = 1.74) in the early relapse group, which is in line with the previously published study [120]. However, the difference was not significant (p = 0.62), which may be due to the fact that the numbers of patient samples were low.

3.2 Identification of circulating miRNAs as prognostic markers in NSCLC patients

3.2.1 Clinical characteristics of cohort 2

This study focused on serum samples collected via venipuncture from 210 early-stage lung adenocarcinoma patients (cohort 2) (Table 18). Within this cohort, there was a slightly higher fraction of patients (31%) with stage IIIa tumors. Patients with stage Ia (20%) and Ib (20%) tumors were more common than those with stages IIa (12%) and IIb (17%). Patients received adjuvant chemotherapy (35%) more often than adjuvant radiotherapy (14%). Within a follow-up time of 36.3 ± 10 months, most of the disease events (n = 81) were located at distant sites (27%) and nine out of 88 occurred locally. Fifteen out of 81 patients developed a second

tumor. To analyze recurrence-free survival (RFS) the second tumor relapse events were censored. Fifty patients died within 19 ± 9 months.

3.2.2 Distribution and correlation of miRNA expression data sets

The normalized expression values (ΔCp values) of each selected miRNA were assessed by analyzing the distribution of each miRNA expression dataset. *miR-21-5p*, *miR-142-3p*, and *miR-486-5p* were found to have high miRNA levels (0 to -5 ΔCp) (Figure 7). The miRNA levels of *miR-30d-5p*, *miR-125b-5p*, *miR-331-3p*, and *miR-20b-5p* were in a medium range (-5 to -10 ΔCp) and *miR-29b-3p* (-5 to -15 ΔCp) was observed to have a biphasic curve with miRNA levels at medium ranges (-5 to -10 ΔCp) and relatively low levels (-10 to -15 ΔCp). Monophasic curves were seen for seven out of eight miRNAs. *miR-29b-3p* was observed to have the highest number of patient samples with absent calls.

Interestingly, patients with stage IIIa had significantly lower *miR-29b-3p* expression levels in comparison to stage I (p = 0.002) or II (p = 0.053), respectively (Figure 8).

All miRNAs were positively correlated with one another, albeit different strengths (Figure 9). *miR-142-3p* and *miR-331-3p* showed a high correlation (0.96) to each other. Moreover, *miR-20b-5p* and *miR-486-5p* showed high correlation to each other (0.92) as well as *miR-30d-5p* to *miR-20b-5p* (0.87), *miR-486-5p* (0.89) and to *miR-21-5p* (0.91).

These data suggested that the miRNA expression data sets of *miR-486-5p*, *miR-20b-5p*, and *miR-30d-5p* were related with each other, however, most miRNA expression data sets were distinct from each other. *miR-29b-3p* showed the lowest correlation with all other miRNAs, which might be explained due to its biphasic nature.
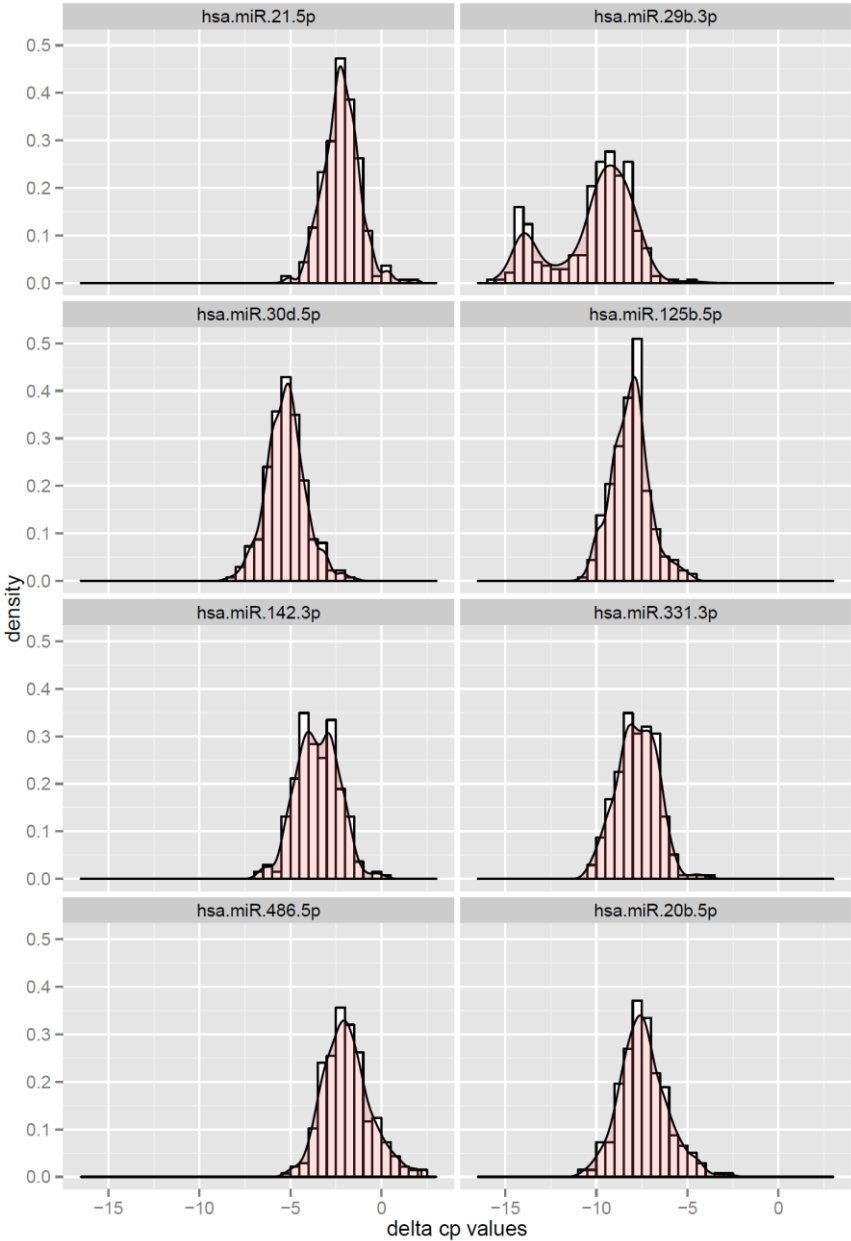
Figure 7 Kernel density plot of miRNAs. Kernel density estimate from different miRNA expression levels (ΔCp).
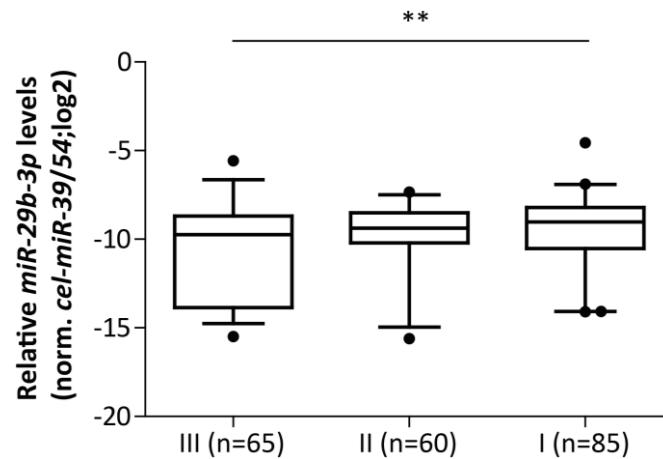
Figure 8 *miR-29b-3p* expression in serum samples of lung adenocarcinoma at different stages. The *miR-29b-3p* expression levels were determined in cohort 2 at stage III (n = 65), stage II (n = 60), and stage I (n = 85). The miRNA values were normalized using the mean of *cel-miR39/54*. Box and Whiskers: 2.5-97.5% percentile. p-values were tested using Mann-Whitney test.
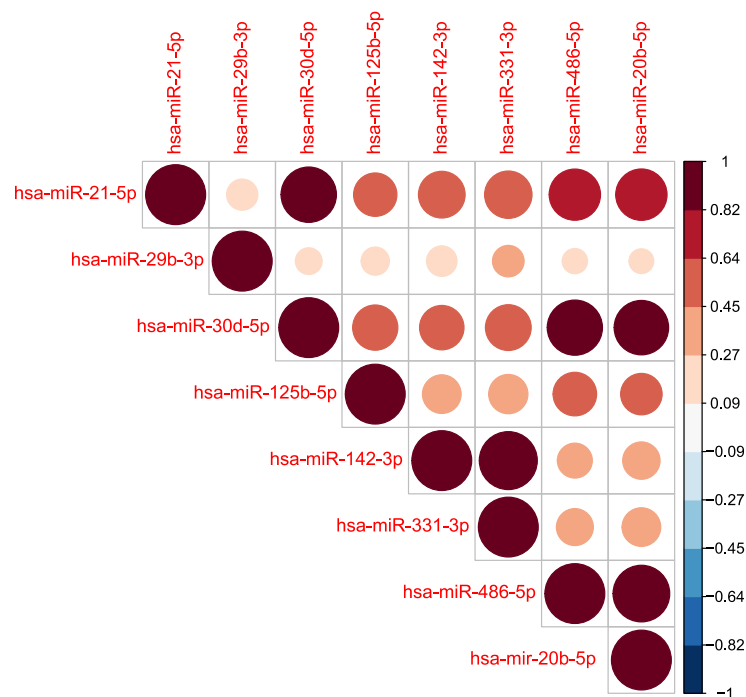
Figure 9 miRNA correlation plot. The miRNAs selected for analysis in serum samples of cohort 1 (n = 210) were analyzed in a pairwise correlation matrix plot.

3.2.3 *miR-20b-5p* and *miR-486-5p* identified to be affected by hemolysis

Hemolysis during blood collection has an impact on the content of miRNAs in serum or plasma [111]. In order to evaluate the impact of hemolysis in this patient cohort, a miRNA-based hemolysis indicator measuring *miR-23a/miR-451a* ratio was used. If the ΔCp is higher than seven the risk of hemolysis is high (n = 129). On the other hand, if the ΔCp is lower than

seven the indication is no hemolysis (n = 81) (Figure 10). These results were corroborated by visually rating red colored serum samples (indicating hemolysis, data not shown). All samples that showed ΔCp higher than seven value derived from the *miR-23a-3p*/*miR-451a* ratio were visually rated as red. Each of the eight analyzed miRNAs was tested to be affected by hemolysis. Therefore, samples that were indicated as hemolytic (n = 47) (excluding samples that have a ΔCp above eight, Figure 10) were compared to those samples that were not indicated as hemolytic samples (n = 129) (Table 20). Hereby, a high correlation of *miR-486-5p* and *miR-20b-5p* with the hemolytic samples was identified, which had fold changes above 1.5 and therefore regarded as potentially hemolytic. Although *miR-30d-5p* also showed a significant p-value it had a low fold change (FC = 1.32). Hence, this miRNA was regarded as potentially not hemolytic due to its low fold change. Since *miR-20b-5p* and *miR-486-5p* were affected by hemolysis, the following analyses in this study were performed without these two miRNAs.

To exclude recurrence-free survival (RFS) or overall survival (OS) to be biased by hemolysis, survival-rates were analyzed using Kaplan-Meier plots (Figure 11): No significant difference could be observed for RFS (p = 0.72) or OS (p = 0.93). In conclusion, hemolysis in this cohort did not play a role in these two outcomes.
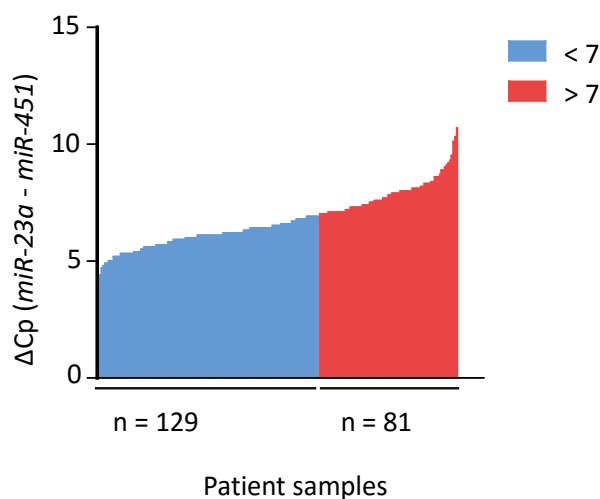
Table 20: Differential miRNA expression between hemolytic (n = 47) vs non-hemolytic samples (n = 129)

miRNA-ID	FC	p-value
miR-20b-5p	1.92	<1.00E-04
miR-21-5p	1.13	2.85E-01
miR-23a-3p	0.86	3.76E-01
miR-29b-3p	1.30	3.66E-01
miR-30d-5p	1.32	1.40E-02
miR-125b-5p	1.19	9.69E-02
miR-142-3p	0.86	1.01E-01
miR-331-3p	0.93	3.25E-01
miR-451a	2.33	<1.00E-04
miR-486-5p	1.91	<1.00E-04

Figure 10 Hemolysis in serum samples. Hemolysis in serum samples was indicated if the expression level was above seven (red). Samples with a ΔCp value below seven (blue) were considered as potentially not hemolytic. The miRNA values were normalized using the mean of *cel-miR-39/54*.
In Table 20 the fold changes and p-values of the eight selected miRNAs were analyzed within cohort 2 (excluding samples that have a ΔCp > eight). p-values were calculated by Mann-Whitney test.
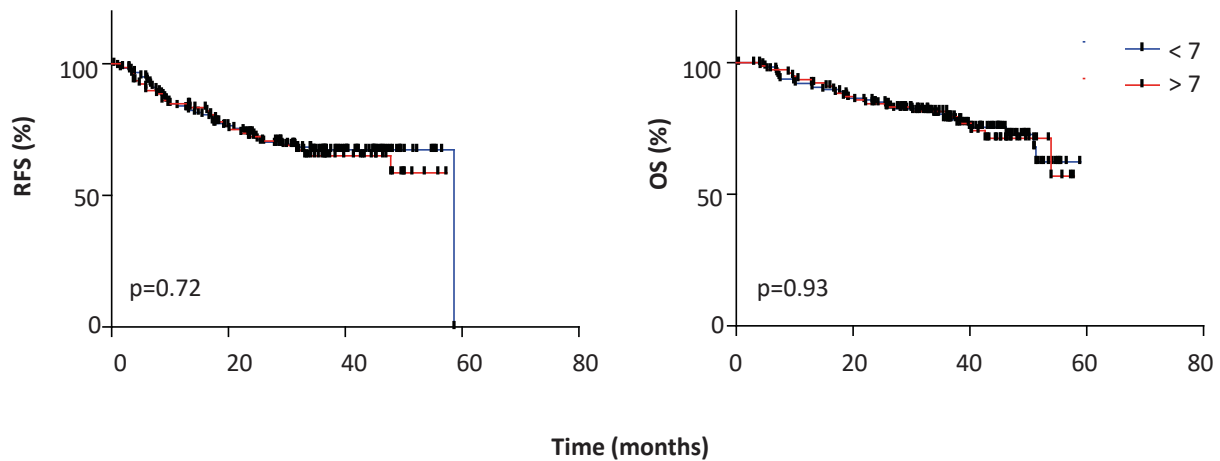
Figure 11 Influence of hemolysis on RFS and OS. Patient samples indicated as potentially hemolytic (n = 81; red line) were compared to those, which were not (n = 129; blue line). Clinical endpoints such as recurrence-free survival (RFS) (left side) and overall-survival OS (right side) were plotted. p-values were tested using log-rank test.

3.2.4 Analysis of prognostic potential of circulating miRNAs

As each of the eight selected miRNAs were shown to have prognostic potential, a combined analysis using a miRNA panel was evaluated in serum of patients with early-stage lung adenocarcinoma. Table 21 shows the results of univariable Cox models (only one miRNA in the model: Single) as well as the hazard-ratios and p-values from one multivariable model (all miRNAs entered the model: Combined). The hazard ratio (HR) indicates the risk to relapse. Using univariable analysis, no miRNA was associated with overall survival. Using the multivariable approach, only *miR-29b-3p* showed a p = 0.05 and therefore could be associated with overall survival.

Table 21: Univariable and multivariable Cox-models for the assessment of miRNAs with overall survival

| miRNA-ID | Single | | | | Combined | | | |
	HR	95% lower	95% upper	P	HR	95% lower	95% upper	P
miR-21-5p	1.04	0.79	1.39	0.77	1.68	0.82	3.43	0.16
miR-29b-3p	0.89	0.79	1.01	0.06	0.88	0.78	1.00	0.05
miR-30d-5p	1.03	0.79	1.33	0.84	0.95	0.44	2.08	0.90
miR-125b-5p	1.05	0.79	1.39	0.75	1.11	0.74	1.65	0.61
miR-142-3p	0.85	0.65	1.11	0.22	1.16	0.49	2.73	0.74
miR-331-3p	0.82	0.62	1.08	0.16	0.56	0.22	1.41	0.22
miR-486-5p	1.06	0.86	1.31	0.59	1.17	0.60	2.27	0.64
miR-20b-5p	1.01	0.82	1.25	0.93	0.78	0.45	1.36	0.38

HR: hazard ratio; Single: Univariable analysis; Combined: Multivariable analysis; 95% upper/lower: 95% upper/lower confidence interval; P: p-value

Multivariable analysis with all miRNAs as in Table 21 shows the potential of miRNAs that could predict overall survival. The best miRNA candidates in a panel calculated by the concordance index (C-index) were *miR-331-3p*, *miR125b-5p*, and *miR-29b-3p* (Table 22). However, the selected panel could not significantly discriminate patients with high and low risk overall survival.

Table 22: Assessing miRNAs with overall survival and improvement in combination with staging

	Panel				Likelihood-ratio test
	HR	95% lower	95% upper	P	P (Stage I/II vs IIIa)
miR-29b-3p	0.89	0.79	1.01	0.07	
miR-125b-5p	1.28	0.92	1.77	0.14	0.06
miR-331-3p	0.77	0.56	1.05	0.10	

HR: hazard ratio; Panel: miRNA panel calculated by C-index; 95% upper/lower: 95% upper/lower confidence interval; P: p-value

Staging is one of the strongest prognostic factors for survival. Therefore, the additional value of the marker panel to staging was determined. A likelihood-ratio test was used to test if the miRNA panel could contribute to an additional value. Stage I and II were grouped together and compared against stage IIIa. The additional value of the miRNA panel against staging "Stage I/II vs IIIa" revealed a p = 0.06 (Table 22). This suggested that the miRNA-panel (*miR-331-3p*, *miR125b-5p*, *miR-29b-3p*) together with staging information indicated a trend to predict survival, but could not significantly differentiate patients from high-risk and low-risk groups.

Finally, a miRNA panel was assessed as a suitable marker panel for recurrence-free survival (RFS). However, again no stable panel of miRNAs could be identified to predict RFS within the patient cohort 2, which indicated weak associations of the measured miRNAs with RFS (data not shown).

In summary, the potential of circulating miRNAs to stratify patients into high and low-risk patients according to the recurrence of the tumor or the overall survival was analyzed. To identify relevant miRNAs associated with prognosis in early stages of patients with lung adenocarcinoma, circulating miRNAs were screened within a cohort of n = 40 patients. *miR-142-3p* was validated in an independent cohort (n = 114) to be associated with prognosis [120]. Based on this study, further serum samples were collected (n = 275). The samples were divided in two cohorts due to different blood collection techniques. Eight circulating miRNAs were selected and studied in both cohorts. Circulating miRNAs isolated from venipuncture were higher abundant than those isolated from arterial blood. Sequential blood samples taken

from venous and arterial blood (n = 13) supported this finding. Therefore, the eight selected miRNAs were analyzed only from one cohort (n = 210). In this study, two commonly reported miRNA biomarker candidates (*miR-20b-5p, miR-486-5p*) were observed to be affected by hemolysis. Univariable and multivariable Cox models were generated based on the miRNA expression values and tested with overall and relapse-free survival. A panel of miRNAs (*miR-29b-3p, miR-125b-5p,* and *miR-331-3p*) was analyzed, which, however, could neither be associated with overall survival nor the relapse-free survival. A benefit of the miRNA panel beyond staging could not be determined.

3.3 EGFR-TKI resistance in NSCLC cells using a co-culture model

3.3.1 Gefitinib treatment results in reduced cell viability of HCC827 and PC-9 NSCLC cells in a dose-dependent manner

Since miRNAs are involved in the progression of NSCLC tumors and in therapy resistance to EGFR-TKI [117], the transcriptional regulation by small non-coding RNAs and mRNAs in EGFR-TKI resistant NSCLC was analyzed.

To investigate miRNAs contributing to an aggressive phenotype, a co-culture model using gefitinib sensitive lung adenocarcinoma cells with lung fibroblasts was used to generate resistance. NSCLC cell lines harboring the activating inframe deletion (del E746-A750) of *EGFR* have been reported to respond to inhibitors such as gefitinib or erlotinib [133]. To test this finding, HCC827 and PC-9 cells harboring this deletion and the lung cancer cell line A549 that did not harbor this deletion were tested for their response to gefitinib and erlotinib. The cell viability was reduced in a dose-dependent manner in gefitinib-hypersensitive HCC827 (IC50: 0.0008 µM) and sensitive PC-9 (IC50: 0.1250 µM) after 72 h. Treatment with erlotinib resulted in a slightly reduced IC50 values in comparison to gefitinib for HCC827 (IC50: 0.0989 µM) and PC-9 cells (0.4626 µM) after 72 h. After treatment, there were still 40% viable cells even at high concentrations (10 µM). This may be due to the pre-existence of *MET* amplification, i.e. before gefitinib treatment [134]. As expected, treatment of A549 cells with gefitinib did not result in a reduction of cell viability even at a concentration of 10 µM (Figure 12).
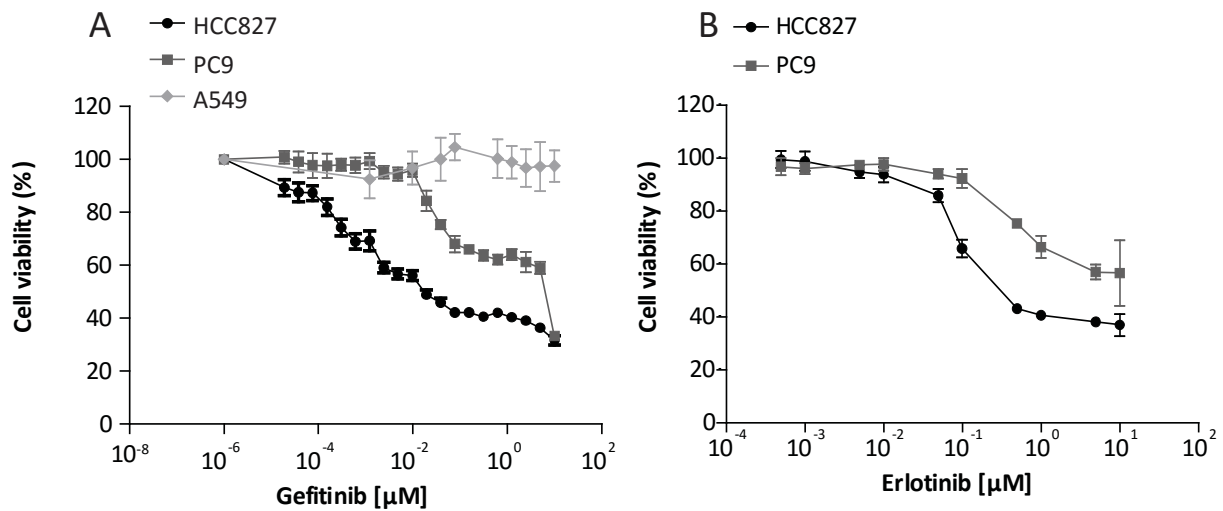
Figure 12 Cell viability of HCC827 and PC-9 cells after dose-dependent titration of EGFR-TKIs. HCC827 and PC-9 cells were treated with **A)** gefitinib or **B)** erlotinib and incubated for 72 h until measurement. A549 cells were included as a resistant cell line against gefitinib. Values were calculated as mean. The standard deviation was calculated from six replicates for each concentration.

3.3.2 Co-culture with lung fibroblasts induces resistance of NSCLC cell lines towards gefitinib

To drive cells into resistance towards EGFR-TKI, a co-culture model was used according to Wang *et al*. [46]. A cell viability assay was employed in order to determine the optimal medium for the tumor cell line HCC827 and the fibroblast cell lines MRC-5 and CCD-19LU (CCL-210), respectively. EMEM medium showed slightly increased cell viability in comparison to culturing cells with RPMI 1640. Therefore, if cells were cultured together, EMEM was used (Figure 13).
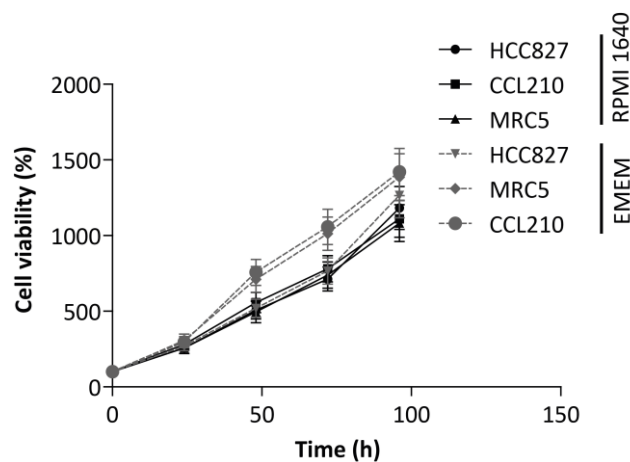
Figure 13 Cell viability of HCC827 tumor cells and fibroblast cells in different culture media. HCC827, MRC-5, and CCL-210 were cultured for 96 h in RPMI1640 or EMEM culture medium.

HCC827 cells were cultivated in bottom chambers of a transwell insert (1 µm) and treated with increasing concentrations of gefitinib (0.05 µM – 0.5 µM). The inhibitor was washed after 1 h of treatment and then combined with the lung fibroblasts CCD-19LU (CCL-210) (Figure 14 A) or MRC-5 (Figure 14 B) and co-cultured for 72 h. Reduced cell viability of the lung tumor cell line HCC827 after gefitinib treatment was observed (0.05 µM to 0.5 µM) ranging from approximately 57% residual viability (0.5 µM) to 49% (0.05 µM) (Figure 14 B). After co-culturing with MRC-5 or CCD-19LU, the treated HCC827 cells became less sensitive towards gefitinib within 72 h. The most effective restoration of cell viability was achieved at 0.5 µM gefitinib treatment and co-culture with 6 x 10^4 fibroblasts. Therefore, in the following experiments, a TKI concentration of 0.5 µM was used. A similar finding was observed for PC-9 cells after co-culturing with MRC-5 cells within 72 h (Figure 15 B). Furthermore, co-culture conditions with lower than 10% FCS resulted in lower resistance of HCC827 cells after gefitinib treatment (data not shown). Therefore, co-culture conditions with 10% FCS were chosen.
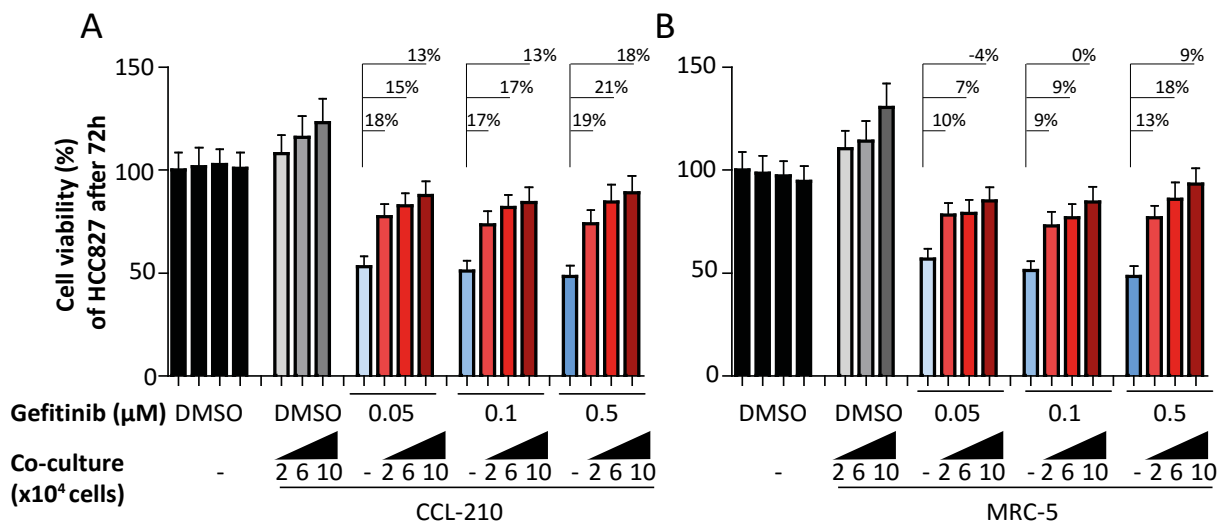
Figure 14 Determination of the co-culture condition. Cell viability of HCC827 cells after co-culture with fibroblast cells **A)** CCL-210 or **B)** MRC-5 cells was tested. Each co-culture after gefitinib treatment (red bars) was tested for the increase of cell viability after comparing to co-culture alone (gray bars) and gefitinib treatment alone (blue bars). Measurements were taken after 72 h. Samples were normalized to a DMSO control (black bars). Standard deviations were calculated from three replicates.
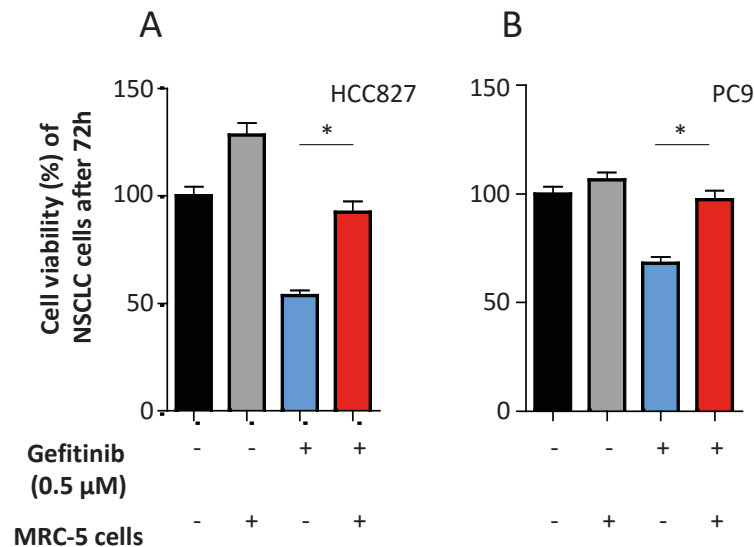
Figure 15 Co-culturing HCC827 or PC-9 NSCLC cells with MRC-5 fibroblasts results in reduced sensitivity towards gefitinib. A) HCC827 or **B)** PC-9 cells were cultured with or without gefitinib (0.5 µM) in the presence or absence of MRC-5 cells for 72 h. Standard deviations were calculated from two independent experiments.

3.3.3 Cell cycle analysis of co-cultured NSCLC cells

To characterize the cell cycle of co-cultured cells, the cells were stained with propidium iodide. The population of dying cells was 1.8 x and 2.7 x increased in treated HCC827 and PC-9 cells, respectively, in comparison to co-cultured cells, as indicated by the sub-G1 phase fraction. Co-cultured gefitinib treated HCC827 (1.8 x fold change) (Figure 16 A) and PC-9 (2.7 x fold change) (Figure 16 B) cells showed a trend for increased DNA synthesis (S)-phase after 48 h compared to only gefitinib treated cells.
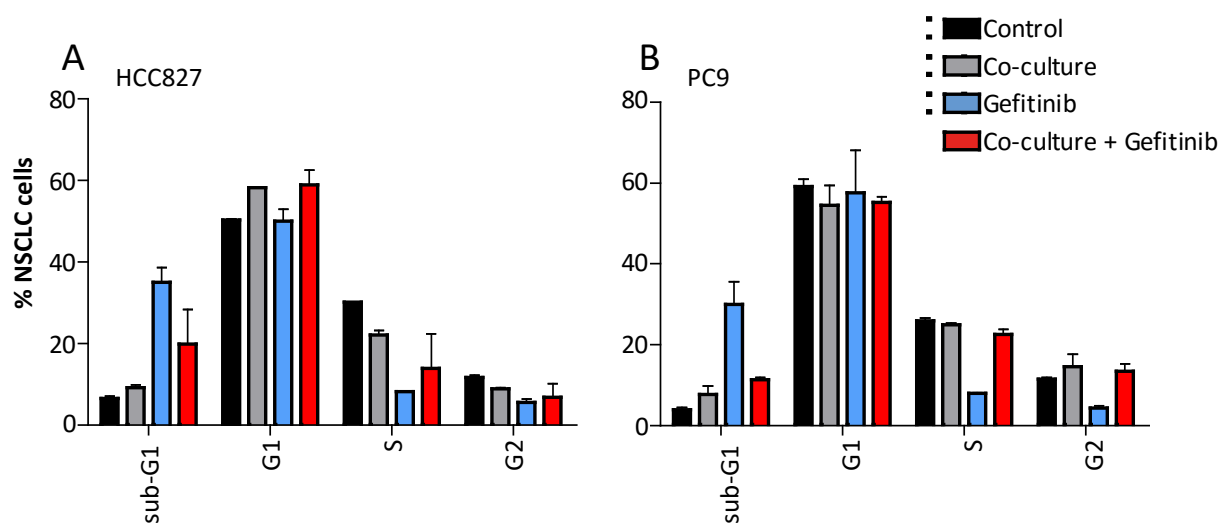
Figure 16 Cell cycle analysis of co-cultured HCC827 or PC-9 cells with fibroblast cells MRC-5. Propidium iodide staining was employed to determine cell cycle changes of **A)** HCC827 or **B)** PC-9 cells after co-culture. Standard deviations were calculated from at least two replicates.

3.3.4 EGFR and MET activity in resistant HCC827 cells

To demonstrate the reduction of EGFR activity after gefitinib treatment, the phosphorylation status of the EGFR family after drug exposure with gefitinib in HCC827 cells was analyzed. Since the NSCLC cell line HCC827 harbors an activating mutation (del E746-A750), it triggers downstream pathways of EGFR. At first, the total protein expression of different receptors (EGFR, MET, ERBB2, ERBB3) in untreated HCC827, MRC-5, and CCD-19LU (CCL-210) cells was determined (Figure 17 A). The lung tumor cells had a strong EGFR and MET expression, whereas both receptor proteins were expressed markedly lower in the lung fibroblast cells MRC-5 and CCD-19LU. The other receptor proteins ERBB2 and ERBB3 were not or poorly expressed in the tumor and fibroblast cells.

In order to determine the activation of EGFR in the co-culture model, a multiplex bead-based phosphorylation assay (Luminex) using a pan-specific antibody against the phospho-tyrosine residues of EGFR, MET, ERBB2, ERBB3, ERBB4, IGF and IR after gefitinib treatment and co-culture was applied (IGF and IR could not be measured in neither the co-culture nor the HGF culture).

As expected, the phosphorylation levels of EGFR showed high MFI (Mean fluorescent intensity) signals in DMSO treated cells (Control) (15,353 MFI). Almost no difference was observed and the MFI levels remained at high levels after co-culture alone (14,463 MFI). However, the signal was reduced 29-fold after 24 h in gefitinib treated (0.5 µM) HCC827 cells (529 MFI) (Figure 17 C). Yet, after co-culture with MRC-5 cells, the phosphorylation of EGFR was slightly increased by 1.9-fold (982 MFI).

MET was found to show high MFI signals in DMSO treated cells (Control) (13,855 MFI) and remained at high MFI levels after co-culture (8,805 MFI). MET phosphorylation was observed to be downregulated after gefitinib treatment (107 MFI), but increased 14-fold after subsequent co-culture (982 MFI). Phosphorylation signals of ERBB2 and ERBB3 were markedly reduced after gefitinib treatment. However, the signal was not rescued anymore after co-culture. ERBB4 phosphorylation was not detected. The results were corroborated using hepatocyte growth factor (HGF) induction (Figure 17 D), which is a prominent inducer of EGFR-TKI resistance [45]. EGFR phosphorylation signal was reduced after gefitinib treatment (1,497 MFI) and did not show any differences after resistance induction (1,499 MFI) as in the co-culture. As expected the phosphorylation signal of MET was increased (1.3-fold) after HGF induction, however, it was not as effective as after co-culture (14-fold). Maybe different signals secreted by the fibroblast cells have a greater effect on the phosphorylation signal of MET than HGF induction alone.

As a negative control for the phosphorylation status (MFI signal), lysates from unstimulated HeLa cells were used and lysates from Hek293 cells stimulated with fetal calf serum (FCS) were used as positive control and measured (Figure 17 B). Stimulation with FCS in Hek293 cells clearly induced signals in all analyzed proteins ranging from 10,000 to 25,000 MFI. Unstimulated HeLa cells showed signals ranging from 70 MFI to 408 MFI. To compare the phosphorylation signals of each protein between samples, equal amounts of protein input were used.

In conclusion, these data shoed that gefitinib treatment reduced the phosphorylation of EGFR and MET. Co-culture with MRC-5 cells after gefitinib treatment rescued the phosphorylation of MET, which is known to induce resistance after gefitinib treatment [46].
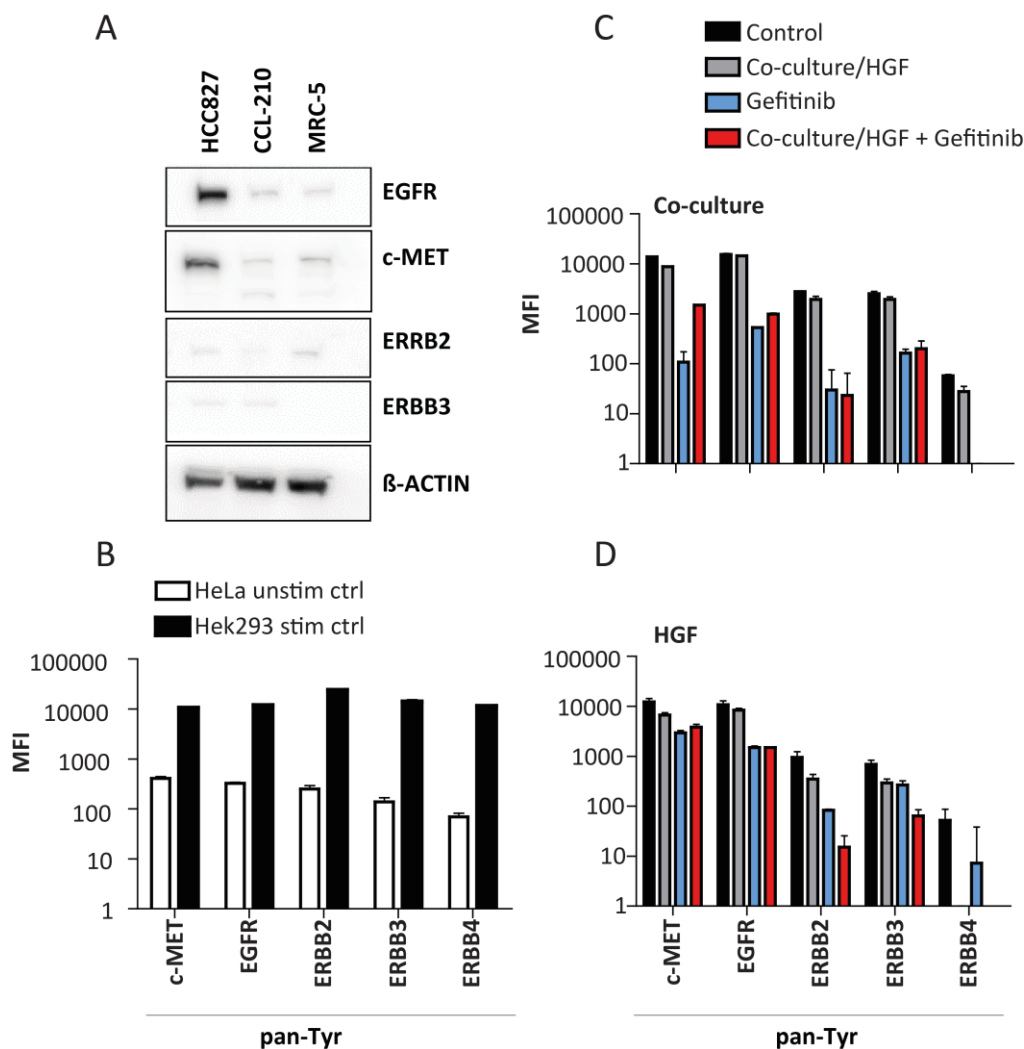
Figure 17 Total and active EGFR family and MET status. A) Total protein status of single cultivated HCC827 tumor cells, fibroblasts cell lines CCD-19LU (CCL-210) and MRC-5 is shown. Protein lysates were isolated after 24 h co-culture, quantified by BCA and equal amounts (20 µg) were analyzed. Molecular weight: EGFR:170 kDa; MET precursor: 170 kDa; ERBB2: 185 kDa; ERRB3: 185 kDa, ß-ACTIN: 42 kDa. **B-D)** Luminex analysis of EGFR family and MET. **B)** Phosphorylation of proteins from stimulated Hek293 (positive control) and unstimulated HeLa lysates (negative control). Phosphorylation signals of proteins from **C)** co-cultured or **D)** HGF induced HCC827. MFI: Mean fluorescent intensity. Multiplex-Luminex analysis was used

to assess phosphorylation signals of MET, EGFR, ERBB2, ERBB3, and ERBB4 by a pan-tyrosine antibody. Standard deviations were calculated from two experiments with three technical replicates.

3.3.5 MTOR/AKT signaling pathway in resistant HCC827 cells

HGF activates the PI3K/AKT signaling pathway and MTOR is a downstream target of both EGFR and MET. Therefore, the MTOR/AKT signaling pathway was analyzed in the co-culture [134]. The phosphorylation signals of AKT, GSK3A, GSK3B, IGF1R, IR, IRS1, MTOR, p70S6K, PTEN, RPS6, and TSC2 were measured using the multiplex bead-based immunoassay system (Luminex).

Consistent with the previously shown data (Figure 17 B), in which the phosphorylation signal of MET was increased in resistant cells after gefitinib treatment, the phospho-signals of most proteins were downregulated after reduction of EGFR activity using gefitinib (Figure 18 B). Co-culture or HGF (Figure 18 C) induction alone did not dramatically change MFI signals in comparison to the DMSO control. Activation of AKT (4.8-fold), GSK3A (5.3-fold), IRS1 (4.4-fold), MTOR (1.1-fold), RPS6KB1 (p70S6K) (12.5-fold), RPS6 (7.9-fold), and TSC2 (2.2-fold) were observed in resistant HCC827 cells after gefitinib treatment. Data from Figure 18 C (HGF induction of HCC827 cells) corroborate these results. Phosphorylation of GSK3B after gefitinib treatment did not result in a clear reduction because it was not observed to be reduced after gefitinib treatment in Figure 18 B.

The internal control (GAPDH) was not observed to change MFI signals between the different samples. In this assay, three controls were used to assess the phosphorylation signal of the different proteins (Figure 18 A). As a negative control, cell lysates from phosphatase treated HeLa cells were used. As a positive control, cell lysates from insulin stimulated HepG2 cells and IGF-1 stimulated MCF-7 cells were used. The negative control showed signals near background level. Equal amounts of protein were used to analyze between different samples.

These data indicated that activation of MET through the co-culture or HGF may lead to the activation of the MTOR/AKT signaling pathway resulting in reduced sensitivity towards gefitinib.
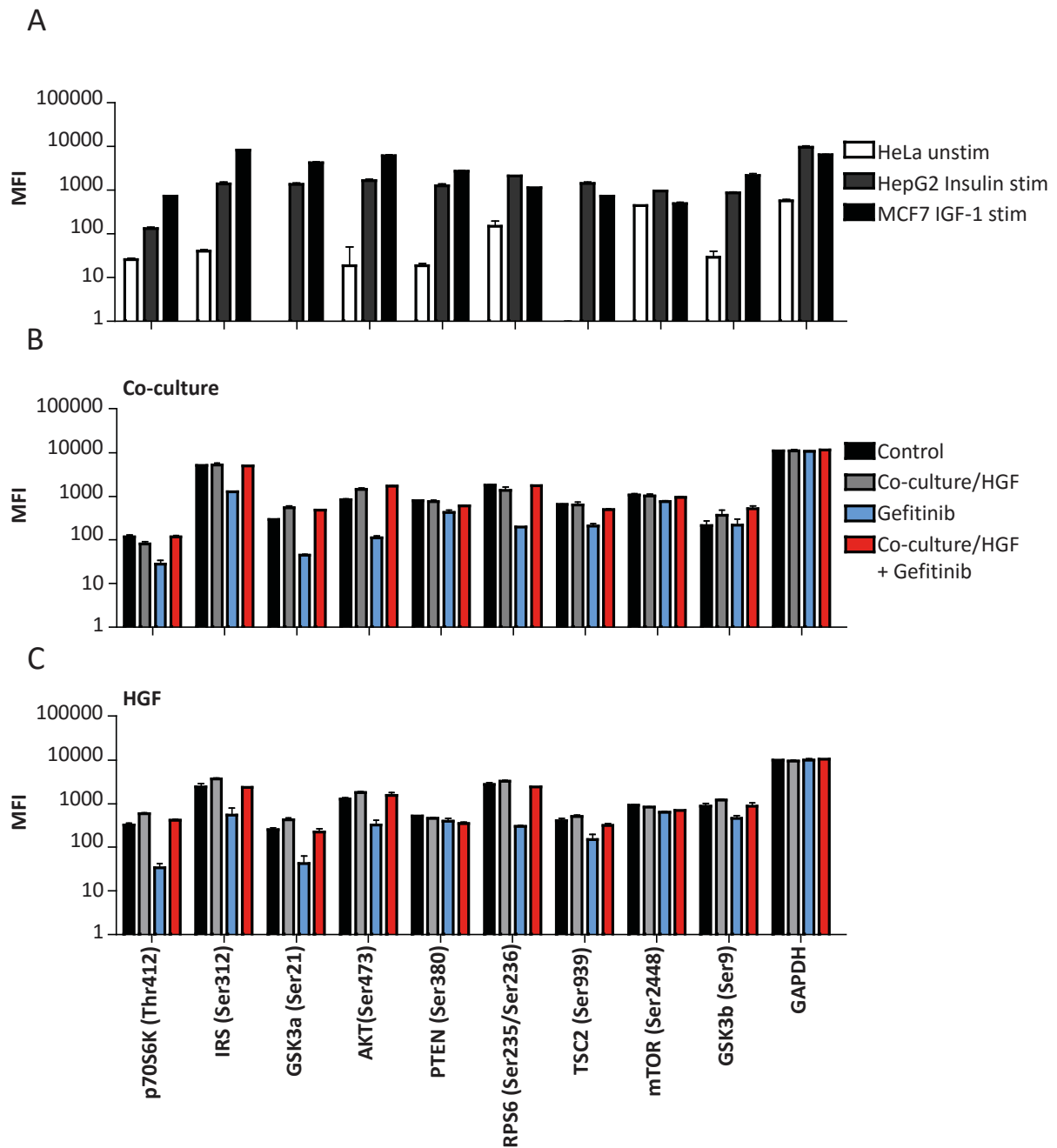
Figure 18 Phospho-signals of MTOR/AKT pathway. Luminex analysis was performed for the MTOR/AKT signaling pathway. **A)** Phosphorylation of stimulated HepG2 stimulated with Insulin (positive control), MCF7 stimulated with IGF-1 (positive control), and unstimulated HeLa lysates (negative control). **B)** HCC827 cells were cultured with or without gefitinib (0.5 µM) in the presence or absence of MRC-5 cells for 48 h. Phosphorylation signals of proteins of **C)** HGF induced HCC827. Protein lysates were quantified by BCA assay. Equal amounts of protein (20 µg) were loaded. MFI: Mean fluorescent intensity. Standard deviations were calculated from two experiments with three technical replicates.

3.4 Identification of paracrine factors in co-culture medium

3.4.1 Paracrine factors secreted by fibroblasts induce resistance of HCC827 towards gefitinib

To further identify factors that might induce resistance towards gefitinib in HCC827 cells, the cell culture medium from fibroblasts was tested (Figure 19 B). Therefore, cell culture medium from MRC-5 lung fibroblasts was centrifuged and the supernatant was applied on gefitinib treated HCC827 cells. Thereby, the HCC827 tumor cells responded as in the co-culture setting. This suggested that fibroblast-derived analytes in the culture medium were necessary to induce resistance in the NSCLC cells towards gefitinib. In order to avoid gefitinib uptake by fibroblast cells, lung tumor cells were washed after treatment. To test whether cell survival after treatment was specific for fibroblasts, the MRC-5 cells were replaced with lung tumor cells A549 (Figure 19 A). Thereby, the resistance of the *EGFR*-mutant HCC827 cells was markedly reduced suggesting that the co-culture with fibroblast cells is required to overcome gefitinib mediated cell toxicity.
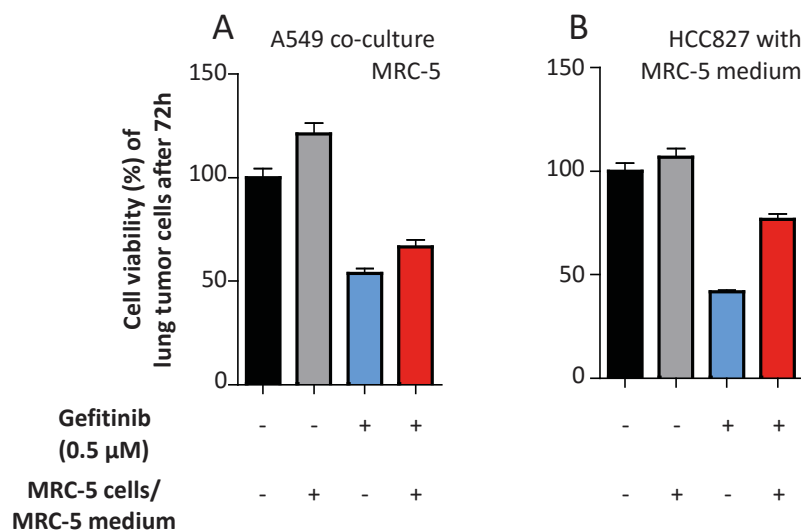
Figure 19 Factors secreted by lung fibroblast cells results in resistance of HCC827 cells to gefitinib. A) HCC827 cells were cultured with (0.5 µM) or without gefitinib in the presence or absence of A549 cells for 72 h. **B)** HCC827 cells were cultured with (0.5 µM) or without gefitinib in the presence or absence of undiluted cell culture medium from MRC-5 fibroblast cells. Standard deviations were calculated from three replicates.

3.4.2 HGF is secreted by fibroblasts into the co-culture medium

As HGF is a known inducer of resistance, the quantity of HGF in the co-culture medium was assessed by ELISA with the cell culture media of the co-culture model (HCC827/MRC-5) and of the separate cultivations (HCC827 or MRC-5) (Figure 20). Human HGF was not measurable in only growth media with or without 10% FCS. The lung tumor cell line

HCC827 alone also did not secrete HGF into the medium, irrespective of treatment with gefitinib. However, after co-culture with MRC-5, 4 ng/ml HGF was detected in the medium. When MRC-5 cells were incubated alone, an even higher concentration of HGF (5 ng/ml) was observed.
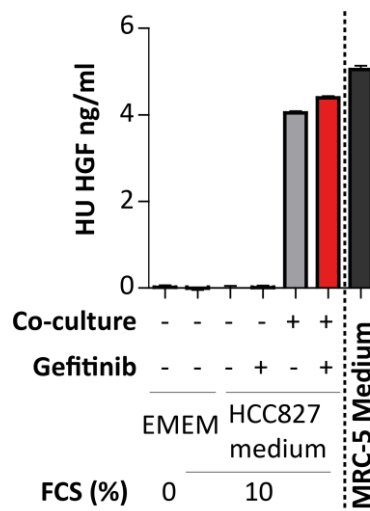
Figure 20 HGF ELISA of cell culture medium from HCC827 co-culture. HCC827 cells were cultured with or without gefitinib (0.5 µM) in the presence or absence of MRC-5 cells for 48 h. Cells were incubated for 48 h in co-culture with cell culture medium 10% FCS or without. Cell culture medium from HCC827 cells alone, in co-culture, as well as medium from MRC-5 cells was analyzed using ELISA kit (Invitrogen) for human HGF levels. The amount of HGF was measured using a standard curve. Standard deviations were calculated from two experiments.

To identify other cytokines involved in the co-culture system, a bead-based multiplex system was used. Therefore, HGF levels were technically validated in the supernatant of HCC827 co-culture (Figure 21 A) and PC-9 co-culture (Figure 21 B) with MRC-5 cells using the Luminex system. Similar to the ELISA analysis, HGF from the supernatants of HCC827 or PC-9 single cultures were present at background levels. Media from co-culture with MRC-5 showed markedly increased levels of HGF. The single culture medium of MRC-5 cells showed the highest levels (1852 MFI) of HGF. The HGF levels were within the linear portion of the standard curve, which was measured using the 5-parameter logistics curve (5-PL) (data not shown). The measurements were within tolerable %coefficients of variation (CV < 25%).
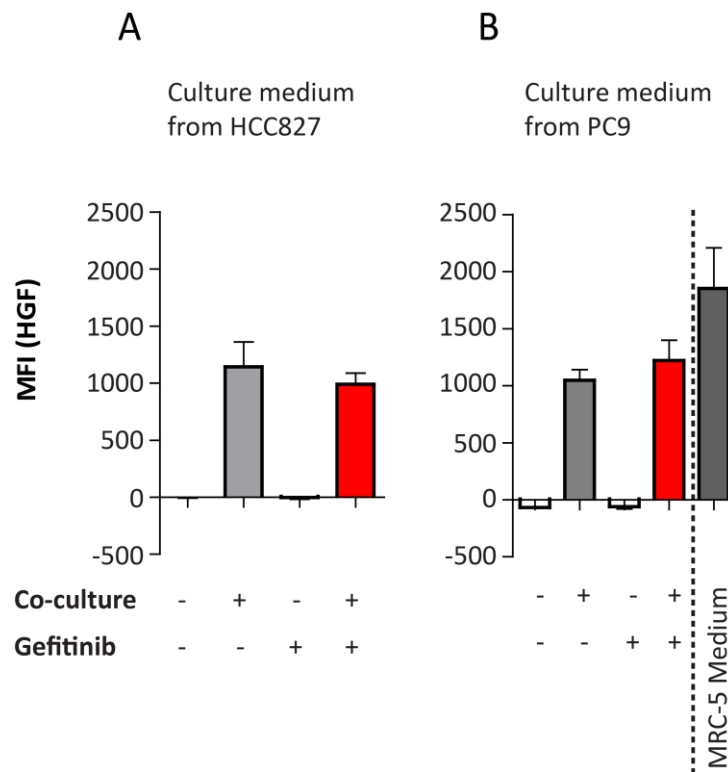
Figure 21 Luminex analysis of HGF in cell culture media of HCC827 and PC-9 co-cultures. A) HCC827 or **B)** PC-9 cells were cultured with or without gefitinib (0.5 µM) in the presence or absence of MRC-5 cells. After 48 h co-culture, the cell culture medium of HCC827 and PC-9 cells was taken and 25 µl cell culture medium was analyzed for HGF (bead region: 62) expression using a bead-based immunoassay (BioRad). Standard deviations were calculated from three experiments. MFI, mean fluorescent intensity.

3.4.3 Screening of cytokines involved in gefitinib resistance

Further cytokines that might be involved in the induction of resistance to gefitinib were searched. Therefore, cytokines in the supernatant of HCC827 (Figure 22 A) and PC-9 (Figure 22 B) co-cultured cells were screened. In total, 41 cytokines were measured using the multiplex bead-based immunoassay (Supplemental Figure 1; Supplemental Table 1). Subsequently, six analytes (GRO, IL6, IL8, MCP1, CXCR3 (IP10) and VEGF) were selected because the abundances of these cytokines were within measurable ranges. Although CSF2 was slightly below the range of the quality control samples (data not shown), this analyte was also included.

No analyte was observed in both cell lines HCC827 and PC-9 to be at low levels in the single culture medium and increased in the culture medium of co-cultured NSCLC tumor cells as it was observed with HGF.

IL6 and IL8 showed similar patterns between the two cell lines (HCC827 and PC-9), i.e. the MFI of the analytes were increased after co-culture (Figure 22 A/B). However, the MFI of IL6 and IL8 in the single culture medium of HCC827 cells already had a high background level above 1,500 MFI for IL6 and above 6,000 MFI for IL8 cells and was therefore not

considered for further analysis. Moreover, CSF2, CXCR3, and VEGF were increased within the HCC827 and PC-9 co-culture medium. The MFI of CXCR3 in comparison to the other analytes was markedly reduced in the culture media of MRC-5 cells. On the other hand, within the co-cultured PC-9 cells, CXCL1, CXCR3, VEGF and CCL2 showed increased MFI levels in comparison to the single cultures (Figure 22 B). The changes of CXCR3 and CCL2 in the cell culture medium from single to co-culture were nearly 100-fold and more than 20,000-fold, respectively.

Human cytokine standards containing all analytes of interests in the assay were used as controls (data not shown). A dilution curve for each analyte was determined. In addition, two human cytokine quality control samples were included, which contained all analytes at predefined concentrations, whereby one quality control sample showed increased MFI values over all analytes in comparison to the second control sample.

In conclusion, the analytes VEGF and CSF2 showed the same pattern as HGF in the cell culture medium of HCC827/MRC-5 co-culture levels.
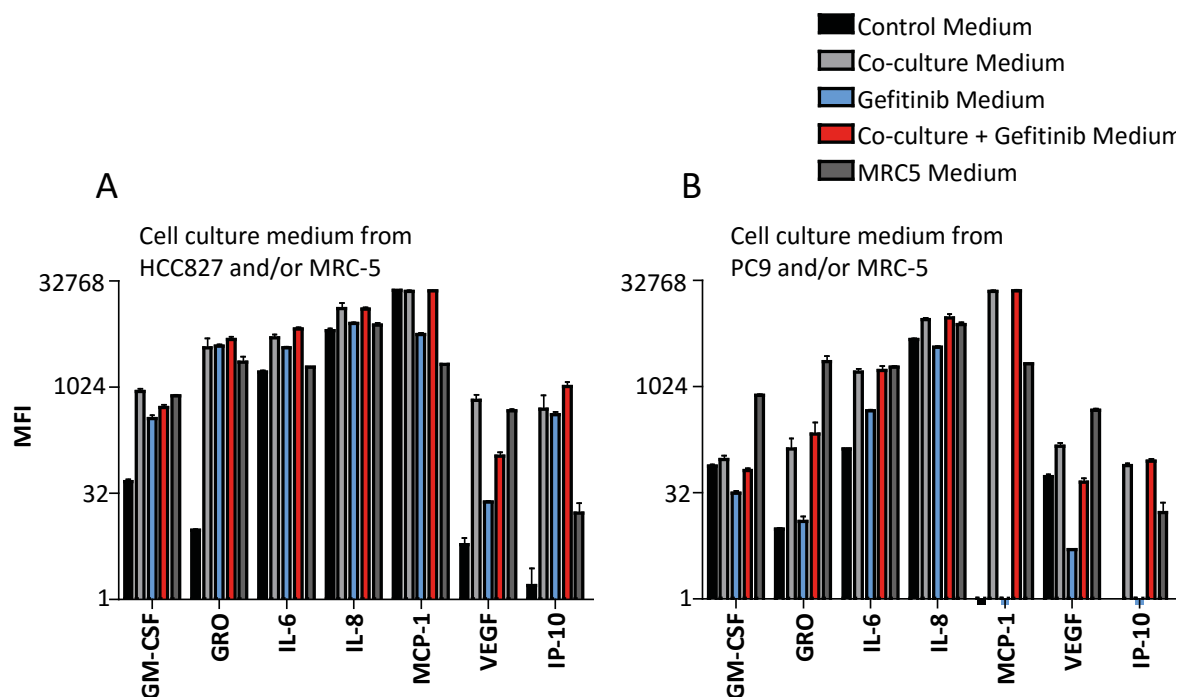
Figure 22 Multiplex bead based analysis of cytokines and chemokines in the cell culture medium of HCC827 and PC-9 cells. HCC827 and PC-9 cells were cultured with or without gefitinib (0.5 µM) in the presence or absence of MRC-5 cells. After 48 h co-culture, the cell culture medium of **A)** HCC827 and **B)** PC-9 cells was harvested, and the human cytokine/chemokine magnetic bead panel was analyzed from 25 µl cell culture medium. Seven out of 41 measured analytes (CSF2 (GM-CSF) (20), CXCL1 (GRO) (26), IL6 (57), IL8 (63), CCL2 (CCL2) (67), VEGF (78), CXCR3 (IP-10) (65)) are presented. Standard deviations were calculated from three experiments with three technical replicates. MFI, mean fluorescent intensity.

3.4.4 Upregulation of *MET* and *GM-CSFR* in HCC827 cells in comparison to MRC-5 cells

The receptors corresponding to the selected analytes in section 3.4.3 were analyzed by qPCR using cell lysates from HCC827 and MRC-5 cells in order to determine in which cell type they were more abundant. To determine the abundance of the receptor for HGF, the mRNA levels of *MET*; for *CSF2*: *CSF2RA*; and for *VEGFA*: *VEGFR1* (*KDR*) and *VEGFR2* (*Flt1*) were analyzed. *MET* levels were decreased after gefitinib treatment (FC = 0.63). *CSF2RA* showed increased levels (FC = 5.3) after gefitinib exposure in comparison to DMSO. However, differential mRNA expression between the different culture conditions was only minor in comparison to the more striking results if mRNA levels of the fibroblast cell line MRC5 were compared to the tumor cell line HCC827. The mRNA levels of *MET* were higher (FC = 37.4) in comparison to MRC-5 cells (Figure 23 A). In line with the results from *MET*, *CSF2RA* was also higher (FC = 40.4) in HCC827 cells in comparison to in MRC-5 cells (Figure 23 B). In contrast, *KDR* (FC = 305.9) (Figure 23 C) and *Flt1* (FC = 1.6) (Figure 23 D) were more abundant in the fibroblast cell line MRC-5 than in HCC827. In summary, these results suggested that ligands such as HGF and CSF2 were more abundant in the cell culture medium of fibroblast cells and/or in the co-culture medium. *MET* and *CSF2RA* were found to be more abundant in HCC827 cells than in fibroblasts.
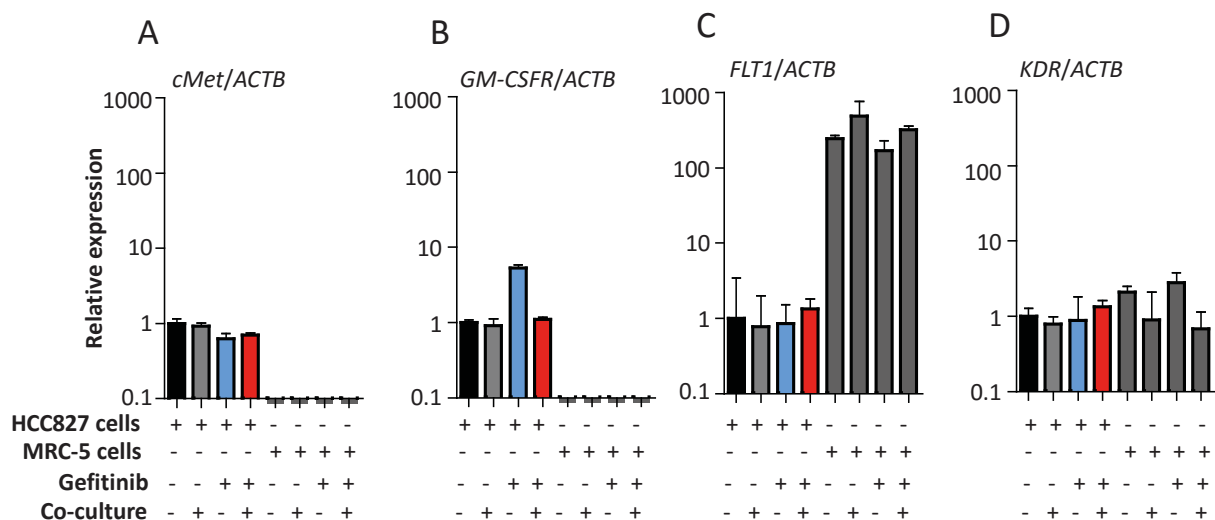
Figure 23 mRNA expression of selected receptors in HCC827/MRC-5 co-culture. HCC827 cells were cultured with or without gefitinib (0.5 µM) in the presence or absence of MRC-5 cells for 48 h. mRNA levels of **A)** *MET* (*cMET*), **B)** *CSF2RA* (*GM-CSFR*), **C)** *FLT1*, and **D)** *KDR* were normalized with the housekeeping gene *ACTB*. mRNAs levels were normalized to HCC827 control. Standard deviations were calculated from three experiments.

3.4.5 Administration of HGF induces resistance to gefitinib in HCC827 and PC-9 cells

Since the genes *MET* and *CSF2RA* were found to be more abundant in tumor cells, HGF and CSF2 ligands were selected for further analysis on their influence after gefitinib treatment by measuring cell viability. These factors are known to target MET or CSF2 receptors, respectively. To evaluate whether HGF or CSF2 could induce resistance in HCC827 after gefitinib treatment, different concentrations of HGF (5-80 ng/ml) or CSF2 (20-40 ng/ml) were administered.

The cell index, reflecting cell adherence, number, viability, and morphology in real-time [122], was shown to be reduced for HCC827 after gefitinib treatment in comparison to gefitinib and subsequent HGF induction (Figure 24 A). Similar results were observed for PC-9 cells (data not shown). HGF was also observed to be markedly higher expressed (566-fold) by fibroblast cells than by HCC827 cells using qPCR (Figure 24 B). Administration of CSF2 with different concentration to HCC827 did not result in reduced sensitivity towards gefitinib (data not shown).

These results suggested that HGF could overcome gefitinib-mediated toxicity in *EGFR*-mutant NSCLC cells.
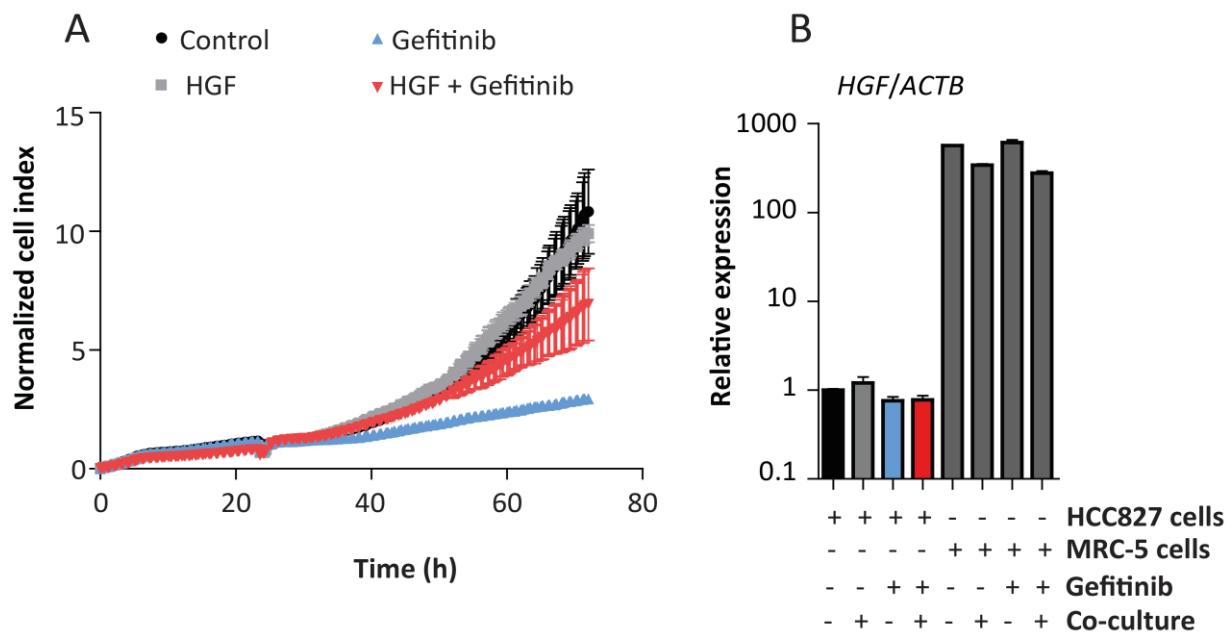
Figure 24 HGF reduces sensitivity towards gefitinib. A) Impedance measurement of HCC827 cells after treatment with gefitinib and/or HGF (20 ng/ml) induction. HCC827 were seeded in E-plates and incubated for 24 h using an xCELLigence (Roche). Standard deviations were calculated from quadruplicates. The cell index was normalized after 24 h. **B)** Relative *HGF* expression was normalized to *ACTB*. HCC827 cells were cultured alone or in co-culture with MRC-5 cells for 48 h. The mRNAs from the different culture conditions were compared to HCC827 control. Standard deviations were calculated from three experiments.

3.5 miRNA profiling of co-cultured NSCLC cells

To analyze miRNAs involved in EGFR-TKI resistant HCC827 cells, 731 miRNAs were profiled using qRT-PCR arrays with three biological replicates (n = 12). Those miRNAs with a median Cp value > 35 in equal to or more than 75% (9/12) of samples (n = 453) were excluded from the analysis (Figure 25 A). All other miRNAs (n = 278) were included. To compare the miRNAs between the samples, the miRNA data was median normalized. The median of n = 278 miRNAs was Cp = 32.1 (Figure 25 B).
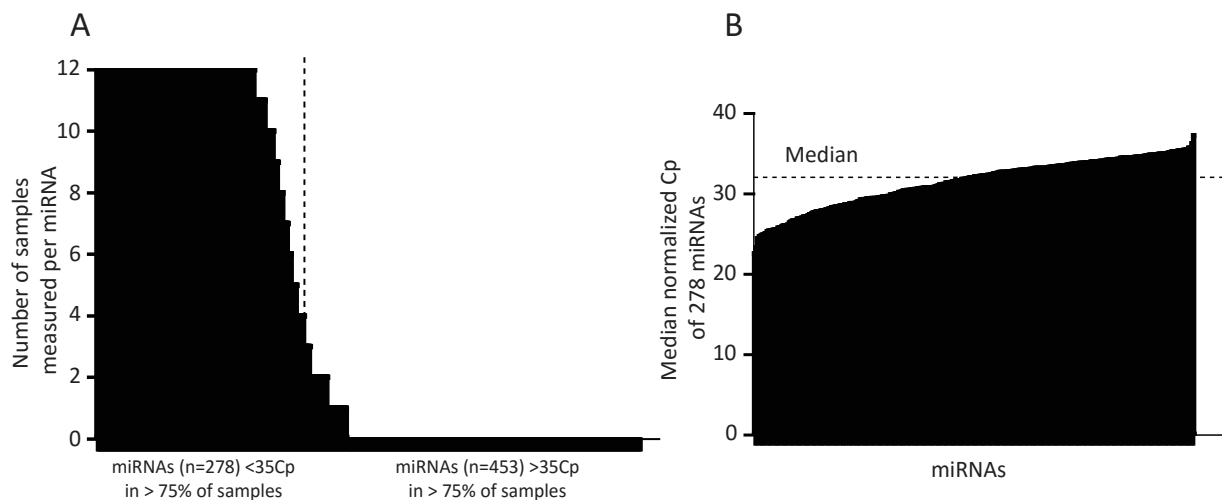
Figure 25 miRNA profiling of HCC827 co-culture. HCC827 cells were cultured with or without gefitinib (0.5 µM) in the presence or absence of MRC-5 cells for 48 h. For each sample, n = 731 human miRNAs were measured. **A)** Penalized miRNAs. **B)** Median normalization of not penalized miRNAs.

3.5.1 Selection of miRNA candidates from the screening experiment

For miRNA analysis, the HCC827 tumor cells were grown under four different conditions for 48 h, i.e.:

- Separately cultured (HCC -/-),
- Treated with gefitinib but separately cultivated (HCC +/-),
- Not treated but cultivated in co-culture (HCC -/+),
- Treated and cultivated in co-culture (HCC +/+).

To select and narrow down the number of miRNAs, a linear fold change (FC) ≥ 1.5 and an unpaired two-tailed Student t-Test $p < 0.05$ was applied. Subsequently, all miRNAs were ranked according to their FC. The miRNAs were also tested using a false discovery rate (q-value). All of the selected miRNAs had a q-value < 0.2. MRC-5 cells were also screened and analyzed for differential expression after treatment and subsequent co-culture. However, no differentially expressed miRNA could be validated by comparing +/+ vs +/- (data not shown).

The comparison: HCC +/+ vs HCC +/- was the main comparison to select potential miRNAs that may be involved in the resistance to gefitinib. In total, 31 miRNAs were found to be deregulated if a FC ≥ 1.5 and a $p < 0.05$ was applied and miRNAs had a median Cp ≤ 35 (Figure 26 A; Supplemental Table 2). From these 31 miRNA, 19 were found to be downregulated while twelve were upregulated. To further narrow down the number of miRNAs for validation, the selection was done using a FC ≥ 2. *miR-205*, *miR-181a-2-3p*, *miR-181a-3p*, *miR-181a-5p*, *miR-181b-5p* were found to be downregulated while *miR-503-5p*, *1296-5p*, *miR-222-5p*, *let-7a-2-3p*, *miR-941, miR-29b-1-5p* were upregulated in the resistant lung tumor cells (Table 23). Although *miR-181a-5p* and *miR-181a-3p* showed slightly lower than FC = 2, these miRNAs were taken into account because they belong to the *miR-181* cluster with *miR-181b-5p*. Here, *miR-29b-3p*, which is the major form of the mir-29b-1 precursor was also observed to be differentially regulated. However, *miR-29b-1-5p* was selected because it showed a higher FC, and although it was earlier denoted as the miRNA* strand or the minor form of the *mir-29b-1* precursor, reports have shown potential functional miRNA* species [135].

Table 23: Selected deregulated miRNAs from miRNA array profiling and analysis of HCC +/+ vs HCC +/-

miRNA ID	p-value	q-value	Fold change	Median Cp
miR-205	2.50E-02	1.63E-01	0.42	32.50
miR-181a-2-3p	2.56E-02	1.63E-01	0.46	31.67
miR-181b-5p	6.01E-04	4.61E-02	0.47	29.44
miR-181a-5p	2.91E-03	6.53E-02	0.52	27.03
miR-181a-3p	6.63E-04	4.61E-02	0.60	33.04
miR-503-5p	9.19E-03	8.97E-02	2.02	28.56
miR-1296	1.72E-02	1.39E-01	2.05	34.60
miR-222-5p	9.03E-03	8.97E-02	2.34	33.86
let-7a-2-3p	6.39E-03	7.52E-02	2.46	32.07
miR-941	1.75E-02	1.39E-01	2.51	33.20
miR-29b-1-5p	2.79E-03	6.53E-02	2.66	30.98
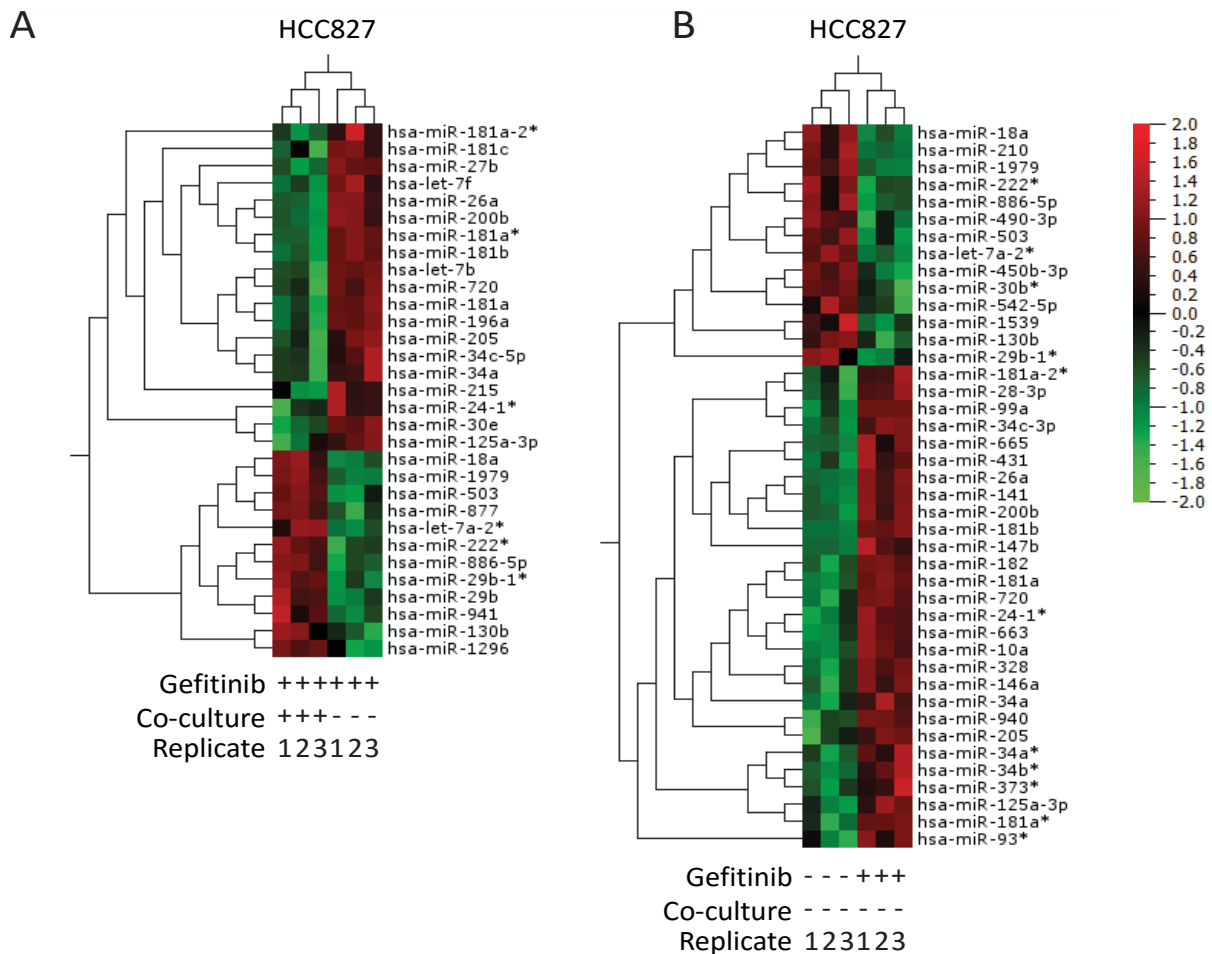
Figure 26 HeatMap of deregulated miRNAs involved in resistance of HCC827 cells towards gefitinib. A) Co-culture & gefitinib treated HCC827 (HCC +/+) cells compared to HCC827 cells treated with gefitinib in single culture (HCC +/-). **B)** HCC827 cells treated with gefitinib in single culture (HCC +/-) compared against untreated cells in single culture (HCC -/-). miRNAs were selected if FC was above 1.5 and p < 0.05. Each group consists of three experiments. Red: Upregulation; Green: Downregulation.

3.5.1.1 Deregulated miRNAs in HCC827 under different culture conditions

To identify miRNAs directly regulated by downregulation of EGFR activity, HCC +/- vs HCC -/- was compared (Figure 26 B; Supplemental Table 3). In this analysis, 42 miRNAs were differentially expressed if the same filter criteria were used as mentioned above. All miRNAs that were selected in the main test (HCC +/+ vs HCC +/-) were inversely regulated. From the 42 miRNAs, 15 were downregulated while 27 were upregulated. For example, *miR-205*, *miR-181a-2-3p*, *miR-181a-3p*, *miR-181a-5p*, *miR-181b-5p* were found to be upregulated, while *miR-503-5p*, *miR-222-5p*, *let-7a-2-3p*, *miR-29b-1-5p* were downregulated in the gefitinib treated HCC827 cells in comparison to not treated HCC827 cells.

To identify differentially expressed miRNAs after treatment in co-cultured HCC827 cells, a test that compares HCC +/+ vs HCC -/+ was done. Here, eleven miRNAs were found to be differentially expressed. *miR-181-5p* and *-3p* were observed to be upregulated in HCC +/+ in

comparison to HCC -/+. This suggested that regulation of *miR-181a-5p* and *-3p* is markedly influenced by downregulation of EGFR activity even in co-cultured cells, i.e. when other signaling pathways were activated (Supplemental Table 4).

To identify differentially regulated miRNAs due to the co-culture with MRC-5, HCC -/+ vs HCC -/- were compared. Here, only three miRNAs (*miR-30c-1-3p*, *miR-490-3p*, and *miR-891b*) were observed to be deregulated (Supplemental Table 5).

An appropriate set of reference genes was selected such as *miR-103*, *miR-423-5p*, *miR-191*, *SNORD49A*, *SNORD38B*, and *U6*, which were designated as potential housekeeping genes and tested using Normfinder [127], where for each gene a stability value was estimated, which is reflected by the standard deviation (SD). Using this method, *SNORD49A* was found to have the best stability value (SD = 0.004), *miR-191* and *miR-103* showed a stability value at SD = 0.005 and *U6* showed the lowest stability at SD = 0.021 (data not shown). Since normalization using miRNAs as housekeepers is more appropriate for miRNAs as target molecules, *miR-191* was used in validation experiments as normalizing gene [136].

3.5.2 Validation of selected miRNAs in HCC827 and PC-9 cells

In a validation study, the selected miRNAs from the profiling were analyzed using three biological replicates of HCC827 cells. Here, *miR-1296-5p*, *miR-941*, and *miR-222-5p* showed a median Cp above 35 across all 12 samples and were, therefore, were excluded. The remaining eight miRNA candidates from the miRNA profiling were validated in HCC827 cells (Table 24; Figure 27). Consistent with the screening data, five miRNAs (*miR-181a-3p*, *miR-205-5p*, *miR-181a-2-3p*, *miR-181b-5p*, *miR-181a-5p*) were downregulated, while three miRNAs (*miR-503-5p*, *miR-29b-1-5p*, and *let-7a-2-3p*) were upregulated by comparing HCC+/+ vs HCC+/-. Among the eight miRNAs, *miR-181a-2-3p* did not show significant deregulation.

Table 24: Validation of selected miRNAs in gefitinib-treated co-cultured HCC827 cells

miRNA ID	pVal	Fold change	Median Cp
miR-181a-3p	1.69E-03	0.51	34.17
miR-205-5p	1.17E-02	0.52	33.47
miR-181a-2-3p	1.13E-01	0.56	34.04
mir-181b-5p	3.89E-02	0.58	30.20
miR-181a-5p	4.36E-03	0.61	27.13
miR-1296	6.78E-01	0.89	36.26
miR-941	9.17E-01	0.96	35.35
miR-222-5p	3.85E-01	1.63	37.13
miR-503-5p	1.90E-02	1.81	29.05
miR-29b-1-5p	3.68E-02	1.83	33.68
let-7a-2-3p	1.80E-03	3.71	35.00
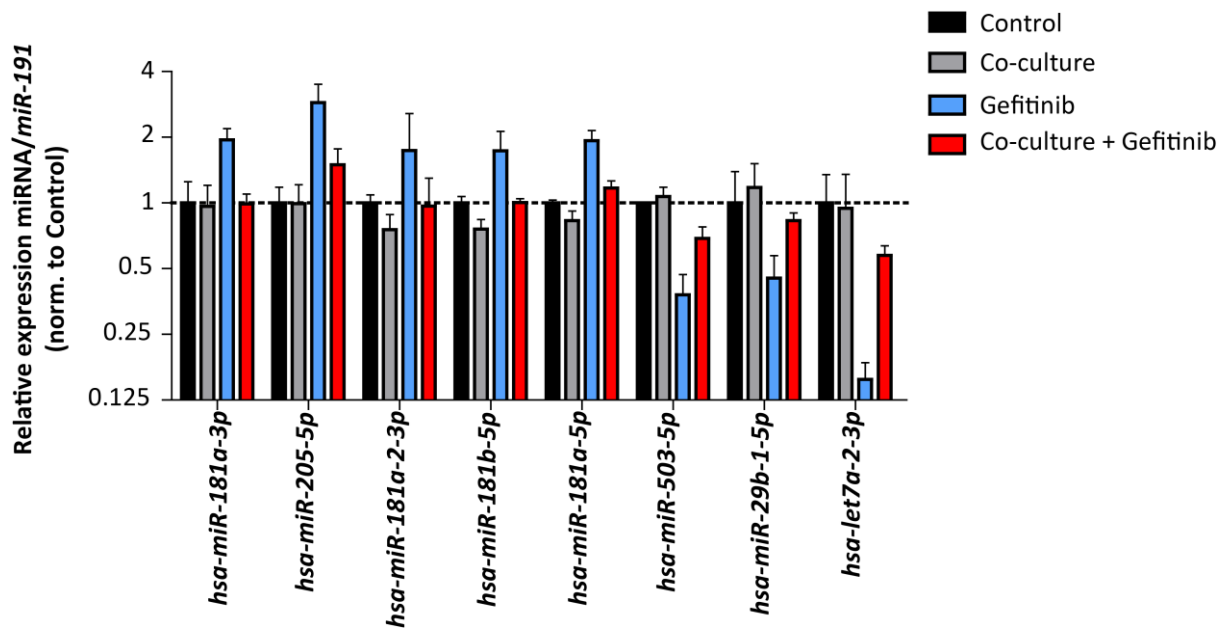
Figure 27 Validation of selected miRNAs in HCC827 co-culture. HCC827 cells were cultured with or without gefitinib (0.5 µM) in the presence or absence of MRC-5 cells for 48 h. miRNAs were measured and normalized against *miR-191*. Relative expression was calculated by comparing to HCC827 control. A log2 base scale was used for y-axis. Values above or below the dotted line indicate an up- or downregulation, respectively, of the miRNA in comparison to control HCC827 cells. Standard deviations were calculated from three experiments.

In addition to the technical validation in the same cell line, the differential expression of the eight selected miRNAs was tested not only in HCC827 (Figure 28 A) but also in the second gefitinib-sensitive cell line PC-9 (Figure 28 B) comparing +/+ vs +/- at different time points (24 h, 48 h, and 72 h). In the HCC827 cell line, all miRNAs were observed to show the same direction of regulation as observed in the profiling study and in the first validation. However, in PC-9 cells, the expression of *let-7a-2-3p*, *miR-181a-3p*, miR-*181a-5p*, *miR-205-5p*, *miR-181b-5p*, *miR-181a-2-3p* were not the same at each time-point as in the HCC827 cell line. These miRNAs were therefore also excluded from further analysis. Only *miR-503-5p* and *miR-29b-1-5p* were upregulated in PC-9 and HCC827 by comparing +/+ vs +/- at different time points.
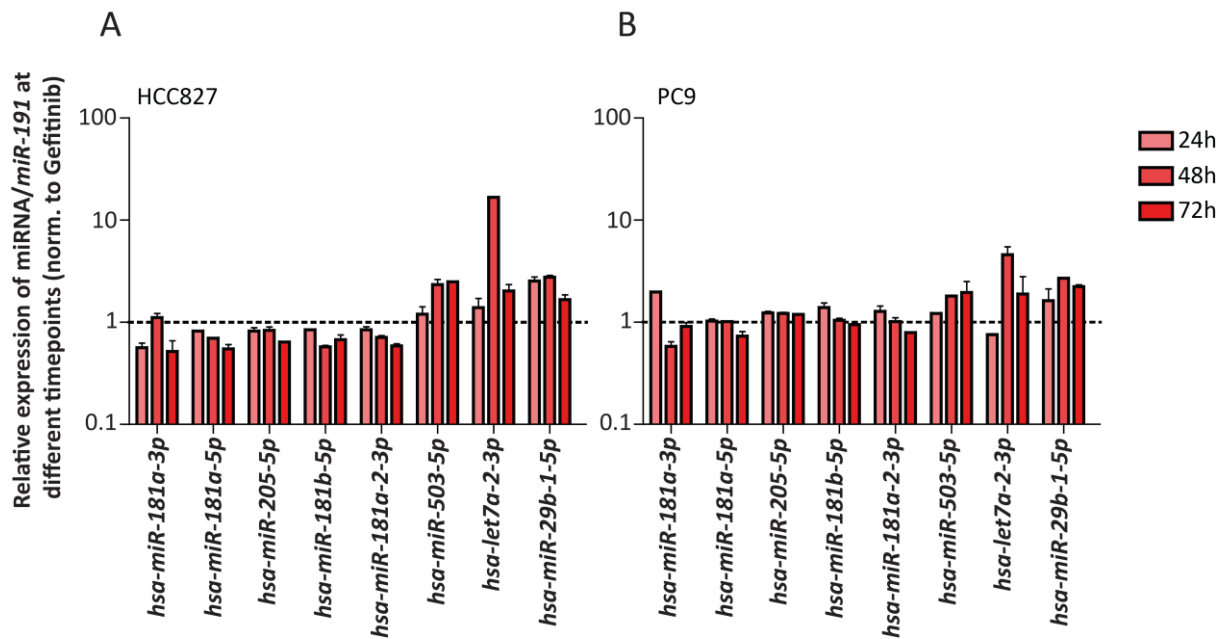
Figure 28 Validation of selected miRNAs in HCC827 and PC-9 cells after co-culture and gefitinib treatment against gefitinib treatment only at different time points. A) HCC827 or **B)** PC-9 cells were cultured alone and treated with gefitinib (0.5 µM) or co-cultured with MRC-5 cells and treated with gefitinib for 24 h, 48 h, and 72 h. miRNAs were measured and normalized against *miR-191*. A log2 base scale was used for y-axis. Values above or below the dotted line indicate an up- or downregulation, respectively, of the miRNA in comparison to gefitinib treatment. Standard deviations were calculated from three experiments.

To identify miRNAs to be influenced by HGF, which was shown to be the major factor to induce resistance, the most interesting miRNAs (including *miR-503-5p* and *miR-29b-1-5p*) were then tested for differential expression after gefitinib treatment and subsequent HGF induction. To assess miRNA regulation in HGF-triggered EGFR-TKI resistant lung tumor cells, soluble HGF was administered to treated cells. The same regulation pattern of *miR-29b-1-5p* and *miR-503-5p* as in co-cultured cells was observed (Figure 29). Since *miR-29b-1-5p* and *miR-29a-3p* derive from the same precursor and are clustered together within a proximal distance of 10kb they are believed to be co-expressed [137]. Interestingly, Garofalo *et al*. already described *miR-29a-3p* to be downregulated in HCC827 and PC-9 cells after gefitinib treatment. Ectopic overexpression of *miR-29a-3p* in gefitinib exposed HCC827 and PC-9 cells resulted in reduced apoptosis and increased cell viability [117]. Therefore, *miR-503-5p* was considered as the most interesting candidate as nothing was known about the regulation of this miRNA in EGFR-TKI resistant cells. The main focus of this study was to assess the impact of the deregulation of this miRNA.

In summary, the data from the screening and validation study suggested that *miR-503-5p* was upregulated in resistant HCC827 and PC-9 cells. Moreover, the selected miRNAs, in particular *miR-503-5p*, could compensate their expression after co-culture or HGF induction if the EGFR activity was reduced upon gefitinib treatment.
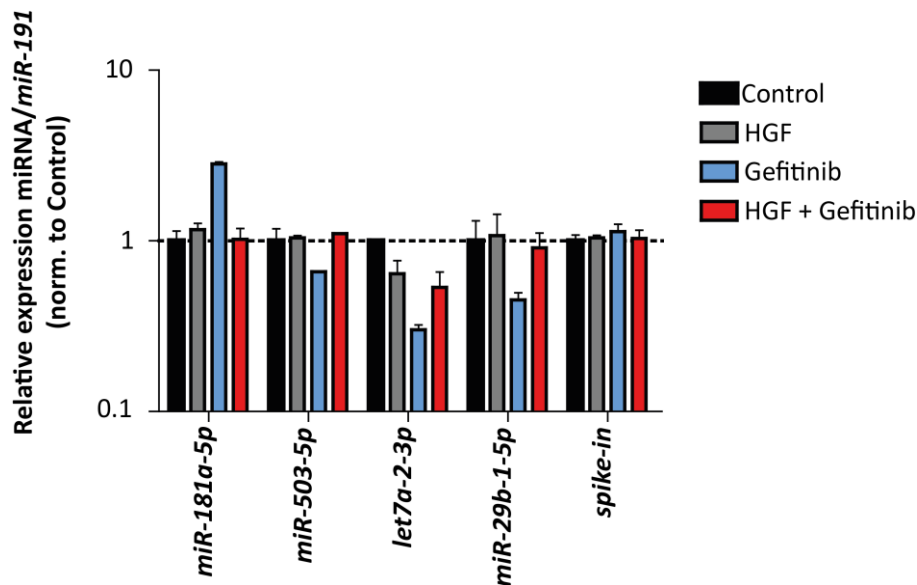
Figure 29 Regulation of selected miRNAs in HGF induced HCC827 cells after gefitinib treatment. HCC827 cells were cultured with or without gefitinib (0.5 µM) in the presence or absence of HGF (20 ng/ml) cells for 48 h. miRNAs were measured and normalized against *miR-191*. Relative expression was calculated by comparing to HCC827 control. A base-10 log scale was used for y-axis. Values above or below the dotted line indicate an up- or downregulation, respectively, of the miRNA in comparison to control HCC827 cells. Standard deviations were calculated from three experiments.

3.5.3 *miR-503-5p* expression in different lung cancer cell lines after treatment with gefitinib

To further elucidate the role of *miR-503-5p* in conferring resistance, its expression was analyzed for differential expression after gefitinib treatment in different lung cancer cell lines containing wild-type (wt) *EGFR*. Here, significant differential expression of *miR-503-5p* was observed in HCC827 cells after gefitinib treatment in comparison to DMSO control (FC = 0.50). PC-9 cells showed also a slight downregulation (FC = 0.81; p = 0.3). Other lung cancer cell lines such as A549 (wt) (FC = 0.84), H2030 (wt) (FC = 1.28), H1650 (FC = 0.87), and H1975 (FC = 1.07) did not show significant downregulation (Figure 30). Interestingly, H1650 has the same deletion of *EGFR* (delE746-A750) but no deregulation of *miR-503-5p* was observed. EGFR-TKI resistance in H1650 cells has been suggested to be due to loss of PTEN [138] since IC50 of H1650 was found at 1.9 µM. Moreover, H1975 was described to be less sensitive towards gefitinib due to T907M gatekeeper mutation [40]. Stably resistant HCC827 (HCC827GR2 and GR4) also showed no significant differential expression of *miR-503-5p* (FC = 1.15 and 1.16). HCC827GR2 and GR4 showed lower IC50 than the HCC827 cells. The resistant HCC827 were also identified as HCC827 cells using SNP based multiplex human cell line authentication test [139], which was performed at the DKFZ Core Facility (data not shown).

These results suggested that *miR-503-5p* levels were reduced after treatment in gefitinib hypersensitive cells but not in gefitinib-resistant cells.

Cell line	IC50 (µM)	EGFR
HCC827 wt	< 10⁻³	delE746-A750
PC9	0.13	delE746-A750
A549	> 10	wt
H1650	1.9	delE746-A750
H1975	> 10	L858R; T790M
HCC827-GR2	> 5	delE746-A750
HCC827-GR4	>5	delE746-A750
H2030	>10	wt
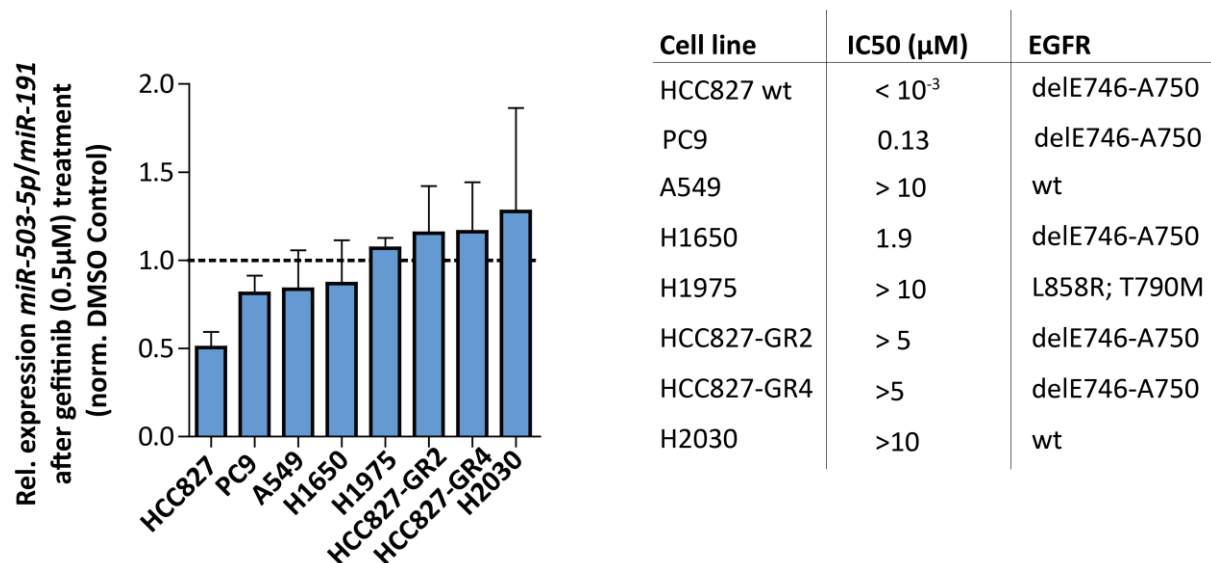
Figure 30 Expression of *miR-503-5p* in different lung cancer cell lines after gefitinib treatment. Relative expression of *miR-503-5p* normalized to *miR-191* in different lung cancer cell lines after treatment with 0.5 µM gefitinib. Relative expression was calculated by comparing to DMSO control. Values above or below the dotted line indicate an up- or downregulation, respectively, of the miRNA in comparison to control cells (DMSO). Standard deviations were calculated from three experiments. IC50 and *EGFR* mutation status (from COSMIC database: http://cancer.sanger.ac.uk\cell_lines) are listed for each of the cell lines on the right panel.

3.6 Gene expression profiling of co-cultured HCC827 and PC-9 cells

To further explore the molecular mechanism of EGFR-TKI resistant NSCLC cells, the genome-wide transcriptome of HCC827 and PC-9 cells was analyzed. Profiling was done using Illumina microarrays to identify common mRNAs associated with gefitinib resistance.

The data was quantile normalized and hierarchical clustering of mRNAs showed expected group clusters of HCC827 (Figure 31 A) and PC-9 (Figure 31 B).
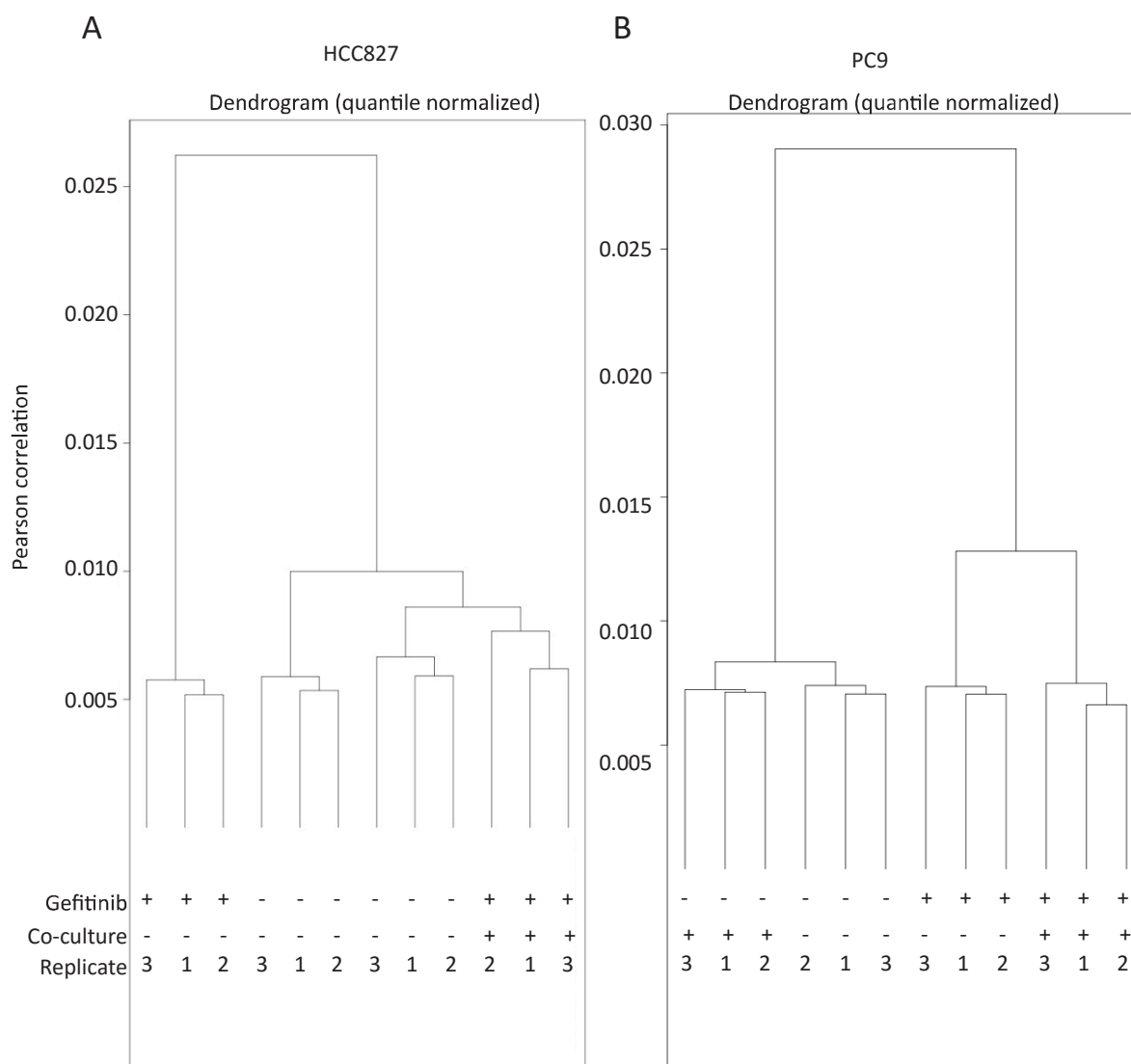
Figure 31 Dendrogram of HCC827 and PC-9 co-cultured cells. A) HCC827 and **B)** PC-9 were cultured with or without gefitinib (0.5 µM) in the presence or absence of MRC-5 cells for 48 h. Hierarchical clustering of quantile normalized data of all Illumina (ILMN) probes from microarray data is shown.

The differential expression of mRNAs was analyzed with the following comparison: (+/+) vs (+/-). Illumina probes were defined as differentially expressed if they showed a FC ≥ 1.5 and $p < 0.05$ (t-Test). In total, 1017 probes were upregulated in HCC827 cells and 238 in PC-9 cells (Figure 32 A). Between both cell lines, 145 probes overlapped. On the other hand, 1018 of them were found to be downregulated in HCC827 cells and 211 in PC-9 cells. In both cell lines, 92 probes were downregulated (Figure 32 B). A total of 237 were identified to be differentially regulated (10 Illumina probes were excluded (initially n = 247) because they showed discrepancies in the regulation between HCC827 and PC-9 cells). To check overlap between the other comparisons, all probes from both cell lines were analyzed using a Venn-Diagram (Figure 32 C). Most of them from the main test overlapped with those from the

comparison (+/-) vs (-/-). Interestingly, most of the probes showed inverse regulation to the main test.
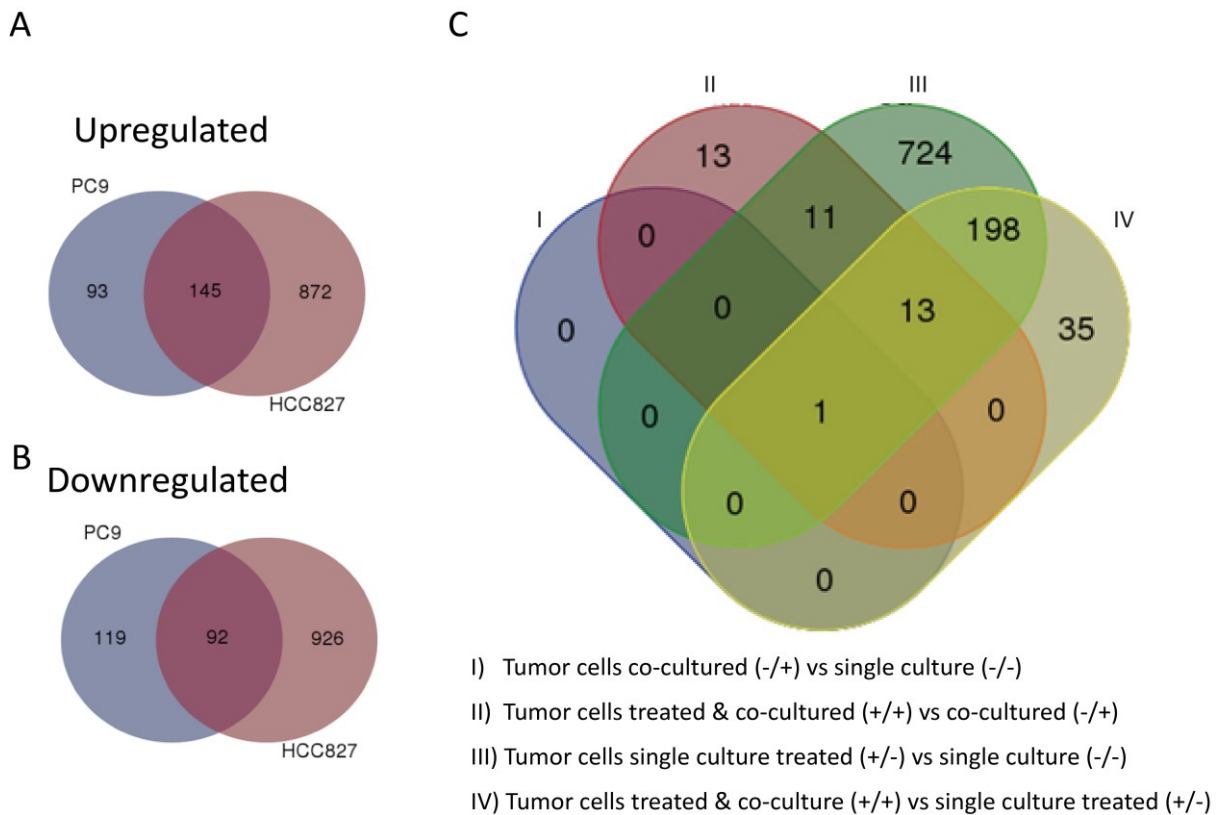
Figure 32 Venn-Diagram of ILMN probe IDs between different analyzed groups within co-cultured HCC827 and PC-9 cells. ILMN probe IDs with FC > 1.5 and a pVal < 0.05 were selected and identified to be **A)** upregulated or **B)** downregulated in both the HCC827 and PC-9 cells. **c)** Differentially expressed Illumina probe Ids from both HCC827 and PC-9 cells between different analyzed groups.

Some Illumina probe Ids were designed to target a specific splice isoform for which multiple isoforms are known or the probes were designed such as that they target all splice isoforms of a gene. Therefore, the 237 Illumina probes corresponded to 211 single transcripts for HCC827 and PC-9 cells. From the 211 mRNAs, 84 were downregulated and 127 were upregulated in the comparison (+/+) vs (+/-) (Supplemental Table 6). The data from the microarray was technically validated using 40 selected mRNAs out of 211 genes (19%) using qRT-PCR. A high correlation between array data and PCR data was found indicating that the microarray data were reliable ($R^2 = 0.78$; Pearson: 0.89; Figure 33).

Using Gene Ontology analysis, an enrichment of genes coding for proteins involved in cell death and vesicle mediated transport upon treatment with gefitinib was identified to be upregulated (Table 25). Enrichment of cell cycle genes, DNA replication and cellular response to stress were downregulated. After treatment and co-culture, genes associated with

cell cycle genes were upregulated while enrichment of genes associated with vesicle-mediated transport was downregulated (Table 26).
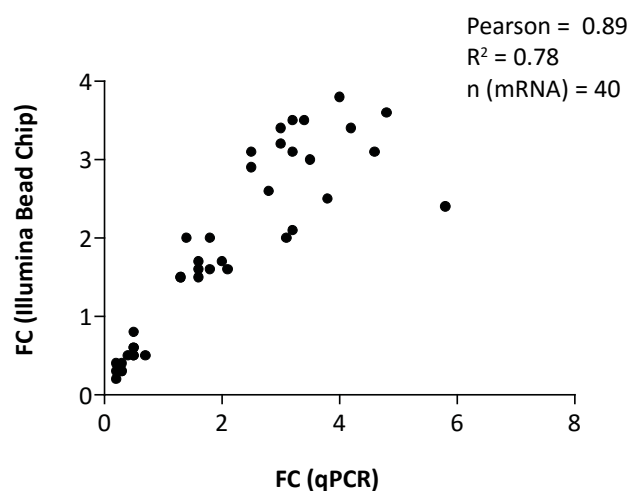
Figure 33 Correlation analysis of microarray and qPCR. Pearson correlation of 40 genes between microarray and qPCR comparing the fold changes of co-culture treated against only treated samples.

Table 25: GO analysis of ILMN microarray data +/- vs -/-

Category	Term	Count	%	PValue	List Total	Pop Hits	Pop Total	Benjamini	Regulation
GOTERM_BP_FAT	GO:0008219~cell death	32	9.38	1.66E-05	258	719	13528	9.73E-03	Up
GOTERM_BP_FAT	GO:0006915~apoptosis	24	7.04	1.16E-03	258	602	13528	1.14E-01	Up
GOTERM_BP_FAT	GO:0016192~vesicle-mediated transport	25	7.33	2.66E-04	258	576	13528	6.51E-02	Up
GOTERM_BP_FAT	GO:0007049~cell cycle	127	32.40	9.87E-75	317	776	13528	1.68E-71	Down
GOTERM_BP_FAT	GO:0000279~M phase	88	22.45	7.92E-69	317	329	13528	6.76E-66	Down
GOTERM_BP_FAT	GO:0006260~DNA replication	48	12.24	3.28E-35	317	190	13528	5.10E-33	Down
GOTERM_BP_FAT	GO:0006259~DNA metabolic process	74	18.88	8.99E-38	317	506	13528	1.53E-35	Down
GOTERM_BP_FAT	GO:0033554~cellular response to stress	50	12.76	1.18E-15	317	566	13528	9.48E-14	Down

Table 26: GO analysis of ILMN microarray data +/+ vs +/-

Category	Term	Count	%	PValue	List Total	Pop Hits	Pop Total	Benjamini	Regulation
GOTERM_BP_FAT	GO:0007049~cell cycle	37	31.36	2.27E-20	99	776	13528	7.21E-18	Up
GOTERM_BP_FAT	GO:0000279~M phase	23	19.49	1.30E-15	99	329	13528	3.17E-13	Up
GOTERM_BP_FAT	GO:0006974~response to DNA damage stimulus	21	17.80	1.86E-12	99	373	13528	2.22E-10	Up
GOTERM_BP_FAT	GO:0048015~phosphoinositide-mediated signaling	10	8.47	1.35E-08	99	88	13528	8.02E-07	Up
KEGG_PATHWAY	hsa03030:DNA replication	11	9.32	8.49E-13	52	36	5085	4.42E-11	Up
GOTERM_BP_FAT	GO:0006323~DNA packaging	5	6.17	1.78E-03	61	117	13528	1.98E-01	Down
GOTERM_BP_FAT	GO:0016192~vesicle-mediated transport	7	8.64	4.17E-02	61	576	13528	6.51E-01	Down
GOTERM_BP_FAT	GO:0030182~neuron differentiation	8	9.88	3.12E-03	61	438	13528	2.42E-01	Down
GOTERM_BP_FAT	GO:0000904~cell morphogenesis involved in differentiation	6	7.41	4.47E-03	61	244	13528	2.93E-01	Down

3.7 Identification of *GABARAPL1* as a target of *miR-503-5p*

3.7.1 Selection of mRNAs from microarray experiments using miRNA prediction

To predict putative targets of *miR-503-5p*, miRNA prediction algorithms such as TargetScan 6.2 are commonly used. This data prediction algorithm predicts 385 transcripts with conserved sites for *miR-503-5p* (if using one transcript per gene having the highest aggregate

P_{CT} [140]). However, several target prediction databases enable to select putative miRNA targets from different algorithms. In order to determine putative *miR-503-5p* mRNA targets, an overlap of the Ingenuity pathway analysis (IPA), including experimentally validated interactions from TarBase, miRecords, the prediction algorithm TargetScan, and manual search of miRNA-related findings from the peer-reviewed literature was employed. Ingenuity listed a total of 770 putative targets of *miR-503-5p*. In combination, the *in-silico* data with 770 putative targets and the microarray data analysis with 211 selected mRNAs revealed an overlap of eight putative genes, four out of which showed expression inversely correlated to *miR-503-5p* expression, i.e. all four selected genes (*ZMAT3*, *GABARAPL1*, *DCLK1*, and *OSBPL7*) were inversely regulated to the miRNA in the main test (+/+ vs +/-) (Figure 34 A). In a next step, the selected mRNAs were validated in HCC827 co-culture (Figure 34 B). *DCLK1* had Cp values above 35 and were therefore excluded. Here, only Gamma-aminobutyric acid receptor-associated protein-like 1 (*GABARAPL1*) was identified to be significantly upregulated upon gefitinib treatment (FC = 3.4). However, its expression was downregulated in HCC +/+ vs +/- (FC = 0.46). According to TargetScan 6.2, *GABARAPL1* is a predicted conserved target of *miR-503-5p* with a 7mer-1A seed match, which stands for an exact match comprising the seed from positions 2-7 of the mature miRNA followed by an 'A' at target position 1 [75] (Figure 35). The probability of conserved targeting (P_{CT}), a metric used to assess the predicted miRNA-mRNA pairing, revealed a P_{CT} = 0.73. High aggregate P_{CT} indicates a high confidence with low false-discovery rate for biologically conserved target sites [140].

In summary, the selection of mRNAs from the screening list using a miRNA-target filter suggested a miRNA/mRNA pairing (*miR-503-5p/GABARAPL1*) in gefitinib resistant cells.
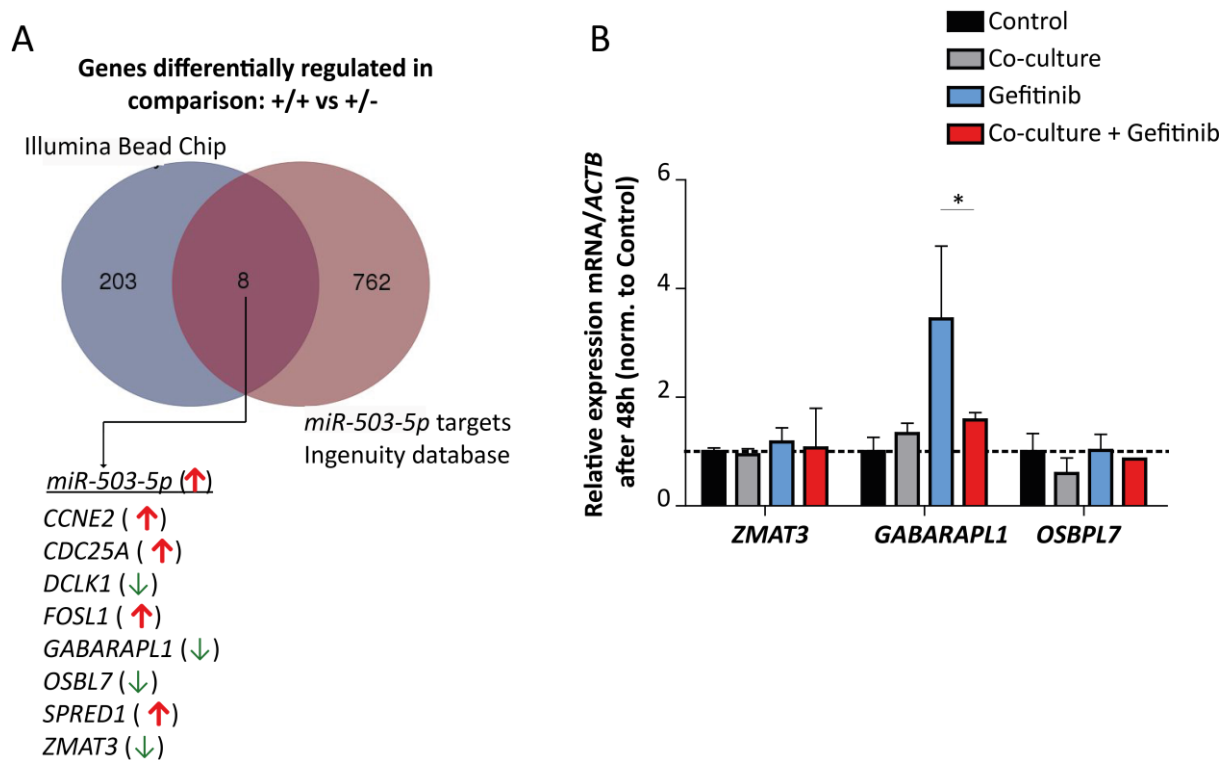
Figure 34 Validation of mRNAs in HCC827 co-culture. A) Differentially expressed genes in HCC +/+ vs HCC +/- from Illumina Bead Chip analysis were overlapped with putative *miR-503-5p* target genes from Ingenuity database. **B)** HCC827 cells were cultured with or without gefitinib (0.5 µM) in the presence or absence of MRC-5 cells for 48 h. mRNA levels of *ZMAT3*, *GABARAPL1* and *OSBPL7* were assessed. Values are presented from two independent experiments each with three replicates. Relative expression was calculated by comparing to HCC827 control. Values above or below the dotted line indicate an up- or downregulation, respectively, of the miRNA in comparison to control cells (DMSO treated). Red arrow: Upregulated; Green arrow: Downregulated.
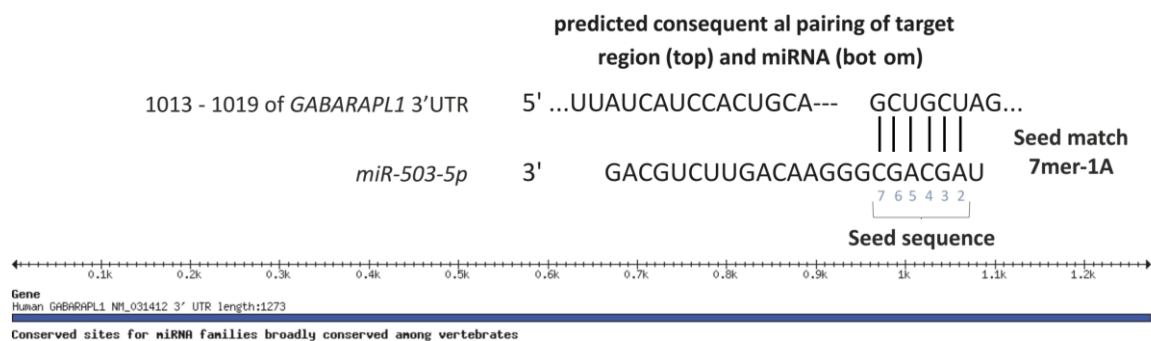
Figure 35 3'UTR of *GABARAPL1*. Predicted pairing of 7mer-1A seed region for *miR-503-5p* at the *GABARAPL1* 3'UTR site. *miR-503-5p* was predicted as a conserved miRNA by TargetScan 6.2.

3.7.2 Validation of *GABARAPL1* as target of *miR-503-5p*

To test the miRNA-target interaction, exogenous double-stranded miRNA mimics were transiently transfected into HCC827 cells and the expression of the miRNA and known mRNA target sequence was analyzed.

Transfecting HCC827 cells using RNAiMAX (FC < 0.1) was more efficient than using the transfection reagent HiPerfect (FC > 0.45) (Supplemental Figure 2).

In order to find an interaction between *miR-503-5p* and *GABARAPL1* regulation, the miRNA was overexpressed by transiently transfecting double-stranded RNA molecules at 40 nM for 48 h and 72 h (Figure 36 A). Significant reduction of endogenous mRNA levels of *GABARAPL1* after ectopic overexpression of *miR-503-5p* was observed after 48 h (p = 0.001; FC = 0.78) and 72 h (p < 0.001; FC = 0.59). To further elucidate the regulation of endogenous protein levels of GABARAPL1 after ectopic overexpression of *miR-503-5p*, a Western Blot of the small molecular weight protein (15 kDa) was performed. The protein level of GABARAPL1 was decreased upon *miR-503-5p* overexpression (Figure 36 B).

Inhibiting the expression of *miR-503-5p* should lead to the derepression of *GABARAPL1*. As expected, no reduction of *GABARAPL1* but a slight increased tendency was observed, which, however, was not significant (p = 0.22; FC = 1.2) (Figure 36 C).

Direct targeting of *GABARAPL1* by *miR-503-5p* was tested by a luciferase reporter assay containing the full length 3'UTR of *GABARAPL1*. The luciferase activity was significantly reduced (p = 0.02; FC = 0.80) in HCC827 cells when *miR-503-5p* was co-transfected with *GABARAPL1* 3'UTR vector in comparison to a non-targeting miRNA (ctrl#2) (Figure 37). As expected, co-transfection of *miR-503-5p* with *GABARAPL1* 3'UTR, in which the binding site for *miR-503-5p* was truncated did not significantly alter luciferase activity (p = 0.14; FC = 1.03). Moreover, co-transfection of *miR-503-5p* with empty pmirGLO vector also did not significantly alter luciferase activity (p = 0.13; FC = 0.89).

In summary, these results suggested that *miR-503-5p* directly targets *GABARAPL1* and downregulated its expression on mRNA and protein level.
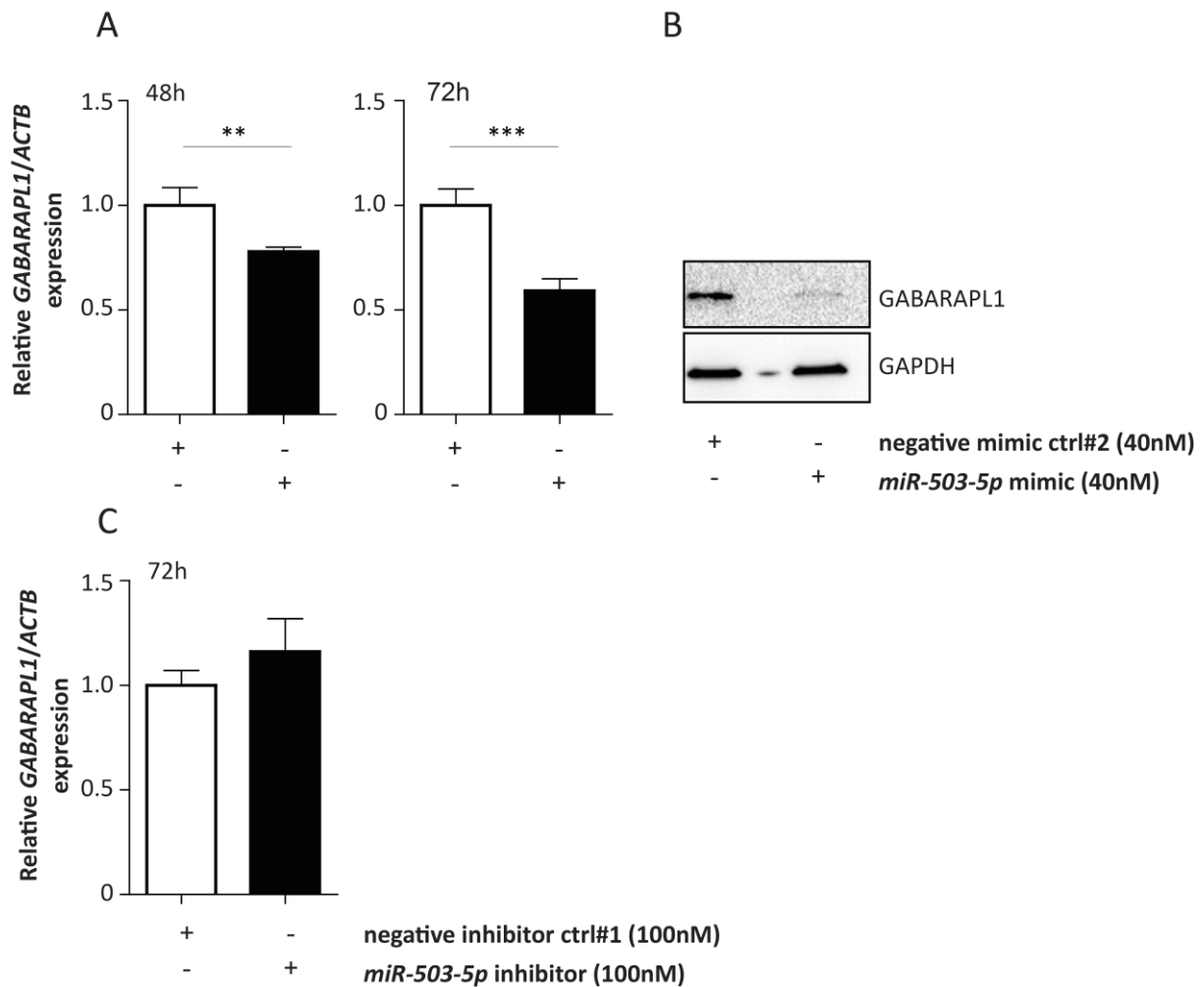
Figure 36 Expression of *GABARAPL1* after *miR-503-5p* overexpression and inhibition. HCC827 cells were transiently transfected with **A)** miRIDIAN *miR-503-5p* mimics (GE) at 40 nM using RNAiMAX (Invitrogen). *GABARAPL1* downregulation was determined at a 48 h and 72 h post-transfection time. **B)** Proteins were harvested after 48 h and assessed for GABARAPL1 expression (Molecular weight: 14 kDa). GAPDH (Molecular weight: 37 kDa) was used as loading control. **C)** HCC827 cells were transiently transfected with miRIDIAN *miR-503-5p* Hairpin inhibitor (GE) at 100 nM using RNAiMAX (Invitrogen) and assessed for the derepression of target mRNA levels of *GABABRAL1* after 72 h. mRNA normalization was performed using *ACTB*. Linear relative fold changes are shown. Statistical analysis employed the unpaired two sided t-Test (**p < 0.01; ***p < 0.001). Standard deviations were calculated from three experiments.
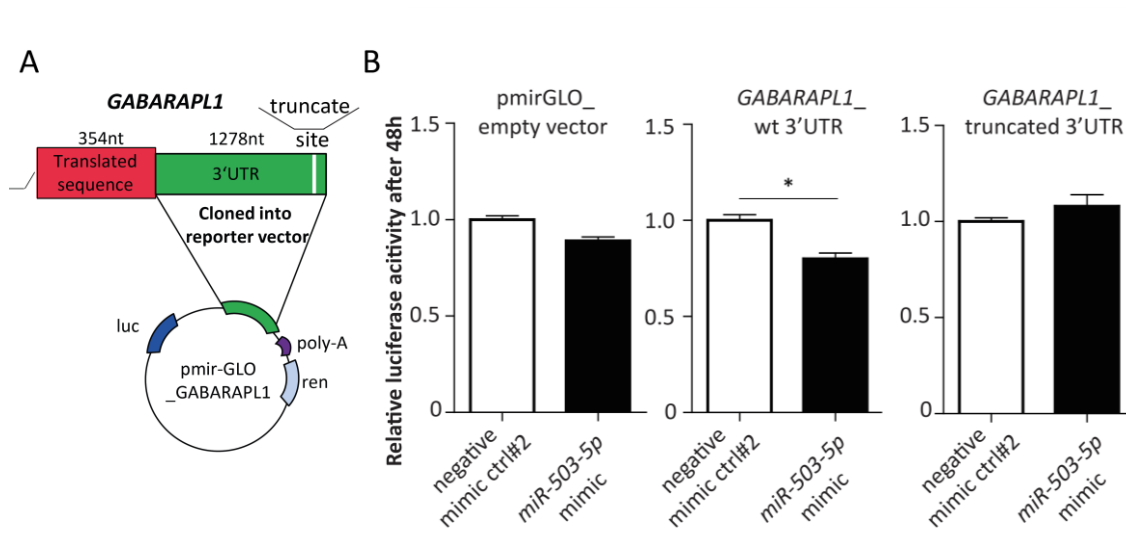
Figure 37 Direct interaction of *miR-503-5p* and *GABARAPL1* identified by 3'UTR Luciferase assay. A) *GABARAPL1* 3´UTR containing a seed region for *miR-503-5p* was cloned into pmirGLO luciferase vector containing firefly luiferase (luc) and a renilla reporter (ren) for normalization. **B)** HCC827 cells were transfected with empty pmirGLO vector, pmirGLO containing *GABARAPL1* 3´UTR, and pmirGLO containing truncated *GABARAPL1* 3'UTR and co-transfected with mimic *miR-503-5p* (40 nM) or miRNA negative mimic control#2 (40 nM). Statistical analysis employed the unpaired two sided t-Test (*p < 0.05). The graphs show values out of three independent experiments each with six replicates.

3.8 Autophagy regulation in HCC827 co-culture

3.8.1 Increase of autophagy markers SQSTM1 (p62), LC3B-II after Bafilomycin A1 treatment

One of the most commonly used approaches to assess autophagy is to determine the conversion from endogenous LC3B-I to LC3B-II, whereby the LC3B-II indicates the lipidated form of LC3B (LC3B-II). Moreover expression of the autophagy marker SQSTM1 (p62) is commonly assessed by Western Blot. Inhibition of late stage autophagy by Bafilomycin A1, a specific inhibitor of the vacuolar-type H+-ATPase [141] results in the increase of autophagosomes (Figure 38 A).

Blocking the fusion resulted in the increase of SQSTM1 and LC3B-II after 24 h using different concentrations of Bafilomycin A1 indicating accumulation of these proteins within the autophagosome and thus defective autophagy (Figure 38 B). GABARAPL1 was also observed to be increased after Bafilomycin A1 treatment. Moreover, different time points 6 h - 48 h were also tested, which showed comparable results (data not shown).

GABARAPL1 belongs to the Atg8 family and shares 29% sequence similarity with LC3 [142, 143]. It can also be lipidated forming GABARAPL1-II. However, here it could not be determined whether the second lower band is the lipidated form of GABARAPL1 or the result of cross-reaction with GABARAP, which shows 86% similarity with GABARAPL1 (UniProt

Alignment, data not shown). The siRNA-mediated knockdown of *GABARAPL1* resulted in the reduction of the upper band (Figure 40). However, the lower band did not disappear suggesting that cross-reaction with another protein with high sequence similarity such as GABARAP is the more likely reason for the lower band.
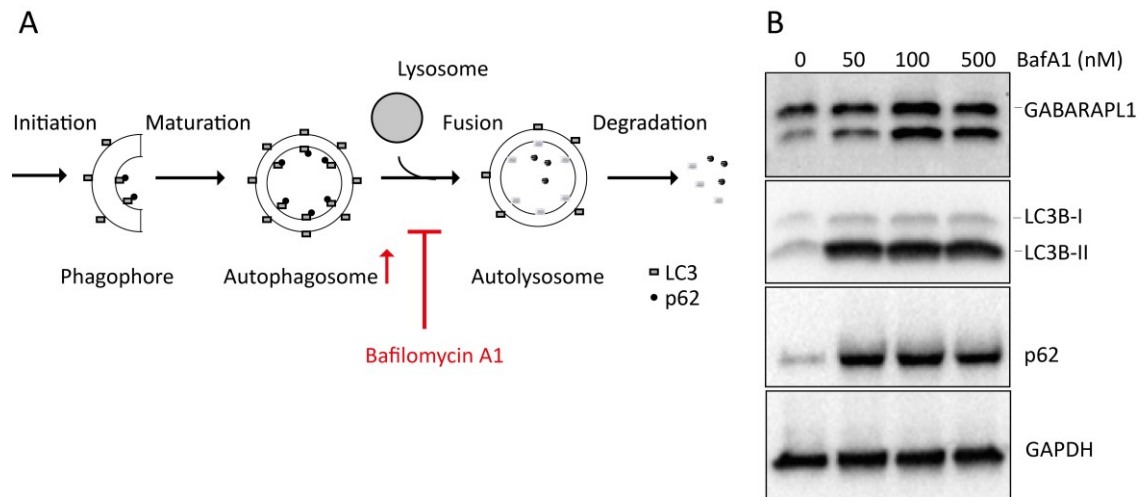
Figure 38 Autophagy markers after Bafilomycin A1 treatment. A) Schematic representation of autophagic pathway. Bafilomycin A1 (BafA1) inhibits fusion of autophagosome and lysosomes. **B)** Expression of autophagy markers LC3B, SQSTM1 (p62) and GABARAPL1 after treatment of HCC827 cells with DMSO and different concentration of BafA1 (50-500 nM) for 24 h. GAPDH was used as loading control. The second lower band of GABARAPL1 is discussed in section 3.8.1. Molecular weight: GABARAPL1: 14 kDa; SQSTM1: 62 kDa; LC3B: 14; 16 kDa.

3.8.2 Deregulation of autophagic activity after gefitinib treatment and subsequent co-culture

To test GABARAPL1 protein expression in co-culture, GABARAPL1 was measured on Western Blot. After gefitinib treatment, a known inducer of autophagy [144], GABARAPL1 was upregulated after 48 h and 72 h (HCC+/- vs -/-: 1.4 x and 1.5 x) but decreased by 20% in HCC+/+ vs +/- (Figure 39 A/B) after 48 h and 72 h. These results were corroborated in cells cultured with HGF and gefitinib treatment, where GABARAPL1 was observed to be upregulated (HCC+/- vs -/-: 1.3 x – 1.4 x), while the comparison HCC+/+ vs +/- showed a decrease by 50% (Supplemental Figure 4).

To identify autophagy regulation in co-cultured cells, SQSTM1 (p62) levels were measured. SQSTM1 is an adapter protein that can bind many different proteins to form protein complexes. For example, it can bind LC3 and other substrates to the inner surface during the maturation of the phagophore to transport it to autophagosomes for degradation. If autophagy is defective, SQSTM1 accumulates in the cytoplasm [145-147]. SQSTM1 levels were observed to be marginally reduced upon gefitinib treatment in comparison to DMSO

treatment after 48 h and 72 h (HCC+/- vs -/-: 0.9 x) (Figure 39 A/B). Although gefitinib is an inducer of autophagy, decrease of SQSTM1 was marginal maybe due its low concentration (0.5 µM). Upon co-culture, SQSTM1 levels were increased in comparison to treated cells after 48 h and 72 h (HCC+/+ vs +/-: 1.2 x and 1.3 x) (Figure 39 A/B). These results were corroborated from *in-vitro* culture after HGF administration (HCC+/+ vs +/-: 2.1 x) (Supplemental Figure 4).

Moreover, conversion of LC3B-I to LC3B-II could also be clearly observed after gefitinib treatment for 72 h. Gefitinib treatment resulted in increased levels of LC3B-II in comparison to DMSO control (1.7 x). Co-culture after gefitinib treatment resulted in the reduction of LC3B-II (0.7 x). Increase of the lipidated form of LC3B (LC3B-II) between the different culture conditions is associated with deregulated autophagic activity

In this study, slightly increased levels of SQSTM1 and decreased levels of LC3B-II were found in resistant HCC827 cells while GABARAPL1 showed inverse regulation indicating deregulation of autophagic activity.
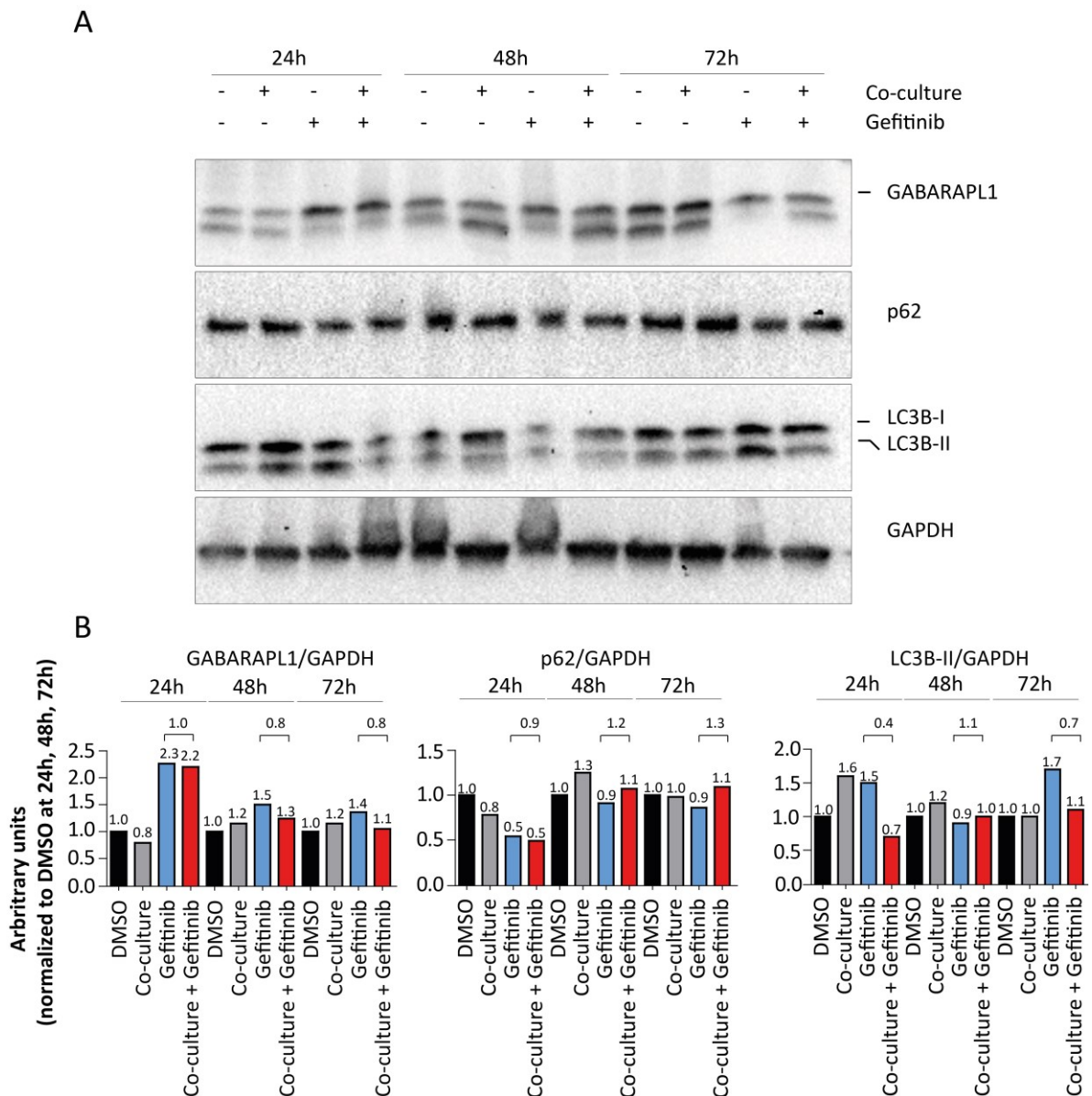
Figure 39 Expression of SQSTM1 (p62) and GABARAPL1 in resistant HCC827 cells. HCC827 cells were cultured with or without gefitinib (0.5 μM) in the presence or absence of **A)** MRC-5 cells for 24-72 h. **B)** Densitometric analysis of GABARAPL1, SQSTM1, and LC3B-II. The analysis was performed using ImageLab 5.2.1. Protein levels were normalized to internal GAPDH levels. Predicted molecular weight: SQSTM1: 62kDa, LC3B: 14, 16 kDA, GABARAPL1:14 kDa.

3.8.3 Accumulation of SQSTM1 after *GABARAPL1* knockdown indicates defective autophagy

Since *miR-503-5p* has a plethora of targets, this study focused on the possible role of GABARAPL1 as it was found to interact with this miRNA. To assess the role of GABARAPL1 in autophagy, the autophagy marker SQSTM1 (p62) was measured after knockdown of *GABARAPL1*. Four different siRNAs were used to knockdown *GABARAPL1*. The siRNA-mediated knockdown of *GABARAPL1* showed 5% - 19% expression depending on the siRNA (Supplemental Figure 3). Three out of four (siGABARAPL1#6, #8, and #9)

were considered as effective siRNAs and were selected for further analysis. Upon knockdown of *GABARAPL1*, the expression of SQSTM1 was clearly increased after 48 h (#6: 2.4 x; #8: 1.6 x; #9: 3.3 x) (Figure 40 A/C). This suggested that reduction of GABARAPL1 results in defective autophagy.

The siRNA-mediated knockdown of *GABARAPL1* expression resulted in slightly increased LC3B-II expression after 24 h and 48 h (Figure 40 B). The increase of LC3B-II expression may be the result of compensating the loss of GABARAPL1 and is therefore increased [148]. Transfection with siRNAs against *GABARAPL1* reduced the GABARAPL1 protein to more than 95% in all siRNA-mediated transfections.

These data suggested that siRNA-mediated knockdown of *GABARAPL1* results in increased SQSTM1 levels indicating accumulation of this protein due to defective autophagy.
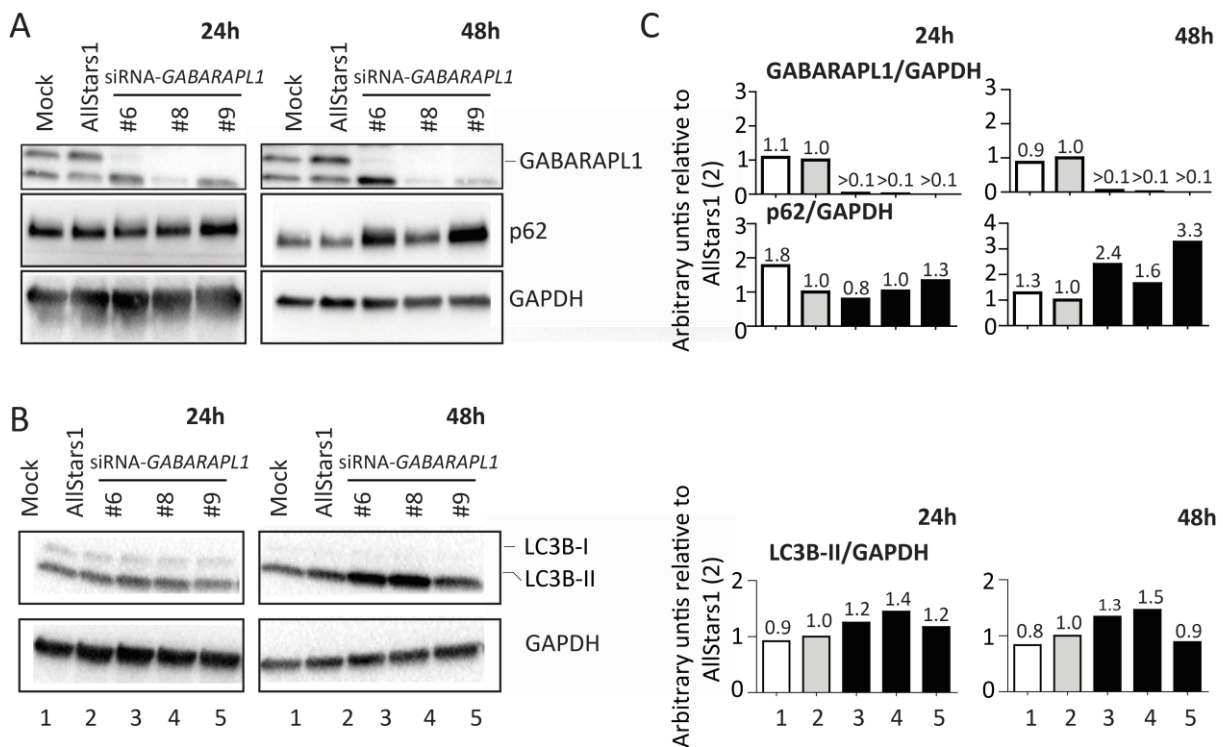
Figure 40 Expression of SQSTM1 (p62) and GABARAPL1 after siRNA-mediated knockdown of GABARAPL1. HCC827 cells were transfected with three different siRNAs (10 nM) against *GABARAPL1* and AllStars1 (10 nM) or Mock for **A)** 24 h and 48 h. **B)** LC3B expression was measured after treatment as described in A). **C)** Densitometric analysis of GABARAPL1, SQSTM1 and LC3B-II was performed using ImageLab 5.2.1. Molecular weight: SQSTM1: 62kDa, LC3B: 14, 16 kDA, GABARAPL1:14 kDa. (24 h/48 h). 1: Mock, 2: AllStars1, 3-5: siRNA-mediated knockdown of *GABARAPL1*#6, #8, and #9.

In summary, miRNAs and mRNAs were investigated in the development of resistance using a gefitinib co-culture model. Gefitinib-sensitive HCC827 and PC-9 cells were co-cultured with lung fibroblasts (MRC-5).

Global miRNA analysis revealed expression changes associated with EGFR-TKI resistance. Eleven miRNAs were selected, out of which *miR-503-5p* was validated in both cell lines. Inhibition of EGFR activity by gefitinib resulted in the reduction of *miR-503-5p*. The subsequent co-culture following treatment with gefitinib resulted in the increase of *miR-503-5p*. Although the expression of *miR-503-5p* was reduced after gefitinib treatment in HCC827 cells, no difference of this miRNA was found in other lung cancer cells, which had lower sensitivities to gefitinib.

Subsequently, global gene expression profiling revealed 211 differentially expressed mRNAs in the resistant HCC827 and PC-9 cells. Based on the gene expression profile, an enrichment of genes that are involved in cell migration and apoptosis was found after treatment with gefitinib. In the resistant cells, genes associated with apoptosis were downregulated, whereas cell cycle genes were upregulated. To determine potential miRNA target genes of *miR-503-5p*, the global gene expression profiling was compared with miRNA prediction databases. Several predicted target genes of *miR-503-5p* were identified. Among these, *GABARAPL1* was verified as a putative target. Ectopic overexpression of *miR-503-5p* resulted in a significant reduction of *GABARAPL1* mRNA and protein. Moreover, direct interaction was shown by 3'UTR luciferase reporter assay. Deregulation of autophagy was indicated by the reduced protein levels of SQSTM1 and increased LC3B-II after gefitinib treatment. Resistant HCC827 cells showed an accumulation of SQSTM1 but lower LC3B-II protein content. Since GABARAPL1 has been suggested to play a role in autophagy, siRNA-mediated knockdown of *GABARAPL1* resulted in the accumulation of SQSTM1. This indicated that autophagy was defective in NSCLC with reduced GABARAPL1 expression.

4 Discussion

Improving the stratification of lung cancer patients through biomarkers can help clinicians to select the optimal strategy for patient care. Circulating miRNAs have been suggested as stable, non-invasive biomarkers in body fluids such as serum in cancer detection [93, 94]. The identification of prognostic tumor-specific circulating miRNA profiles in patients with operable NSCLC may provide a blueprint for better patient care and treatment. Moreover, circulating miRNAs can serve as cost-effective markers to enable monitoring before and after patients' therapy, or furthermore, for the risk assessment of operable or not operable NSCLC patients. Many miRNA markers have been suggested as diagnostic and prognostic markers in NSCLC [85, 101, 102, 104, 120]. In this study, miRNAs were not only evaluated in the context of the progression of the tumor at early stages of NSCLC patients, but also after therapy in NSCLC cells. In order to focus on a specific signaling pathway, NSCLC cells that harbor the druggable target EGFR were analyzed after treatment. Moreover, miRNA regulation was studied in EGFR-TKI treated NSCLC cells. Although patients with activating mutations in *EGFR* respond well to EGFR-TKI treatment, almost all NSCLC patients ultimately develop resistance to these agents [149, 150]. Since miRNAs are known to be key molecules in tumor progression, this research assessed both their potential as prognostic markers as well as their functional relevance to contribute to a metastatic phenotype in NSCLC. Therefore, the aim of this PhD work was:

- **Firstly,** to identify circulating miRNAs as prognostic markers for early-stage lung adenocarcinoma.

- **Secondly**, to evaluate the involvement of miRNAs in NSCLC tumor progression. In therapy resistance, miRNAs were hypothesized to be involved in mediating the resistance towards gefitinib in lung cancer cells via the induction of stromal cells. Therefore, the crosstalk between tumor cells and stromal fibroblasts and its underlying miRNA signaling network in NSCLCs that may modulate gefitinib resistance was elucidated.

4.1 Circulating miRNAs as markers for early-stage lung adenocarcinoma.

4.1.1 Pre-analytical consideration for circulating miRNA analysis

For the analysis of circulating miRNAs, it is critical to have adequately defined pre-analytical parameters that are standardized for the collection of a blood sample. In particular, the differences between miRNA expression levels from different blood sampling, via venipuncture or arterial sampling, are still poorly understood. In this present study, two cohorts of 65 patients (blood drawn via arterial catheter) and 210 patients (blood drawn via venipuncture) were measured. The increased expression for all selected miRNAs in samples in which blood was drawn via venipuncture in comparison to samples withdrawn via an arterial catheter was observed. To further evaluate differences in blood drawings that influence miRNA expression, serum samples from the same patient were derived from venous blood before and on the day of surgery, as well as after the induction of anesthesia via an arterial catheter. Again, almost all the selected miRNAs showed an increase in samples isolated from venous blood. It remains elusive, however, whether the induction of anesthesia or the vessel puncture procedure is critical for the findings.

Kahn *et al*. identified different expression levels of three biomarkers: Squamous Cell Carcinoma antigen (SCC), Carcinoembrionic Antigen (CEA), and CYFRA 21-1. The expression level of SCC was dependent on the procedure of blood withdrawal. Its expression was increased in samples in which blood was taken via arterial catheter through the induction of anesthesia in comparison to samples via venipuncture [121].

Thorpe *et al*. reported that blood collection by different blood drawing procedures resulted in differences in the ovarian cancer serum marker prolactin. Their study found that prolactin levels were markedly increased at the time of surgery in comparison to samples prior to surgery [151]. Differential expression of miRNAs in arterial and peripheral venous plasma was already observed in patients with gastric cancer. However, they observed decreased and increased miRNA expression in peripheral venous samples in comparison to arterial blood [152].

As miRNAs are known to be deregulated under hypoxic conditions [153, 154], different oxygen levels in arterial and venous blood may influence miRNA regulation.

miRNAs have been shown to be taken up by recipient cells and to be communicators between cells [97]. Therefore, one may also speculate that miRNA expression levels withdrawn from arterial blood should be higher in comparison to blood withdrawn via venipuncture, as miRNAs may be absorbed and taken up by cells, because blood flows first from arterial to venous circulation. This is, however, contradictory to the results presented here, in which

most of the miRNAs have been shown to be higher in venous blood than in arterial blood. One can assume that the increase of specific miRNAs in serum samples from blood withdrawn via venipuncture might derive from actively secreting tumor cells. Moreover, the passive leakage of miRNAs via apoptosis or necrosis might also be possible [155]. It is also likely that differences are caused due to the different composition of arterial and venous blood, which results in different PCR efficiencies, and thus, differently measured miRNA expression levels. Further studies must be conducted in order to clarify the differential expression of miRNA withdrawn from venous and arterial blood.

From internal discussions, in this study, it is known that serum from blood drawn via arterial catheters is subjected to one freeze and thaw cycle to room temperature. The decreased miRNA expression may be due to the release of miRNAs from exosomes or AGO proteins and their subsequent degradation via RNases after a freeze and thaw cycle. Although the found differences were subtle, they were systematic.

Although Mitchell *et al.* reported no difference of miRNAs after freeze and thaw cycles [93], Grasedieck *et al.* showed that the repeated freeze and thaw cycles of miRNAs at room temperature decreased miRNA levels [96]. The differences in miRNA expression between both studies may be explained by several reasons. For example, Mitchell *et al.* [93] performed studies using plasma, whereas Grasedieck *et al.* [96] used serum samples. Moreover, in both studies repeated freeze and thaw cycles were performed with low numbers of miRNAs. Global miRNA analysis might provide a broader picture as to whether certain miRNA populations are expressed differentially after repeated freeze and thaw cycles. Therefore, the changes in miRNA expression levels cannot only be influenced by different blood drawing procedures, but also by freeze and thaw cycles.

In order to minimize variation in miRNA expression analysis, serum sample sets should be considered for pre-analytical variables such as blood withdrawal as well as freeze and thaw cycles.

4.1.2 Evaluation of circulating miRNA candidates as prognostic markers in NSCLC

As in a previous study, *miR-142-3p* was identified to be associated with the early recurrence of NSCLC [120], this miRNAs was again studied in another cohort of n = 65 patients, which were sampled via an arterial catheter. Again, the miRNA expression of *miR-142-3p* showed a tendency to be increased in patients with an early recurrence of lung adenocarcinoma.

In this study, hemolysis was evaluated in serum samples. *miR-20b-5p* and *miR-486-5p* were identified as strongly correlated with hemolytic miRNA *miR-451a*. However, hemolysis was not associated with overall or recurrence-free survival. *miR-486-5p* has previously been

described as a prognostic biomarker for NSCLC [104]. Hemolysis has been shown to affect miRNA expression levels elsewhere [111], in particular, *miR-16* and *miR-451a*. It remains elusive, however, as to whether hemolysis in this study as well as others occurs during blood processing or as a result of a disease.

After excluding the hemolytic miRNAs, the prognostic potential of a miRNA panel in early-stage (I-IIIa) lung adenocarcinoma patients was evaluated. These miRNAs were selected as they were described to play a role as prognostic or diagnostic markers in NSCLC in different studies [101, 102, 104-107, 120, 129-131]. A panel of miRNAs was calculated using Cox-regression models as prognostic markers. As a result of the tumor heterogeneity among patients, the use of a biomarker panel was expected to be more sensitive and specific than single markers [156].

miR-29b-3p expression showed the strongest prognostic association. This miRNA has previously been described in NSCLC to promote tumor invasiveness. Patients with high-c-MYC and low *miR-29b* levels were associated with poor OS and RFS [157]. *miR-29b-3p*, *miR-125b-5p*, and *miR-331-3p* were identified as a panel, but were not able to significantly discriminate high-risk and low-risk patients. The combining of staging information and the miRNA panel was not significantly beneficial to stratify high and low-risk patients.

In conclusion, this study evaluated the prognostic potential of a miRNA panel in early-stage (I-IIIa) lung adenocarcinoma patients. Increased *miR-142-3p* levels were identified and associated with poor prognosis in early-stage lung adenocarcinoma.

This study highlights the importance of pre-analytical variables for the analysis of circulating miRNAs from serum samples. It showed that blood-collection via venipuncture results in higher expression levels of selected circulating miRNAs in comparison to blood-collection via an arterial catheter. Moreover, the expression of *miR-20b-5p* and *miR-486-5p* in serum of NSCLC were found to be strongly associated with hemolysis.

4.2 Role of miRNAs in therapy resistance of lung adenocarcinoma cells

4.2.1 Acquired resistance mechanisms towards EGFR-TKI of lung adenocarcinoma

In order to further evaluate the involvement of miRNAs in the progression of NSCLC, a resistance model towards gefitinib was used, which Wang *et al.* have described [46].

In this study, NSCLC cells that harbor an inframe deletion of exon 19 in *EGFR* were used. The inframe deletion of exon 19 is an activating mutation [149]. Up to 10 to 20% of patients from Europe and 40 to 60% of Asians carry an activation mutation of *EGFR* [36, 158].

Therapy with the first generation EGFR-TKI inhibitor gefitinib has shown remarkable tumor shrinkage and an improvement in progression-free survival [25]. Patients, however, do commonly develop a resistance towards the targeted therapy [149]. This study used a NSCLC resistance model towards gefitinib to identify the differential regulation of miRNAs and target genes. Not all cells died from the gefitinib treatment, which may be due to the presence of a pre-existing *MET* amplification, which allows these cells to survive the treatment [44]. The administration of gefitinib results in a kinase-dependent reduction of cell viability. The model from Wang *et al.* enables a fast-track model to analyze molecules that affect EGFR-TKI sensitivity. The co-culture system, in comparison to stable EGFR-TKI resistant cells, enables the analysis of the interaction between tumor and fibroblast cells. Moreover, the EGFR-TKI gefitinib allows a more physiological condition through a reduction of tyrosine kinase activity, whereas other studies instead use artificial approaches by shRNA-mediated *EGFR* knockdown [117], which is kinase-independent, as it identifies the deregulation of downstream targets.

To further explore the paracrine factors that induce the resistance of gefitinib treated NSCLC cells, a panel of growth factors, cytokines and chemokines were analyzed.

The cell culture medium of fibroblasts alone resulted in the resistance of HCC827 cells to gefitinib. The reduced levels of HGF in the co-culture medium, in comparison to the MRC-5 culture medium, may be a consequence of the binding of HGF, which is produced by MRC-5 cells, to the membrane receptor MET on the surface of HCC827 cells. In this study, HGF was identified to be prominently secreted and able to induce resistance in HCC827 cells. This finding is consistent with other reports that demonstrated an HGF-mediated resistance towards gefitinib [46]. Several MET inhibitors were tested using the co-culture system [159] and in clinical trials [160], however, no inhibitor received the FDA's approval to be used in cases of lung cancer.

In this study, VEGF was also found to be a putative target to overcome insensitivity towards gefitinib in HCC827 cells. In EGFR-TKI-resistant lung cancer cells, HGF may induce VEGF. These results were consistent with Takeuchi and his colleagues, who showed that MET activation in PC-9 cells by HGF resulted in increased VEGF production [161]. Increased VEGF production is known to induce tumor angiogenesis [162], and is a potential mechanism to overcome the EGFR blockade [163].

CSF2 was another factor that was found to be increased in the co-culture relative to the single tumor cell culture medium. The mRNA levels of the cell membrane receptor *CSF2RA* was increased in the tumor cell lines in comparison to the fibroblasts, which suggests that the

ligand may bind to the CSF2 receptor. Administration of CSF2, however, did not result in insensitivity towards gefitinib (data not shown). CSF2 was also found to be upregulated in EGFR-TKI resistant HNSCC cells [164].

In this study, the IL6 and IL8 signaling proved to be increased in the co-culture, but decreased in the single culture. Although the abundance of IL6 and IL8 was already very high in the cell culture medium, the activation of the IL6 receptor may require high levels of the ligand to induce insensitivity towards gefitinib. Reports have found the TGF-beta-IL6 axis mediates resistance towards erlotinib treatment in a mouse model [165]. Moreover, it has been shown that metformin can sensitize EGFR-TKI resistant lung cancer cells by decreasing IL6 signaling [166]. Interestingly, the IL6R/JAK1/STAT3 signaling has been reported to induce resistance towards the irreversible EGFR-TKI afatinib, which is also critical to the interaction between fibroblast cells MRC-5 and lung cancer cells [167]. The IL8 signaling has also been suggested to be involved in resistance towards gefitinib. Liu *et al*. demonstrated that the suppression of IL8 in PC-9 cells resistant to gefitinib resulted in the increase of dead cells in combination with gefitinib through the reduction of the stemness-related genes (*ALDH1A1*, *NANOG*, and *SOX2*). Moreover, increased IL8 expression was associated with poor progression-free survival of EGFR-TKI treated lung adenocarcinoma patients [168].

In breast cancer, GRO (CXCL1) has also been described to be involved and overexpressed in metastatic sites. It can attract $CD11b^+Gr1^+$ myeloid cells, which in turn results in increased cell survival [169].

Moreover, Zhang *et al*. have reported activation of the AXL kinase as one of the main reasons for acquired resistance to treatment to both gefitinib and erlotinib in *EGFR*-mutant NSCLC patients. HCC827 cells that were resistant to erlotinib showed increased *AXL* expression and were shown to have an aggressive phenotype (increased cell migration and associated with epithelial-to-mesenchymal transition properties) *in-vitro* and *in-vivo.* The siRNA-mediated knockdown of *AXL* was shown to increase sensitivity to erlotinib in *EGFR*-mutant HCC827 cells, although not in erlotinib-resistant cell lines [170].

In summary, HGF secreted from fibroblast cells was the strongest inducer of resistance towards gefitinib in NSCLC cells HCC827 and PC-9.

4.2.2 *miR-503-5p* identified to be involved in gefitinib resistant lung adenocarcinoma cells

To determine differentially expressed miRNAs in resistant and sensitive cells, miRNAs between gefitinib treated cells versus subsequently co-cultured cells were analyzed. A total of 31 miRNAs were observed to be differentially regulated.

miR-503-5p was found to be the most interesting candidate involved in the gefitinib-insensitive HCC827 cells. Within this study, *miR-503-5p* was found to be inhibited by reducing EGFR activity using gefitinib in HCC827 cells. Other cell lines with wild-type *EGFR* or lung cancer cell lines with lower sensitivity towards gefitinib showed nearly no regulation after gefitinib treatment. The co-culture or HGF alone did not change *miR-503-5p* expression, however, in cases that cells were pre-treated with gefitinib, the co-culture or HGF treatment resulted in the restoration of *miR-503-5p* expression. This result suggests that *miR-503-5p* can only compensate its expression after co-culture or HGF induction if the EGFR activity is reduced. Its expression may be dependent on a certain threshold. To identify the downstream factors of EGFR and MET responsible for *miR-503-5p* deregulation, transcription factors binding to upstream sequences of *miR-503-5p* must be studied. For example, it has been found that MET induces the activation of ELK1 transcription factor, which can induce the expression of the *miR-23a-27a-2-2 cluster*. Interestingly, *miR-27a* was able to downregulate the expression of *MET* and *EGFR* by binding to their 3'UTR and/or by downregulating the expression of *SPRY2* [171]. Therefore, it would be of interest to identify transcription factors that regulate miRNAs, for example the binding of ELK1 at promoter regions of *miR-503-5p*, through the application of chromatin immunoprecipitation experiments.

miR-503-5p is located on the X-chromosome and clusters with other miRNAs such as *miR-424*, *miR-542*, and the *miR-450* family. Reports have shown that *miR-503-5p* promotes tumor progression in other cancer types. Patients with esophagal cancer that have a high expression of *miR-503-5p* had poorer disease-free survival [172]. *miR-503-5p* was found to be overexpressed in adenocarcinomas in comparison to adenomas and normal mucosa [173]. Ectopic overexpression in colon adenocarcinoma cells resulted in increased malignant transformation and was shown to confer tumorigenicity *in-vivo*. The inhibition of *miR-503-5p* resulted in decreased cell proliferation, migration, and cell invasion, but in increased apoptosis, which might partly be due to the regulation of the tumor-suppressor *FBXW7*. However, it has also frequently been reported to have tumor suppressive functions in lung cancer. For example, it has been reported to regulate the anti-apoptotic protein BCL2 or PI3K p85 and IKBKB [174-176]. Li *et al*. showed through combined bisulfite restriction analysis

that the expression of *miR-503-5p* is inversely correlated with its methylation status, and moreover, that it can target *FANCA* [175].

It would be beneficial to generate a stable cell line that could constitutively express the miRNA or to use an inducible system. Further insight into long-term expression analysis may be achieved through a stable transfection of *miR-503-5p*, as it allows to be used in xenograft models to analyze tumor growth *in-vivo*.

Within the screening data of this study, further miRNAs have also been identified by other groups to play a role in the resistance of EGFR-TKI NSCLC cells. For example, here it was shown that *miR-34a* was upregulated after gefitinib treatment, but downregulated after subsequent co-culture. Zhou *et al*. also identified *miR-34a* upregulation after gefitinib treatment. This miRNA was found to induce apoptosis in the very same cells, partially through the reduction of MET expression. By ectopic overexpression of *miR-34a* Zhou *et al*. could show that resistance towards gefitinib is reduced if it is combined with the miRNA [177].

Moreover, *miR-29b-3p* and *5p* and *miR-222-5p* were found to be downregulated after gefitinib treatment and upregulated after subsequent co-culture. Interestingly, Garofalo *et al*. identified *miR-29a* and *miR-29c, miR-222* to be downregulated after drug exposure with gefitinib in HCC827 and PC-9 cells. The authors have identified these miRNA from a screen after developing a stable knockdown of *MET* and *EGFR* that used shRNA lentiviral particles [117]. The overexpression of *miR-221/222* resulted in more resistant cells towards gefitinib treatment. Interestingly, the opposite arm of the mature *miR-29b-1-5p* sequence, the miR-*29b-3p*, has been associated with overall survival in the serum of early stage NSCLC patients [120].

Within the screening dataset from this PhD work, *miR-181a-5p* was found to be upregulated after gefitinib treatment. This miRNA has been described to be downregulated in most tumors and reported to function as a tumor suppressing gene [178-180]. *miR-181a-5p* belongs to the *miR-181* family, which includes the four different miRNAs *miR-181a*, *b*, *c*, and d. Ectopic overexpression of *miR-181a-5p* was shown to reduce cell migration in COS-1 cells. Moreover, the levels of *miR-181a-5p* were lower in the invasive front of human colonic mucosal cells in relative to tumor-adjacent normal epithelial cells [181].

4.2.3 The autophagy gene *GABARAPL1* is a target of *miR-503-5p*

A global transcriptomic profiling was performed to search for differentially regulated mRNAs involved in the co-culture model. The expression data of HCC827 and PC-9 cells were compared and common mRNAs were selected.

In total, 211 mRNAs were found to be deregulated. Most of the upregulated mRNAs were associated with the cell cycle and the response to a DNA damage stimulus. Genes involved in vesicle mediated transport, neuron differentiation, and cell morphogenesis were downregulated.

Early growth response 1 (*EGR1*) was the top upregulated mRNA in the dataset. Consistent with the presented data, the *EGR1* gene was found to be downregulated after gefitinib treatment [182]. However, EGF stimulation was shown to upregulate *EGR1* expression in *EGFR*-mutant NSCLC cells. Another report described that impaired nuclear translocation of EGR1 results in PTEN loss, and thus results in the acquisition of resistance to gefitinib [183].

The Aurora-A kinase (*AURKA*) family has also been described to be upregulated under the same experimental conditions in the co-cultured treated cells in comparison to only treated cells [184]. Interestingly, the overexpression of *AURKA* has proven to reduce gefitinib sensitivity. The insensitivity towards gefitinib by AURKA could be lowered by transfecting *EGFR* mutant NSCLC cells with the shRNA mediated-knockdown of *AURKA*.

When combining the mRNA data sets from the microarray and database predicting miRNA target genes, four mRNAs were observed to be potentially targeted by *miR-503-5p*. From the four mRNAs, *GABARAPL1* was validated by qRT-PCR, Western Blot and Luciferase Assay System using 3'UTR-reporter constructs to be targeted by *miR-503-5p*. GABARAP, which was first described as an early estrogen-regulated gene [185], was later found to be an ubiquitin-like modifier and involved in intracellular trafficking of GABA$_A$R, a type-A ionotropic receptor and ligand-gated chloride channel mediating inhibitory neurotransmission. GABARAPL1 shares 86% identity with GABARAP [186]. The GABARAP family (GABARAP, GABARAPL1, GABARAPL2, and GABARAPL3) belongs to the Atg8 family. The MAP-LC3 (Microtubule-associated protein light chain 3), which consists of MAP1A (LC3A), MAP1B (LC3B), and MAP1C (LC3C), also belongs to this subfamily of Atg8. GABARAPL1 has been reported to increase the expression of the kappa-type opioid receptor on the cell surface [187]. It can link the receptor GABA$_A$R and tubulin [142]. Chakrama *et al.* associated GABARAPL1 with autophagic vesicles [188], which thereby indicates that it is not only involved in the trafficking of proteins, but is also involved in processes such as autophagy. Autophagy is a catabolic process that involves the degradation of superfluous

cellular components such as intracellular proteins, lipids, and organelles so that the cell maintains homeostasis. The degradation takes place in lysosomes and the degraded products are then exported into the cytoplasm for recycling. The conjugation of Atg8 to the phosphatidylethanolamine (PE) lipid is critical for phagophore formation [189]. Although both the LC3s and GABARAPs are critical during the maturation of the autophagosome for the autophagic process, the GABARAP, including GABARAPL1 and LC3 family members, have been reported to have distinct roles in the autophagic process. Through the deletion of each of the family members, Weidberg *et al.* could show that GABARAPs are essential after the elongation of the phagophore membrane, which the LC3s mediated [190].

4.2.4 Role of autophagy in EGFR-TKI resistant HCC827 cells

Autophagy regulation in the co-culture model was further determined by analyzing the expression of GABARAPL1 and the standard autophagy markers LC3B and SQSTM1. GABARAPL1 and LC3B-II were increased after gefitinib treatment and decreased after subsequent co-culture. This dynamic suggested that autophagic activity has changed.

To further evaluate autophagic activity, the autophagy marker Sequestome 1 (SQSTM1/p62), was taken into consideration. SQSTM1 is also known as an adaptor protein that can target specific cargo via its ubiquitin-associated (UBA) domain and LC3A and B and the GABARAP proteins via its LC3-interacting region (LIR) domain for autophagic processing [191, 192]. In this study, SQSTM1 was slightly accumulated in the resistant cells, which indicated further suppressed autophagy in comparison to cells that were solely treated with gefitinib. Cells with homeostatic metabolism have low SQSTM1 levels due to clearance by autophagy. In mice with deficient autophagy, SQSTM1 was observed to accumulate in the cytoplasm [193]. SQSTM1 is involved in a plethora of cellular functions such as cell growth, survival, and mitosis through the interaction with different binding partners. For example, SQSTM1 has been reported to activate NFKB1 (NF-κB), which leads to cell growth [194]. Activation of NFKB1 has been sown to rescue erlotinib-induced cell death in HCC827 cells *in-vitro* and *in-vivo* by reducing the expression of the inhibitor of NFKB1 (NFKBIA). Moreover, low NFKBIA expression, indicating high-NFKB1 activation, was measured in *EGFR*-mutant lung cancer patients treated with erlotinib with poor progression-free and overall-survival [195]. The accumulation of SQSTM1 was associated with a poor overall rate of survival in patients with NSCLC [196]. SQSTM1 releases and stabilizes nuclear factor erythroid 2-related factor 2 (NFE2L2/Nrf2) from KEAP1, and therefore, activates NFE2L2, which leads to the induction of the antioxidant defence system [197]. Yamadori *et al.* have

shown that NFE2L2 was constitutively activated in the NSCLC cell line PC-9 that harbors the *EGFR*-activation mutation, whereas treatment with EGFR-TKI resulted in the downregulation of NFE2L2. Moreover, their study revealed that the knockdown of *KEAP1* resulted in increased cell growth. Interestingly, their study demonstrated EGFR-TKI resistance in a patient with advanced NSCLC harboring a gene mutation in *KEAP1* [198]. It would, therefore, be interesting to determine a regulation of NFE2L2 by *miR-503-5p* that may contribute to EGFR-TKI resistance in *EGFR*-mutant NSCLC cells.

SQSTM1 has been shown to be regulated by the MTOR pathway, which is critical to the autophagy pathway [199]. The MTOR pathway was analyzed in order to further emphasize the involvement of autophagic processes. Active MTOR is known to suppress autophagy [200]. Using the Luminex system, the phosphorylation status of several members of the MTOR/AKT pathway was analyzed. In this study, phosphorylation of MTOR was shown to be slightly downregulated upon gefitinib treatment. However, after co-culture, p-MTOR was slightly upregulated. RPS6KB1, a downstream target of MTOR, was also shown to be downregulated after gefitinib treatment. Activated RPS6KB1 has been associated with reduced autophagy [201, 202]. However, RPS6KB1 and its substrate RPS6 have been shown to promote autophagy [202, 203]. The dual role of RPS6KB1 in autophagy may be the result of varied experimental settings, i.e. it has a positive role under nutrient deprivation, but under normal conditions and if autophagy is fatal to the cell, it has a negative role on autophagy [204]. Activated AKT has also been shown to suppress autophagy [205]. AKT activation phosphorylates MTOR, which in turn suppresses the autophagic processes. In this study, p-AKT was also shown to be downregulated after gefitinib treatment and increased from subsequent co-culture. Active TSC2 has also been described to repress MTOR [206]. In TSC2-null mouse embryonic fibroblasts (MEFs) reduced autophagy was reported in comparison to TSC2- positive controls [207]. In line with the study, in which phosphorylation of GSK3A and B were shown to be downregulated in cells with associated increased autophagy, Marchand *et al.* have shown that GSK3 inhibition was able to increase autophagic flux [208]. Therefore, in contrast to other reports describing treated resistant tumors with autophagy inhibitors, it would be interesting to identify, upon induction of autophagy, the impact on drug sensitivity in resistant *EGFR* active-mutant NSCLC cells. Specific inhibitors (BEZ235, PI-103), either alone or in combination with EGFR-TKIs were successfully used to target the PI3K/AKT/MTOR pathway in order to sensitize EGFR-TKI resistant HCC827 and PC-9 cells [209, 210]. Moreover, MTOR inhibitors, such as temsirolimus and everolimus, reduced HGF-induced resistance to gefitinib in HCC827 and PC-9 cells and *in-vivo* [211].

The role of autophagy in resistance to EGFR TKI treatment is still poorly understood, as the consequences of autophagy have been shown to be cytoprotective or cytotoxic in different studies. Wei *et al.* have shown evidence of a cytoprotective role of autophagy in *EGFR* mutant lung cancer cells with the inframe deletion of exon 19. In their study, they have shown that inactive BECN1 (Beclin 1) leads to autophagy suppression, promotes tumor growth, and is resistance to EGFR-TKI-driven therapy. They have shown that activated EGFR inhibits autophagy through its binding to BECN1, which leads to its phosphorylation and thus to decreased BECN1-associated VPS34 kinase activity by altering its interaction with inhibitors such as BCL2 and KIAA0226 (Rubicon). The phosphorylation of BECN1 by activated EGFR leads to autophagy suppression and promoted NSCLC growth. The disruption of the EGFR-BECN1 complex by EGFR-TKI erlotinib in cells with active EGFR mutations resulted in the induction of autophagy by enabling the inhibitors to bind to BECN1 [146].

miR-503-5p moderately reduced *GABARAPL1* expression and was predicted to bind hundreds of targets. Therefore, siRNAs, which mimic the action of miRNAs, were used against *GABARAPL1* to specifically silence this gene. The siRNA-mediated knockdown of *GABARAPL1* was utilized to identify its involvement in autophagic activity. Therefore, standard autophagic markers such as LC3B and SQSTM1 were analyzed. As expected, the knockdown of *GABARAPL1* resulted in the accumulation of SQSTM1, which indicated that SQSTM1 was not degraded by autophagy. Since the accumulation of SQSTM1 was also observed in resistant HCC827 cells, as GABARAPL1 was increased, these findings indicated that autophagic processes were suppressed in those cells. Although LC3B-II was found to be increased after GABARAPL1 knockdown, it is possible that LC3B compensates for the function of the GABARAP family [148].

These findings were in line with another report that showed increased oncogenic activity in breast cancer cells with decreased GABARAPL1 expression. The knockdown of *GABARAPL1* resulted in decreased autophagic flux [212]. Moreover, the low expression of *GABARAPL1* was associated with poor prognosis of hepatocellular carcinoma (HCC). The knockdown of *GABARAPL1* in HCC induced cell growth [213].

4.3 Conclusion and Outlook

The aim of this study was to analyze miRNAs involved in NSCLC progression. For this, two approaches were defined, i.e. to identify circulating miRNAs as prognostic markers in early-stage lung adenocarcinoma patients, and secondly, and to analyze the role of miRNAs in EGFR-TKI therapy resistance.

In conclusion, circulating miRNAs were analyzed to stratify patients into high-risk and low-risk patients, according to the progression of the tumor or their overall survival. *miR-142-3p* levels were associated with the prognosis of early-stage lung adenocarcinoma patients. By investigating the potential of circulating miRNAs as prognostic markers, pre-analytical variables such as blood withdrawal and hemolysis were identified to influence miRNA expression levels. Future studies using miRNAs from serum samples should consider these pre-analytical variables.

Moreover, the data presented in this research identified *miR-503-5p* as regulated in resistant NSCLC cells and shown to interact with *GABARAPL1*. The reduction of *GABARAPL1* was partially mediated by the overexpression of *miR-503-5p*. Autophagic activity was deregulated in resistant lung adenocarcinoma cells in comparison to cells that were sensitive to gefitinib. The siRNA-mediated knockdown of *GABARAPL1* resulted in SQSTM1 accumulation, which indicated defective autophagy. Further studies on *miR-503-5p* expression and autophagy regulation in EGFR-TKI resistant lung adenocarcinoma patients might enable novel treatment options.

5 References

1.   Ferlay, J., et al., *Cancer incidence and mortality worldwide: sources, methods and major patterns in GLOBOCAN 2012.* Int J Cancer, 2015. **136**(5): p. E359-86.
2.   Chen, Z., et al., *Non-small-cell lung cancers: a heterogeneous set of diseases.* Nat Rev Cancer, 2014. **14**(8): p. 535-46.
3.   Langer, C.J., et al., *The evolving role of histology in the management of advanced non-small-cell lung cancer.* J Clin Oncol, 2010. **28**(36): p. 5311-20.
4.   Ettinger, D.S., et al., *Non-small cell lung cancer, version 2.2013.* J Natl Compr Canc Netw, 2013. **11**(6): p. 645-53; quiz 653.
5.   Bender, E., *Epidemiology: The dominant malignancy.* Nature, 2014. **513**(7517): p. S2-3.
6.   Goldstraw, P., et al., *The IASLC Lung Cancer Staging Project: proposals for the revision of the TNM stage groupings in the forthcoming (seventh) edition of the TNM Classification of malignant tumours.* J Thorac Oncol, 2007. **2**(8): p. 706-14.
7.   Pepek, J.M., et al., *How well does the new lung cancer staging system predict for local/regional recurrence after surgery?: A comparison of the TNM 6 and 7 systems.* J Thorac Oncol, 2011. **6**(4): p. 757-61.
8.   National Lung Screening Trial Research, T., et al., *Reduced lung-cancer mortality with low-dose computed tomographic screening.* N Engl J Med, 2011. **365**(5): p. 395-409.
9.   Kovalchik, S.A., et al., *Targeting of low-dose CT screening according to the risk of lung-cancer death.* N Engl J Med, 2013. **369**(3): p. 245-54.
10. O'Connor, G.T. and H. Hatabu, *Lung cancer screening, radiation, risks, benefits, and uncertainty.* JAMA, 2012. **307**(22): p. 2434-5.
11. Kulasingam, V. and E.P. Diamandis, *Strategies for discovering novel cancer biomarkers through utilization of emerging technologies.* Nat Clin Pract Oncol, 2008. **5**(10): p. 588-99.
12. de Groot, P. and R.F. Munden, *Lung cancer epidemiology, risk factors, and prevention.* Radiol Clin North Am, 2012. **50**(5): p. 863-76.
13. Cancer Genome Atlas Research, N., *Comprehensive molecular profiling of lung adenocarcinoma.* Nature, 2014. **511**(7511): p. 543-50.
14. Slebos, R.J., et al., *K-ras oncogene activation as a prognostic marker in adenocarcinoma of the lung.* N Engl J Med, 1990. **323**(9): p. 561-5.
15. Kosaka, T., et al., *Mutations of the epidermal growth factor receptor gene in lung cancer: biological and clinical implications.* Cancer Res, 2004. **64**(24): p. 8919-23.
16. Govindan, R., et al., *Genomic landscape of non-small cell lung cancer in smokers and never-smokers.* Cell, 2012. **150**(6): p. 1121-34.
17. Soda, M., et al., *Identification of the transforming EML4-ALK fusion gene in non-small-cell lung cancer.* Nature, 2007. **448**(7153): p. 561-6.
18. Tao, R.H. and I.N. Maruyama, *All EGF(ErbB) receptors have preformed homo- and heterodimeric structures in living cells.* J Cell Sci, 2008. **121**(Pt 19): p. 3207-17.
19. Ferguson, K.M., et al., *EGF activates its receptor by removing interactions that autoinhibit ectodomain dimerization.* Mol Cell, 2003. **11**(2): p. 507-17.
20. Arteaga, C.L. and J.A. Engelman, *ERBB receptors: from oncogene discovery to basic science to mechanism-based cancer therapeutics.* Cancer Cell, 2014. **25**(3): p. 282-303.
21. Ushiro, H. and S. Cohen, *Identification of phosphotyrosine as a product of epidermal growth factor-activated protein kinase in A-431 cell membranes.* J Biol Chem, 1980. **255**(18): p. 8363-5.
22. Zhang, X., et al., *An allosteric mechanism for activation of the kinase domain of epidermal growth factor receptor.* Cell, 2006. **125**(6): p. 1137-49.
23. Yarden, Y. and J. Schlessinger, *Self-phosphorylation of epidermal growth factor receptor: evidence for a model of intermolecular allosteric activation.* Biochemistry, 1987. **26**(5): p. 1434-42.
24. Tomas, A., C.E. Futter, and E.R. Eden, *EGF receptor trafficking: consequences for signaling and cancer.* Trends Cell Biol, 2014. **24**(1): p. 26-34.
25. Mok, T.S., et al., *Gefitinib or carboplatin-paclitaxel in pulmonary adenocarcinoma.* N Engl J Med, 2009. **361**(10): p. 947-57.

26. Rosell, R., et al., *Erlotinib versus standard chemotherapy as first-line treatment for European patients with advanced EGFR mutation-positive non-small-cell lung cancer (EURTAC): a multicentre, open-label, randomised phase 3 trial.* Lancet Oncol, 2012. **13**(3): p. 239-46.

27. Sequist, L.V., et al., *Phase III study of afatinib or cisplatin plus pemetrexed in patients with metastatic lung adenocarcinoma with EGFR mutations.* J Clin Oncol, 2013. **31**(27): p. 3327-34.

28. Paez, J.G., et al., *EGFR mutations in lung cancer: correlation with clinical response to gefitinib therapy.* Science, 2004. **304**(5676): p. 1497-500.

29. Lynch, T.J., et al., *Activating mutations in the epidermal growth factor receptor underlying responsiveness of non-small-cell lung cancer to gefitinib.* N Engl J Med, 2004. **350**(21): p. 2129-39.

30. Stamos, J., M.X. Sliwkowski, and C. Eigenbrot, *Structure of the epidermal growth factor receptor kinase domain alone and in complex with a 4-anilinoquinazoline inhibitor.* J Biol Chem, 2002. **277**(48): p. 46265-72.

31. Hirsch, F.R., et al., *Epidermal growth factor receptor in non-small-cell lung carcinomas: correlation between gene copy number and protein expression and impact on prognosis.* J Clin Oncol, 2003. **21**(20): p. 3798-807.

32. Shigematsu, H., et al., *Clinical and biological features associated with epidermal growth factor receptor gene mutations in lung cancers.* J Natl Cancer Inst, 2005. **97**(5): p. 339-46.

33. Pao, W., et al., *EGF receptor gene mutations are common in lung cancers from "never smokers" and are associated with sensitivity of tumors to gefitinib and erlotinib.* Proc Natl Acad Sci U S A, 2004. **101**(36): p. 13306-11.

34. Sharma, S.V., et al., *Epidermal growth factor receptor mutations in lung cancer.* Nat Rev Cancer, 2007. **7**(3): p. 169-81.

35. Pao, W., et al., *KRAS mutations and primary resistance of lung adenocarcinomas to gefitinib or erlotinib.* PLoS Med, 2005. **2**(1): p. e17.

36. Rosell, R., et al., *Screening for epidermal growth factor receptor mutations in lung cancer.* N Engl J Med, 2009. **361**(10): p. 958-67.

37. Maemondo, M., et al., *Gefitinib or chemotherapy for non-small-cell lung cancer with mutated EGFR.* N Engl J Med, 2010. **362**(25): p. 2380-8.

38. Kobayashi, S., et al., *EGFR mutation and resistance of non-small-cell lung cancer to gefitinib.* N Engl J Med, 2005. **352**(8): p. 786-92.

39. Oxnard, G.R., et al., *Acquired resistance to EGFR tyrosine kinase inhibitors in EGFR-mutant lung cancer: distinct natural history of patients with tumors harboring the T790M mutation.* Clin Cancer Res, 2011. **17**(6): p. 1616-22.

40. Pao, W., et al., *Acquired resistance of lung adenocarcinomas to gefitinib or erlotinib is associated with a second mutation in the EGFR kinase domain.* PLoS Med, 2005. **2**(3): p. e73.

41. Sequist, L.V., et al., *Genotypic and histological evolution of lung cancers acquiring resistance to EGFR inhibitors.* Sci Transl Med, 2011. **3**(75): p. 75ra26.

42. Yu, H.A., et al., *Analysis of tumor specimens at the time of acquired resistance to EGFR-TKI therapy in 155 patients with EGFR-mutant lung cancers.* Clin Cancer Res, 2013. **19**(8): p. 2240-7.

43. Bean, J., et al., *MET amplification occurs with or without T790M mutations in EGFR mutant lung tumors with acquired resistance to gefitinib or erlotinib.* Proc Natl Acad Sci U S A, 2007. **104**(52): p. 20932-7.

44. Engelman, J.A., et al., *MET amplification leads to gefitinib resistance in lung cancer by activating ERBB3 signaling.* Science, 2007. **316**(5827): p. 1039-43.

45. Yano, S., et al., *Hepatocyte growth factor induces gefitinib resistance of lung adenocarcinoma with epidermal growth factor receptor-activating mutations.* Cancer Res, 2008. **68**(22): p. 9479-87.

46. Wang, W., et al., *Crosstalk to stromal fibroblasts induces resistance of lung cancer to epidermal growth factor receptor tyrosine kinase inhibitors.* Clin Cancer Res, 2009. **15**(21): p. 6630-8.

47. Montesano, R., et al., *Identification of a fibroblast-derived epithelial morphogen as hepatocyte growth factor.* Cell, 1991. **67**(5): p. 901-8.

48.   Bottaro, D.P., et al., *Identification of the hepatocyte growth factor receptor as the c-met proto-oncogene product.* Science, 1991. **251**(4995): p. 802-4.

49.   Bhowmick, N.A., E.G. Neilson, and H.L. Moses, *Stromal fibroblasts in cancer initiation and progression.* Nature, 2004. **432**(7015): p. 332-7.

50.   Bartel, D.P., *MicroRNAs: genomics, biogenesis, mechanism, and function.* Cell, 2004. **116**(2): p. 281-97.

51.   Calin, G.A., et al., *Frequent deletions and down-regulation of micro- RNA genes miR15 and miR16 at 13q14 in chronic lymphocytic leukemia.* Proc Natl Acad Sci U S A, 2002. **99**(24): p. 15524-9.

52.   Rodriguez, A., et al., *Identification of mammalian microRNA host genes and transcription units.* Genome Res, 2004. **14**(10A): p. 1902-10.

53.   Lee, Y., et al., *MicroRNA maturation: stepwise processing and subcellular localization.* EMBO J, 2002. **21**(17): p. 4663-70.

54.   Kozomara, A. and S. Griffiths-Jones, *miRBase: annotating high confidence microRNAs using deep sequencing data.* Nucleic Acids Res, 2014. **42**(Database issue): p. D68-73.

55.   Lee, Y., et al., *MicroRNA genes are transcribed by RNA polymerase II.* EMBO J, 2004. **23**(20): p. 4051-60.

56.   Cai, X., C.H. Hagedorn, and B.R. Cullen, *Human microRNAs are processed from capped, polyadenylated transcripts that can also function as mRNAs.* RNA, 2004. **10**(12): p. 1957-66.

57.   Han, J., et al., *Molecular basis for the recognition of primary microRNAs by the Drosha-DGCR8 complex.* Cell, 2006. **125**(5): p. 887-901.

58.   Blaszczyk, J., et al., *Crystallographic and modeling studies of RNase III suggest a mechanism for double-stranded RNA cleavage.* Structure, 2001. **9**(12): p. 1225-36.

59.   Lee, Y., et al., *The nuclear RNase III Drosha initiates microRNA processing.* Nature, 2003. **425**(6956): p. 415-9.

60.   Bohnsack, M.T., K. Czaplinski, and D. Gorlich, *Exportin 5 is a RanGTP-dependent dsRNA-binding protein that mediates nuclear export of pre-miRNAs.* RNA, 2004. **10**(2): p. 185-91.

61.   Lund, E., et al., *Nuclear export of microRNA precursors.* Science, 2004. **303**(5654): p. 95-8.

62.   Carmell, M.A. and G.J. Hannon, *RNase III enzymes and the initiation of gene silencing.* Nat Struct Mol Biol, 2004. **11**(3): p. 214-8.

63.   Bernstein, E., et al., *Role for a bidentate ribonuclease in the initiation step of RNA interference.* Nature, 2001. **409**(6818): p. 363-6.

64.   Lee, Y., et al., *The role of PACT in the RNA silencing pathway.* EMBO J, 2006. **25**(3): p. 522-32.

65.   Khvorova, A., A. Reynolds, and S.D. Jayasena, *Functional siRNAs and miRNAs exhibit strand bias.* Cell, 2003. **115**(2): p. 209-16.

66.   Schwarz, D.S., et al., *Asymmetry in the assembly of the RNAi enzyme complex.* Cell, 2003. **115**(2): p. 199-208.

67.   Gregory, R.I., et al., *Human RISC couples microRNA biogenesis and posttranscriptional gene silencing.* Cell, 2005. **123**(4): p. 631-40.

68.   Meister, G., et al., *Human Argonaute2 mediates RNA cleavage targeted by miRNAs and siRNAs.* Mol Cell, 2004. **15**(2): p. 185-97.

69.   Eulalio, A., E. Huntzinger, and E. Izaurralde, *Getting to the root of miRNA-mediated gene silencing.* Cell, 2008. **132**(1): p. 9-14.

70.   Kiriakidou, M., et al., *An mRNA m7G cap binding-like motif within human Ago2 represses translation.* Cell, 2007. **129**(6): p. 1141-51.

71.   Chendrimada, T.P., et al., *MicroRNA silencing through RISC recruitment of eIF6.* Nature, 2007. **447**(7146): p. 823-8.

72.   Bagga, S., et al., *Regulation by let-7 and lin-4 miRNAs results in target mRNA degradation.* Cell, 2005. **122**(4): p. 553-63.

73.   Wu, L., J. Fan, and J.G. Belasco, *MicroRNAs direct rapid deadenylation of mRNA.* Proc Natl Acad Sci U S A, 2006. **103**(11): p. 4034-9.

74.   Grimson, A., et al., *MicroRNA targeting specificity in mammals: determinants beyond seed pairing.* Mol Cell, 2007. **27**(1): p. 91-105.

75.   Lewis, B.P., C.B. Burge, and D.P. Bartel, *Conserved seed pairing, often flanked by adenosines, indicates that thousands of human genes are microRNA targets.* Cell, 2005. **120**(1): p. 15-20.

76.   Krek, A., et al., *Combinatorial microRNA target predictions.* Nat Genet, 2005. **37**(5): p. 495-500.

77.   Miska, E.A., *How microRNAs control cell division, differentiation and death.* Curr Opin Genet Dev, 2005. **15**(5): p. 563-8.

78.   Sood, P., et al., *Cell-type-specific signatures of microRNAs on target mRNA expression.* Proc Natl Acad Sci U S A, 2006. **103**(8): p. 2746-51.

79.   Lu, J., et al., *MicroRNA expression profiles classify human cancers.* Nature, 2005. **435**(7043): p. 834-8.

80.   Lujambio, A., et al., *A microRNA DNA methylation signature for human cancer metastasis.* Proc Natl Acad Sci U S A, 2008. **105**(36): p. 13556-61.

81.   Calin, G.A., et al., *Human microRNA genes are frequently located at fragile sites and genomic regions involved in cancers.* Proc Natl Acad Sci U S A, 2004. **101**(9): p. 2999-3004.

82.   Dews, M., et al., *Augmentation of tumor angiogenesis by a Myc-activated microRNA cluster.* Nat Genet, 2006. **38**(9): p. 1060-5.

83.   He, L., et al., *A microRNA component of the p53 tumour suppressor network.* Nature, 2007. **447**(7148): p. 1130-4.

84.   Kumar, M.S., et al., *Impaired microRNA processing enhances cellular transformation and tumorigenesis.* Nat Genet, 2007. **39**(5): p. 673-7.

85.   Schwarzenbach, H., et al., *Clinical relevance of circulating cell-free microRNAs in cancer.* Nat Rev Clin Oncol, 2014. **11**(3): p. 145-56.

86.   Johnson, S.M., et al., *RAS is regulated by the let-7 microRNA family.* Cell, 2005. **120**(5): p. 635-47.

87.   Takamizawa, J., et al., *Reduced expression of the let-7 microRNAs in human lung cancers in association with shortened postoperative survival.* Cancer Res, 2004. **64**(11): p. 3753-6.

88.   Yanaihara, N., et al., *Unique microRNA molecular profiles in lung cancer diagnosis and prognosis.* Cancer Cell, 2006. **9**(3): p. 189-98.

89.   Hayashita, Y., et al., *A polycistronic microRNA cluster, miR-17-92, is overexpressed in human lung cancers and enhances cell proliferation.* Cancer Res, 2005. **65**(21): p. 9628-32.

90.   O'Donnell, K.A., et al., *c-Myc-regulated microRNAs modulate E2F1 expression.* Nature, 2005. **435**(7043): p. 839-43.

91.   Patnaik, S.K., et al., *Evaluation of microRNA expression profiles that may predict recurrence of localized stage I non-small cell lung cancer after surgical resection.* Cancer Res, 2010. **70**(1): p. 36-45.

92.   Hanash, S.M., C.S. Baik, and O. Kallioniemi, *Emerging molecular biomarkers--blood-based strategies to detect and monitor cancer.* Nat Rev Clin Oncol, 2011. **8**(3): p. 142-50.

93.   Mitchell, P.S., et al., *Circulating microRNAs as stable blood-based markers for cancer detection.* Proc Natl Acad Sci U S A, 2008. **105**(30): p. 10513-8.

94.   Chen, X., et al., *Characterization of microRNAs in serum: a novel class of biomarkers for diagnosis of cancer and other diseases.* Cell Res, 2008. **18**(10): p. 997-1006.

95.   Lawrie, C.H., et al., *Detection of elevated levels of tumour-associated microRNAs in serum of patients with diffuse large B-cell lymphoma.* Br J Haematol, 2008. **141**(5): p. 672-5.

96.   Grasedieck, S., et al., *Impact of serum storage conditions on microRNA stability.* Leukemia, 2012. **26**(11): p. 2414-6.

97.   Valadi, H., et al., *Exosome-mediated transfer of mRNAs and microRNAs is a novel mechanism of genetic exchange between cells.* Nat Cell Biol, 2007. **9**(6): p. 654-9.

98.   Arroyo, J.D., et al., *Argonaute2 complexes carry a population of circulating microRNAs independent of vesicles in human plasma.* Proc Natl Acad Sci U S A, 2011. **108**(12): p. 5003-8.

99.   van Niel, G., et al., *Exosomes: a common pathway for a specialized function.* J Biochem, 2006. **140**(1): p. 13-21.

100.   Laterza, O.F., et al., *Plasma MicroRNAs as sensitive and specific biomarkers of tissue injury.* Clin Chem, 2009. **55**(11): p. 1977-83.

101. Bianchi, F., et al., *A serum circulating miRNA diagnostic test to identify asymptomatic high-risk individuals with early stage lung cancer.* EMBO Mol Med, 2011. **3**(8): p. 495-503.

102. Boeri, M., et al., *MicroRNA signatures in tissues and plasma predict development and prognosis of computed tomography detected lung cancer.* Proc Natl Acad Sci U S A, 2011. **108**(9): p. 3713-8.

103. Sozzi, G., et al., *Clinical utility of a plasma-based miRNA signature classifier within computed tomography lung cancer screening: a correlative MILD trial study.* J Clin Oncol, 2014. **32**(8): p. 768-73.

104. Hu, Z., et al., *Serum microRNA signatures identified in a genome-wide serum microRNA expression profiling predict survival of non-small-cell lung cancer.* J Clin Oncol, 2010. **28**(10): p. 1721-6.

105. Cui, E.H., et al., *Serum microRNA 125b as a diagnostic or prognostic biomarker for advanced NSCLC patients receiving cisplatin-based chemotherapy.* Acta Pharmacol Sin, 2013. **34**(2): p. 309-13.

106. Yuxia, M., T. Zhennan, and Z. Wei, *Circulating miR-125b is a novel biomarker for screening non-small-cell lung cancer and predicts poor prognosis.* J Cancer Res Clin Oncol, 2012. **138**(12): p. 2045-50.

107. Liu, X.G., et al., *High expression of serum miR-21 and tumor miR-200c associated with poor prognosis in patients with lung cancer.* Med Oncol, 2012. **29**(2): p. 618-26.

108. Chen, X., et al., *Identification of ten serum microRNAs from a genome-wide serum microRNA expression profile as novel noninvasive biomarkers for nonsmall cell lung cancer diagnosis.* Int J Cancer, 2012. **130**(7): p. 1620-8.

109. Chen, C., et al., *Real-time quantification of microRNAs by stem-loop RT-PCR.* Nucleic Acids Res, 2005. **33**(20): p. e179.

110. Pradervand, S., et al., *Concordance among digital gene expression, microarrays, and qPCR when measuring differential expression of microRNAs.* Biotechniques, 2010. **48**(3): p. 219-22.

111. Kirschner, M.B., et al., *The Impact of Hemolysis on Cell-Free microRNA Biomarkers.* Front Genet, 2013. **4**: p. 94.

112. Blondal, T., et al., *Assessing sample and miRNA profile quality in serum and plasma or other biofluids.* Methods, 2013. **59**(1): p. S1-6.

113. Yano, T., et al., *Therapeutic strategy for postoperative recurrence in patients with non-small cell lung cancer.* World J Clin Oncol, 2014. **5**(5): p. 1048-54.

114. Weiss, G.J., et al., *EGFR regulation by microRNA in lung cancer: correlation with clinical response and survival to gefitinib and EGFR expression in cell lines.* Ann Oncol, 2008. **19**(6): p. 1053-9.

115. Wang, Y.S., et al., *MicroRNA-214 regulates the acquired resistance to gefitinib via the PTEN/AKT pathway in EGFR-mutant cell lines.* Asian Pac J Cancer Prev, 2012. **13**(1): p. 255-60.

116. Bryant, J.L., et al., *A microRNA gene expression signature predicts response to erlotinib in epithelial cancer cell lines and targets EMT.* Br J Cancer, 2012. **106**(1): p. 148-56.

117. Garofalo, M., et al., *EGFR and MET receptor tyrosine kinase-altered microRNA expression induces tumorigenesis and gefitinib resistance in lung cancers.* Nat Med, 2012. **18**(1): p. 74-82.

118. Mestdagh, P., et al., *Evaluation of quantitative miRNA expression platforms in the microRNA quality control (miRQC) study.* Nat Methods, 2014. **11**(8): p. 809-15.

119. Raymond, C.K., et al., *Simple, quantitative primer-extension PCR assay for direct monitoring of microRNAs and short-interfering RNAs.* RNA, 2005. **11**(11): p. 1737-44.

120. Kaduthanam, S., et al., *Serum miR-142-3p is associated with early relapse in operable lung adenocarcinoma patients.* Lung Cancer, 2013. **80**(2): p. 223-7.

121. Kahn, N., et al., *Blood-sampling collection prior to surgery may have a significant influence upon biomarker concentrations measured.* Clin Proteomics, 2015. **12**(1): p. 19.

122. Solly, K., et al., *Application of real-time cell electronic sensing (RT-CES) technology to cell-based assays.* Assay Drug Dev Technol, 2004. **2**(4): p. 363-72.

123. Haan, C. and I. Behrmann, *A cost effective non-commercial ECL-solution for Western blot detections yielding strong signals and low background.* J Immunol Methods, 2007. **318**(1-2): p. 11-9.

124. Fulton, R.J., et al., *Advanced multiplexed analysis with the FlowMetrix system.* Clin Chem, 1997. **43**(9): p. 1749-56.
125. Schmittgen, T.D. and K.J. Livak, *Analyzing real-time PCR data by the comparative C(T) method.* Nat Protoc, 2008. **3**(6): p. 1101-8.
126. Livak, K.J. and T.D. Schmittgen, *Analysis of relative gene expression data using real-time quantitative PCR and the 2(-Delta Delta C(T)) Method.* Methods, 2001. **25**(4): p. 402-8.
127. Andersen, C.L., J.L. Jensen, and T.F. Orntoft, *Normalization of real-time quantitative reverse transcription-PCR data: a model-based variance estimation approach to identify genes suited for normalization, applied to bladder and colon cancer data sets.* Cancer Res, 2004. **64**(15): p. 5245-50.
128. Huang da, W., B.T. Sherman, and R.A. Lempicki, *Systematic and integrative analysis of large gene lists using DAVID bioinformatics resources.* Nat Protoc, 2009. **4**(1): p. 44-57.
129. Silva, J., et al., *Vesicle-related microRNAs in plasma of nonsmall cell lung cancer patients and correlation with survival.* Eur Respir J, 2011. **37**(3): p. 617-23.
130. Markou, A., et al., *Clinical evaluation of microRNA expression profiling in non small cell lung cancer.* Lung Cancer, 2013. **81**(3): p. 388-96.
131. Wang, Z.X., et al., *Prognostic significance of serum miRNA-21 expression in human non-small cell lung cancer.* J Surg Oncol, 2011. **104**(7): p. 847-51.
132. Shen, J., et al., *Plasma microRNAs as potential biomarkers for non-small-cell lung cancer.* Lab Invest, 2011. **91**(4): p. 579-87.
133. Cataldo, V.D., et al., *Treatment of non-small-cell lung cancer with erlotinib or gefitinib.* N Engl J Med, 2011. **364**(10): p. 947-55.
134. Turke, A.B., et al., *Preexistence and clonal selection of MET amplification in EGFR mutant NSCLC.* Cancer Cell, 2010. **17**(1): p. 77-88.
135. Yang, J.S., et al., *Widespread regulatory activity of vertebrate microRNA* species.* RNA, 2011. **17**(2): p. 312-26.
136. Peltier, H.J. and G.J. Latham, *Normalization of microRNA expression levels in quantitative RT-PCR assays: identification of suitable reference RNA targets in normal and cancerous human solid tissues.* RNA, 2008. **14**(5): p. 844-52.
137. Baskerville, S. and D.P. Bartel, *Microarray profiling of microRNAs reveals frequent coexpression with neighboring miRNAs and host genes.* RNA, 2005. **11**(3): p. 241-7.
138. Sos, M.L., et al., *PTEN loss contributes to erlotinib resistance in EGFR-mutant lung cancer by activation of Akt and EGFR.* Cancer Res, 2009. **69**(8): p. 3256-61.
139. Castro, F., et al., *High-throughput SNP-based authentication of human cell lines.* Int J Cancer, 2013. **132**(2): p. 308-14.
140. Friedman, R.C., et al., *Most mammalian mRNAs are conserved targets of microRNAs.* Genome Res, 2009. **19**(1): p. 92-105.
141. Yamamoto, A., et al., *Bafilomycin A1 prevents maturation of autophagic vacuoles by inhibiting fusion between autophagosomes and lysosomes in rat hepatoma cell line, H-4-II-E cells.* Cell Struct Funct, 1998. **23**(1): p. 33-42.
142. Wang, H., et al., *GABA(A)-receptor-associated protein links GABA(A) receptors and the cytoskeleton.* Nature, 1999. **397**(6714): p. 69-72.
143. Le Grand, J.N., et al., *GABARAPL1 (GEC1): original or copycat?* Autophagy, 2011. **7**(10): p. 1098-107.
144. Han, W., et al., *EGFR tyrosine kinase inhibitors activate autophagy as a cytoprotective response in human lung cancer cells.* PLoS One, 2011. **6**(6): p. e18691.
145. Sugita, S., et al., *EGFR-independent autophagy induction with gefitinib and enhancement of its cytotoxic effect by targeting autophagy with clarithromycin in non-small cell lung cancer cells.* Biochem Biophys Res Commun, 2015. **461**(1): p. 28-34.
146. Wei, Y., et al., *EGFR-mediated Beclin 1 phosphorylation in autophagy suppression, tumor progression, and tumor chemoresistance.* Cell, 2013. **154**(6): p. 1269-84.
147. So, K.S., et al., *Autophagosome-mediated EGFR down-regulation induced by the CK2 inhibitor enhances the efficacy of EGFR-TKI on EGFR-mutant lung cancer cells with resistance by T790M.* PLoS One, 2014. **9**(12): p. e114000.
148. Maruyama, Y., et al., *LC3B is indispensable for selective autophagy of p62 but not basal autophagy.* Biochem Biophys Res Commun, 2014. **446**(1): p. 309-15.

149.   Gazdar, A.F., *Activating and resistance mutations of EGFR in non-small-cell lung cancer: role in clinical response to EGFR tyrosine kinase inhibitors.* Oncogene, 2009. **28 Suppl 1**: p. S24-31.

150.   Nguyen, K.S., S. Kobayashi, and D.B. Costa, *Acquired resistance to epidermal growth factor receptor tyrosine kinase inhibitors in non-small-cell lung cancers dependent on the epidermal growth factor receptor pathway.* Clin Lung Cancer, 2009. **10**(4): p. 281-9.

151.   Thorpe, J.D., et al., *Effects of blood collection conditions on ovarian cancer serum markers.* PLoS One, 2007. **2**(12): p. e1281.

152.   Zhou, X., et al., *Diagnostic value of a plasma microRNA signature in gastric cancer: a microRNA expression analysis.* Sci Rep, 2015. **5**: p. 11251.

153.   Rupaimoole, R., et al., *Hypoxia-mediated downregulation of miRNA biogenesis promotes tumour progression.* Nat Commun, 2014. **5**: p. 5202.

154.   Kulshreshtha, R., et al., *A microRNA signature of hypoxia.* Mol Cell Biol, 2007. **27**(5): p. 1859-67.

155.   Kosaka, N., et al., *Secretory mechanisms and intercellular transfer of microRNAs in living cells.* J Biol Chem, 2010. **285**(23): p. 17442-52.

156.   Petricoin, E.F., et al., *The blood peptidome: a higher dimension of information content for cancer biomarker discovery.* Nat Rev Cancer, 2006. **6**(12): p. 961-7.

157.   Wu, D.W., et al., *c-Myc suppresses microRNA-29b to promote tumor aggressiveness and poor outcomes in non-small cell lung cancer by targeting FHIT.* Oncogene, 2015. **34**(16): p. 2072-82.

158.   Shi, Y., et al., *A prospective, molecular epidemiology study of EGFR mutations in Asian patients with advanced non-small-cell lung cancer of adenocarcinoma histology (PIONEER).* J Thorac Oncol, 2014. **9**(2): p. 154-62.

159.   Wang, W., et al., *Met kinase inhibitor E7050 reverses three different mechanisms of hepatocyte growth factor-induced tyrosine kinase inhibitor resistance in EGFR mutant lung cancer.* Clin Cancer Res, 2012. **18**(6): p. 1663-71.

160.   Gozdzik-Spychalska, J., et al., *C-MET inhibitors in the treatment of lung cancer.* Curr Treat Options Oncol, 2014. **15**(4): p. 670-82.

161.   Takeuchi, S., et al., *Dual inhibition of Met kinase and angiogenesis to overcome HGF-induced EGFR-TKI resistance in EGFR mutant lung cancer.* Am J Pathol, 2012. **181**(3): p. 1034-43.

162.   Ferrara, N. and T. Davis-Smyth, *The biology of vascular endothelial growth factor.* Endocr Rev, 1997. **18**(1): p. 4-25.

163.   Viloria-Petit, A., et al., *Acquired resistance to the antitumor effect of epidermal growth factor receptor-blocking antibodies in vivo: a role for altered tumor angiogenesis.* Cancer Res, 2001. **61**(13): p. 5090-101.

164.   Box, C., et al., *A novel serum protein signature associated with resistance to epidermal growth factor receptor tyrosine kinase inhibitors in head and neck squamous cell carcinoma.* Eur J Cancer, 2013. **49**(11): p. 2512-21.

165.   Yao, Z., et al., *TGF-beta IL-6 axis mediates selective and adaptive mechanisms of resistance to molecular targeted therapy in lung cancer.* Proc Natl Acad Sci U S A, 2010. **107**(35): p. 15535-40.

166.   Li, L., et al., *Metformin sensitizes EGFR-TKI-resistant human lung cancer cells in vitro and in vivo through inhibition of IL-6 signaling and EMT reversal.* Clin Cancer Res, 2014. **20**(10): p. 2714-26.

167.   Kim, S.M., et al., *Activation of IL-6R/JAK1/STAT3 signaling induces de novo resistance to irreversible EGFR inhibitors in non-small cell lung cancer with T790M resistance mutation.* Mol Cancer Ther, 2012. **11**(10): p. 2254-64.

168.   Liu, Y.N., et al., *IL-8 confers resistance to EGFR inhibitors by inducing stem cell properties in lung cancer.* Oncotarget, 2015. **6**(12): p. 10415-31.

169.   Acharyya, S., et al., *A CXCL1 paracrine network links cancer chemoresistance and metastasis.* Cell, 2012. **150**(1): p. 165-78.

170.   Zhang, Z., et al., *Activation of the AXL kinase causes resistance to EGFR-targeted therapy in lung cancer.* Nat Genet, 2012. **44**(8): p. 852-60.

171.   Acunzo, M., et al., *Cross-talk between MET and EGFR in non-small cell lung cancer involves miR-27a and Sprouty2.* Proc Natl Acad Sci U S A, 2013. **110**(21): p. 8573-8.

172.   Ide, S., et al., *MicroRNA-503 promotes tumor progression and acts as a novel biomarker for prognosis in oesophageal cancer.* Anticancer Res, 2015. **35**(3): p. 1447-51.

173.   Li, L., et al., *Sequential expression of miR-182 and miR-503 cooperatively targets FBXW7, contributing to the malignant transformation of colon adenoma to adenocarcinoma.* J Pathol, 2014. **234**(4): p. 488-501.

174.   Qiu, T., et al., *miR-503 regulates the resistance of non-small cell lung cancer cells to cisplatin by targeting Bcl-2.* Int J Mol Med, 2013. **32**(3): p. 593-8.

175.   Li, N., et al., *Epigenetic silencing of MicroRNA-503 regulates FANCA expression in non-small cell lung cancer cell.* Biochem Biophys Res Commun, 2014. **444**(4): p. 611-6.

176.   Yang, Y., et al., *MiR-503 targets PI3K p85 and IKK-beta and suppresses progression of non-small cell lung cancer.* Int J Cancer, 2014. **135**(7): p. 1531-42.

177.   Zhou, J.Y., et al., *MicroRNA-34a overcomes HGF-mediated gefitinib resistance in EGFR mutant lung cancer cells partly by targeting MET.* Cancer Lett, 2014. **351**(2): p. 265-71.

178.   Shin, K.H., et al., *miR-181a shows tumor suppressive effect against oral squamous cell carcinoma cells by downregulating K-ras.* Biochem Biophys Res Commun, 2011. **404**(4): p. 896-902.

179.   Fei, J., et al., *miR-181a post-transcriptionally downregulates oncogenic RalA and contributes to growth inhibition and apoptosis in chronic myelogenous leukemia (CML).* PLoS One, 2012. **7**(3): p. e32834.

180.   Shi, L., et al., *hsa-mir-181a and hsa-mir-181b function as tumor suppressors in human glioma cells.* Brain Res, 2008. **1236**: p. 185-93.

181.   Ma, Z., et al., *MiR-181a-5p inhibits cell proliferation and migration by targeting Kras in non-small cell lung cancer A549 cells.* Acta Biochim Biophys Sin (Shanghai), 2015.

182.   Maegawa, M., et al., *EGFR mutation up-regulates EGR1 expression through the ERK pathway.* Anticancer Res, 2009. **29**(4): p. 1111-7.

183.   Yamamoto, C., et al., *Loss of PTEN expression by blocking nuclear translocation of EGR1 in gefitinib-resistant lung cancer cells harboring epidermal growth factor receptor-activating mutations.* Cancer Res, 2010. **70**(21): p. 8715-25.

184.   Chen, J., et al., *AURKA upregulation plays a role in fibroblast-reduced gefitinib sensitivity in the NSCLC cell line HCC827.* Oncol Rep, 2015. **33**(4): p. 1860-6.

185.   Pellerin, I., et al., *Identification and characterization of an early estrogen-regulated RNA in cultured guinea-pig endometrial cells.* Mol Cell Endocrinol, 1993. **90**(2): p. R17-21.

186.   Vernier-Magnin, S., et al., *A novel early estrogen-regulated gene gec1 encodes a protein related to GABARAP.* Biochem Biophys Res Commun, 2001. **284**(1): p. 118-25.

187.   Chen, C., et al., *GEC1 interacts with the kappa opioid receptor and enhances expression of the receptor.* J Biol Chem, 2006. **281**(12): p. 7983-93.

188.   Chakrama, F.Z., et al., *GABARAPL1 (GEC1) associates with autophagic vesicles.* Autophagy, 2010. **6**(4): p. 495-505.

189.   Geng, J. and D.J. Klionsky, *The Atg8 and Atg12 ubiquitin-like conjugation systems in macroautophagy. 'Protein modifications: beyond the usual suspects' review series.* EMBO Rep, 2008. **9**(9): p. 859-64.

190.   Weidberg, H., et al., *LC3 and GATE-16/GABARAP subfamilies are both essential yet act differently in autophagosome biogenesis.* EMBO J, 2010. **29**(11): p. 1792-802.

191.   Lamark, T., et al., *NBR1 and p62 as cargo receptors for selective autophagy of ubiquitinated targets.* Cell Cycle, 2009. **8**(13): p. 1986-90.

192.   Pankiv, S., et al., *p62/SQSTM1 binds directly to Atg8/LC3 to facilitate degradation of ubiquitinated protein aggregates by autophagy.* J Biol Chem, 2007. **282**(33): p. 24131-45.

193.   Komatsu, M., et al., *Homeostatic levels of p62 control cytoplasmic inclusion body formation in autophagy-deficient mice.* Cell, 2007. **131**(6): p. 1149-63.

194.   Duran, A., et al., *The signaling adaptor p62 is an important NF-kappaB mediator in tumorigenesis.* Cancer Cell, 2008. **13**(4): p. 343-54.

195.   Bivona, T.G., et al., *FAS and NF-kappaB signalling modulate dependence of lung cancers on mutant EGFR.* Nature, 2011. **471**(7339): p. 523-6.

196.   Inoue, D., et al., *Accumulation of p62/SQSTM1 is associated with poor prognosis in patients with lung adenocarcinoma.* Cancer Sci, 2012. **103**(4): p. 760-6.

197. Komatsu, M., et al., *The selective autophagy substrate p62 activates the stress responsive transcription factor Nrf2 through inactivation of Keap1.* Nat Cell Biol, 2010. **12**(3): p. 213-23.

198. Yamadori, T., et al., *Molecular mechanisms for the regulation of Nrf2-mediated cell proliferation in non-small-cell lung cancers.* Oncogene, 2012. **31**(45): p. 4768-77.

199. Duran, A., et al., *p62 is a key regulator of nutrient sensing in the mTORC1 pathway.* Mol Cell, 2011. **44**(1): p. 134-46.

200. Kamada, Y., et al., *Tor-mediated induction of autophagy via an Apg1 protein kinase complex.* J Cell Biol, 2000. **150**(6): p. 1507-13.

201. Blommaart, E.F., et al., *Phosphorylation of ribosomal protein S6 is inhibitory for autophagy in isolated rat hepatocytes.* J Biol Chem, 1995. **270**(5): p. 2320-6.

202. Shin, J.H., et al., *TAK1 regulates autophagic cell death by suppressing the phosphorylation of p70 S6 kinase 1.* Sci Rep, 2013. **3**: p. 1561.

203. Scott, R.C., O. Schuldiner, and T.P. Neufeld, *Role and regulation of starvation-induced autophagy in the Drosophila fat body.* Dev Cell, 2004. **7**(2): p. 167-78.

204. Daido, S., et al., *Inhibition of the DNA-dependent protein kinase catalytic subunit radiosensitizes malignant glioma cells by inducing autophagy.* Cancer Res, 2005. **65**(10): p. 4368-75.

205. Wang, R.C., et al., *Akt-mediated regulation of autophagy and tumorigenesis through Beclin 1 phosphorylation.* Science, 2012. **338**(6109): p. 956-9.

206. Inoki, K., T. Zhu, and K.L. Guan, *TSC2 mediates cellular energy response to control cell growth and survival.* Cell, 2003. **115**(5): p. 577-90.

207. Parkhitko, A., et al., *Tumorigenesis in tuberous sclerosis complex is autophagy and p62/sequestosome 1 (SQSTM1)-dependent.* Proc Natl Acad Sci U S A, 2011. **108**(30): p. 12455-60.

208. Marchand, B., et al., *Glycogen synthase kinase-3 (GSK3) inhibition induces prosurvival autophagic signals in human pancreatic cancer cells.* J Biol Chem, 2015. **290**(9): p. 5592-605.

209. Sano, T., et al., *The novel phosphoinositide 3-kinase-mammalian target of rapamycin inhibitor, BEZ235, circumvents erlotinib resistance of epidermal growth factor receptor mutant lung cancer cells triggered by hepatocyte growth factor.* Int J Cancer, 2013. **133**(2): p. 505-13.

210. Donev, I.S., et al., *Transient PI3K inhibition induces apoptosis and overcomes HGF-mediated resistance to EGFR-TKIs in EGFR mutant lung cancer.* Clin Cancer Res, 2011. **17**(8): p. 2260-9.

211. Ishikawa, D., et al., *mTOR inhibitors control the growth of EGFR mutant lung cancer even after acquiring resistance by HGF.* PLoS One, 2013. **8**(5): p. e62104.

212. Boyer-Guittaut, M., et al., *The role of GABARAPL1/GEC1 in autophagic flux and mitochondrial quality control in MDA-MB-436 breast cancer cells.* Autophagy, 2014. **10**(6): p. 986-1003.

213. Liu, C., et al., *Low expression of GABARAPL1 is associated with a poor outcome for patients with hepatocellular carcinoma.* Oncol Rep, 2014. **31**(5): p. 2043-8.

6 Appendix
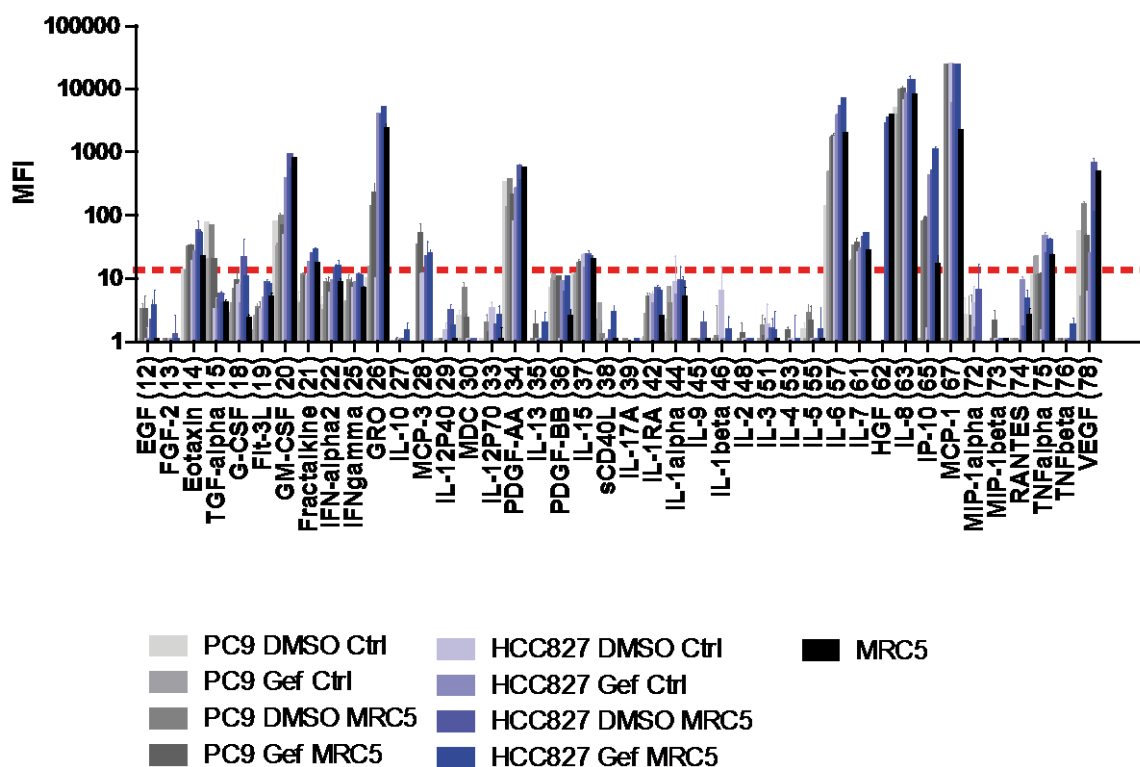
Supplemental Figure 1 Cytokine analysis of supernatant of PC-9 and HCC827 co-culture with MRC-5 cells. Each number for each cytokine depicts the bead region. Note, HGF (62) was measured using a single-Plex assay. Red dotted line: Background. MFI: mean fluorescent intensities.
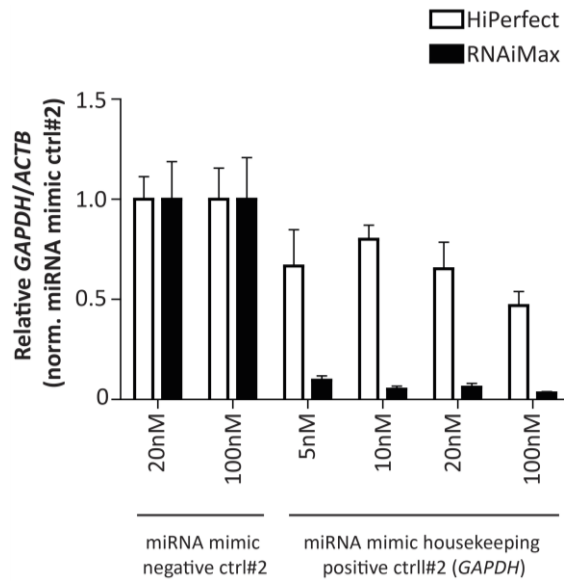
Supplemental Figure 2 Determination of transfection effiency after transient transfection of miRNA mimic molecules. miRIDIAN microRNA Mimics (GE) that targets the 3' UTR of *GAPDH* were transiently transfected at 5-100 nM using HiPerfect (Qiagen) or RNAiMAX (Invitrogen) into HCC827 and analyzed for the decrease of target mRNA levels of *GAPDH*. *GAPDH* downregulation was determined using UPL based method at 48 h post-transfection. *GAPDH* expression from miRNA mimic GAPDH transfected samples was normalized to *GAPDH* expression from samples transfected with miRNA mimic control#2, which is based on *cel-miR-239b* mature sequence Standard deviation were calculated from 3 experiments.
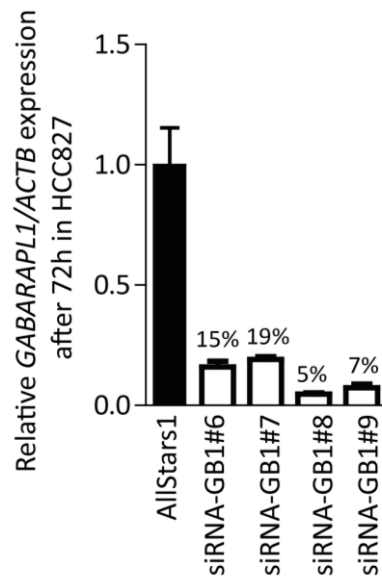
Supplemental Figure 3 *GABARAPL1* expression after siRNA-mediated knockdown of *GABARAPL1*. HCC827 were treated with 4 different siRNAs against *GABARAPL1* #6, #7, #8, and #9 for 72 h.
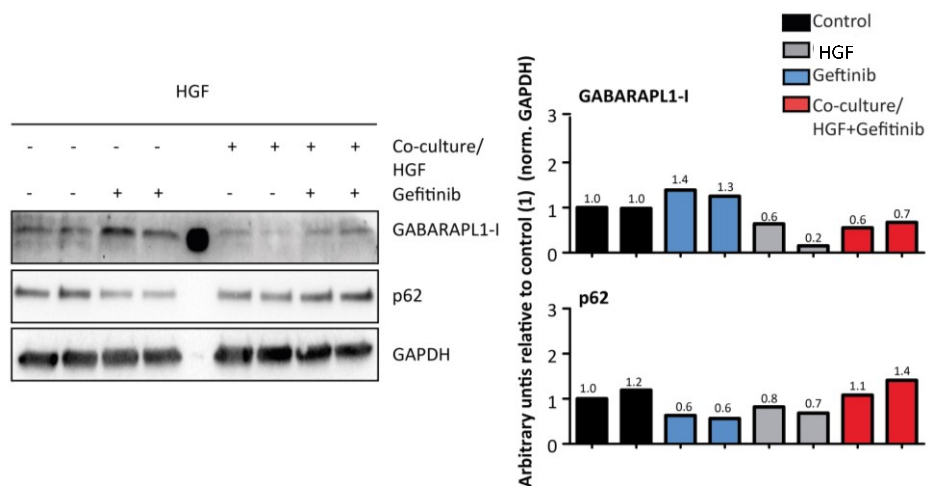
Supplemental Figure 4 Expression of SQSTM1 (p62) and GABARAPL1 in resistant HCC827 cells. HCC827 cells were cultured with or without gefitinib (0.5 μM) in the presence or absence of HGF cells for 48 h. Densitometric analysis of GABARAPL1, SQSTM1, were performed using ImageLab 5.2.1. Protein levels were normalized to internal GAPDH levels. Prediceted molecular weight: SQSTM1: 62kDa, GABARAPL1:14 kDa

Supplemental Table 1 Cytokine data of PC-9 and HCC827 supernatant

Cell line	PC-9								HCC827								MRC-5	
Analytes	DMSO Ctrl	SD	Gef Ctrl	SD	DMSO MRC-5	SD	Gef MRC5	SD	DMSO Ctrl	SD	Gef Ctrl	SD	DMSO MRC5	SD	Gef MRC5	SD	MRC-5	SD
EGF (12)	0.96	1.53	-0.79	0.29	3.13	0.87	3.13	2.29	1.04	0.63	0.63	1.56	2.13	2.38	3.71	2.81	0.79	0.95
FGF-2 (13)	-0.17	0.76	-2.17	1.15	0.17	1.38	0.92	0.95	0.58	0.63	0.17	0.58	1.25	1.39	0.92	0.95	-0.42	0.38
Eotaxin (14)	13.5	0.5	10.83	1.84	31.08	2.1	31.67	3.75	17.75	2.41	25.75	4.44	56.5	25.12	50.5	6.55	21.5	1.32
TGF-alpha (15)	73.17	5.19	18.58	0.76	66.25	3.91	19.08	0.58	3.17	1.66	3.08	0.38	5.5	0.66	3.83	1.88	4.08	0.58
G-CSF (18)	1.96	1.18	2.79	1.01	6.54	1.46	9.13	4.67	7.63	1.15	3.96	1.18	21.21	20.52	10.29	5.26	2.29	0.38
Flt-3L (19)	0.79	0.76	1.46	1.04	3.29	0.76	3.21	1.13	3.13	1.39	4.79	1.04	8.54	1.01	7.71	1.28	4.88	1.09
GM-CSF (20)	76.5	4.13	31.25	2.7	95.42	12.01	66.83	4.4	46.58	4.11	371.33	34.27	897.08	80.09	523.75	54.47	771.83	27.96
Fractalkine (21)	4.21	2.08	3.54	0.29	11.04	1.15	10.46	0.63	10.63	1.15	17.46	0.88	24.38	4.09	27.21	3.51	16.79	0.38
IFN-alpha2 (22)	3.67	1.44	2.75	0.25	8.25	1.75	8.08	2.53	5.67	1.77	9	0.9	14.25	2.63	15.08	4.16	8.42	1.66
IFNgamma (25)	3.83	0.63	2.67	1.59	9	2.61	8.17	2.04	6.83	0.63	8.5	1.52	11	1.3	10.75	0.66	6.83	0.72
GRO (26)	9.79	0.38	12.46	2.32	133.79	54.21	217.04	102.4	9.63	0.25	3892.54	220.26	3717.71	1319.19	4871.96	438.44	2296.71	487.33
IL-10 (27)	-0.79	0.38	-0.29	0.58	-0.54	0.95	1.04	0.14	0.21	0.95	0.71	0.72	1.04	0.29	1.46	0.52	-0.71	0.14
MCP-3 (28)	-1.67	0.76	-1.83	1.01	32.92	8.82	50	24.58	11.25	0.66	-0.5	1.15	21.75	17.03	24.42	4.14	-1	1.75
IL-12P40 (29)	0.33	0.38	-0.5	1.32	0.42	0.14	0.42	0.63	1.42	0.52	-0.75	0.43	3	0.87	1.75	1.39	0.25	0.25
MDC (30)	2.42	0.76	0.83	0.72	6.92	1.66	2.25	0.5	0.42	0.76	-0.67	1.13	0.08	0.29	-0.42	0.29	-1.75	1
IL-12P70 (33)	0.25	1	-0.17	2.13	1.92	0.76	1.33	0.8	3.25	1	1	0.9	1.83	0.52	2.58	1.04	1.08	0.58
PDGF-AA (34)	324.92	6.17	121.75	6.29	356.42	20.44	204.42	5.38	75.92	2.24	255.17	7.59	587.67	77.84	354.5	30.81	539.25	22.64
IL-13 (35)	-1.67	0.95	-1.33	0.52	0.08	1.01	1.83	1.26	0.92	0.38	0.5	1.39	0.92	0.72	1.92	1.01	-0.58	1.01
PDGF-BB (36)	6.75	5.43	9.33	1.7	8.58	1.76	10.25	0.87	0.67	0.14	8.58	0.58	5.92	1.76	10.25	0.9	2.5	0.75
IL-15 (37)	11.75	0.66	10.75	0.75	17.08	3.09	17.42	0.95	22.83	2.47	14.33	1.18	23.42	3.76	21.42	1.88	19.17	1.15
sCD40L (38)	0.75	1.56	2.17	1.7	1.25	0.87	0.75	1	0.08	1.53	0.83	1.01	1.42	1.53	2.92	0.76	0.25	0.5
IL-17A (39)	-1.67	0.38	-1.58	0.29	0.25	2.18	-0.25	0.5	-1.58	0.29	-0.92	1.26	-0.42	0.76	0.83	0.52	-1.33	0.8
IL-1RA (42)	0.54	1.01	1.13	1.56	4.96	1.01	4.88	0.9	5.38	0.87	3.96	3.19	6.79	0.88	6.13	0.66	2.46	0.14

IL-1alpha (44)	1.29	0.76	2.13	4.82	3.88	3.25	0.88	1.75	8.54	13.96	5.21	0.8	9.21	6.28	8.79	2.02	4.96	2.25
IL-9 (45)	-0.08	0.38	-1.67	1.23	0.33	0.72	0.17	1.23	0	0.9	0.17	0.63	1.92	1.15	0.92	0.29	0.5	0.25
IL-1beta (46)	-0.92	0.52	0.08	0.95	1.17	2.57	0.42	0.52	6.25	9.31	0.83	1.15	1	0.5	1.5	1	-0.33	1.61
IL-2 (48)	-1.13	0.75	-1.46	0.29	0.38	1.09	1.29	0.72	0.79	1.59	-0.79	0.76	0.88	1.8	0.88	0.9	-0.13	1.56
IL-3 (51)	0	0.25	0.25	0.25	1.75	0.87	1.17	1.15	1.83	2.13	0.83	0.14	1.58	0.76	1.42	1.61	0.67	0.8
IL-4 (53)	-0.17	0.8	-0.58	0.52	-0.42	2.36	1.42	0.29	0.92	0.76	-0.92	1.26	1	1.64	0.5	1.15	-1.17	1.01
IL-5 (55)	1.5	0.5	0.33	0.29	2.75	1.09	2.08	1.63	0.75	0.43	0.42	1.04	1.08	0.52	1.5	2	0.33	0.76
IL6 (57)	133.83	1.66	464.08	19.84	1638.42	180.17	1747.83	252.08	1671.25	107.48	3701.83	139.95	5095.17	599.05	6784.58	367.25	1950.67	74.6
IL-7 (61)	17.83	1.59	17.33	1.28	31.67	2.31	35.25	8.13	24.92	0.76	28.92	4.29	43.25	9.96	49.67	4.01	26.08	2.13
IL8 (63)	4816.58	180.71	3688.58	141.47	9240.92	445.66	9612.08	1279.01	6451.83	512.58	8165.92	255.78	13287.83	2563.86	13170.33	841.89	7744.5	534.58
CXCR3 (65)	-1.25	0.87	0.83	0.38	77.58	6.53	90.33	7.48	1.58	1.18	412.67	48.05	495.17	294.17	1055.42	162.13	16.75	6.43
CCL2 (67)	0.67	0.76	0.17	0.63	23126.75	478.25	23460.5	536.85	24377.5	73.98	5726.25	333.98	23411.58	622.29	23836.08	196.47	2145	54.06
MIP-1alpha (72)	2.54	2.5	-2.04	1.89	1.04	4.42	2.46	3.01	3.88	3.7	1.63	0.75	6.38	10.83	-0.21	4.01	-1.88	2.5
MIP-1beta (73)	-1.08	0.76	-1	0.9	0.83	0.52	2.08	1.04	0.67	0.38	-0.08	0.58	0.58	1.44	0.58	0.76	0.25	0.5
RANTES (74)	-0.5	0.5	0.5	1.15	0.17	0.76	-0.17	1.15	-0.08	1.91	9	1.73	1.67	2.47	4.67	1.89	2.58	0.8
TNFalpha (75)	10.75	0.9	20.67	0.76	10.83	1.15	11.08	1.38	1.42	0.58	45.83	7.78	23.75	1.15	39.5	3.5	22.33	2.02
TNFbeta (76)	0.21	0.38	-0.63	1.75	0.13	1	0.79	1.26	0.13	0.9	0.63	0.66	0.88	0.25	1.79	0.58	-1.79	0.38
VEGF (78)	54.17	4.4	5	0	146.58	16.55	45	6.38	6	1.52	24	0.75	664.17	135.55	107.08	15.88	473.58	27.55
HGF (62)	-68	1.8	-59.5	19.7	1048.5	92.99	1220	178.28	-25.3	23.69	-20.8	0.35	2769.8	127.63	3344.3	66.11	3830.3	58.34

Supplemental Table 2: miRNA comparison: HCC +/+ vs HCC +/-

miRNA_ID	p-value	q-value	Fold change	Median Cp
hsa-miR-205	2.50E-02	3.63E-01	0.42	32.50
hsa-miR-181a-2*	2.56E-02	3.63E-01	0.46	31.67
hsa-miR-181b	6.01E-04	9.69E-02	0.47	29.44
hsa-miR-24-1*	4.474E-02	4.57E-01	0.50	35.23
hsa-miR-26a	1.94E-03	1.49E-01	0.50	28.37
hsa-miR-181a	2.91E-03	1.50E-01	0.52	27.03
hsa-miR-196a	4.40E-03	1.70E-01	0.56	30.78
hsa-miR-125a-3p	4.23E-02	4.57E-01	0.56	33.37
hsa-miR-30e	1.93E-03	1.49E-01	0.58	31.39
hsa-miR-181a*	6.63E-04	9.69E-02	0.60	33.04
hsa-miR-27b	1.13E-03	1.25E-01	0.62	26.98
hsa-miR-215	4.40E-02	4.57E-01	0.63	34.31
hsa-miR-181c	3.67E-02	4.13E-01	0.63	35.04
hsa-miR-34c-5p	2.88E-02	3.77E-01	0.63	29.27
hsa-miR-34a	2.55E-02	3.63E-01	0.63	27.84
hsa-let-7b	4.66E-03	1.70E-01	0.64	27.56
hsa-miR-200b	2.04E-03	1.49E-01	0.64	28.83
hsa-miR-720	1.49E-02	3.07E-01	0.66	24.50
hsa-let-7f	6.49E-03	1.82E-01	0.66	27.61
hsa-miR-29b	6.39E-03	1.82E-01	1.53	28.19
hsa-miR-18a	3.27E-03	1.50E-01	1.60	28.91
hsa-miR-130b	3.76E-02	4.17E-01	1.67	33.03
hsa-miR-877	9.35E-03	2.21E-01	1.69	33.19
hsa-miR-886-5p	3.29E-03	1.50E-01	1.74	29.31
hsa-miR-503	9.19E-03	2.21E-01	2.02	28.56
hsa-miR-1296	1.72E-02	3.24E-01	2.05	34.60
hsa-miR-222*	9.03E-03	2.21E-01	2.34	33.86
hsa-let-7a-2*	6.39E-03	1.82E-01	2.46	32.07
hsa-miR-1979	4.67E-04	9.69E-02	2.49	23.36
hsa-miR-941	1.75E-02	3.24E-01	2.51	33.20
hsa-miR-29b-1*	2.79E-03	1.50E-01	2.66	30.98

Supplemental Table 3: miRNA comparison: HCC +/- vs HCC -/-

miRNA_ID	p-value	q-value	Fold change	Median Cp
hsa-miR-490-3p	1.43E-02	1.68E-01	0.23	35.72
hsa-miR-100*	1.40E-04	2.54E-02	0.30	35.97
hsa-let-7a-2*	4.87E-04	3.90E-02	0.32	32.07
hsa-miR-222*	1.47E-02	1.68E-01	0.34	33.86
hsa-miR-1539	3.19E-02	2.85E-01	0.43	34.04
hsa-miR-30b*	1.95E-02	2.09E-01	0.43	33.90
hsa-miR-1979	1.44E-03	6.60E-02	0.45	23.36
hsa-miR-503	1.11E-02	1.45E-01	0.49	28.56
hsa-miR-886-5p	1.22E-02	1.54E-01	0.51	29.31
hsa-miR-542-5p	4.11E-02	3.26E-01	0.51	33.03
hsa-miR-29b-1*	3.38E-02	2.90E-01	0.54	30.98
hsa-miR-450b-3p	5.79E-03	1.03E-01	0.54	35.04
hsa-miR-210	4.49E-03	1.02E-01	0.60	28.08
hsa-miR-130b	1.54E-02	1.73E-01	0.61	33.03
hsa-miR-18a	4.27E-03	1.02E-01	0.61	28.91
hsa-miR-141	5.74E-04	3.90E-02	1.53	25.43
hsa-miR-182	1.88E-03	6.60E-02	1.55	28.46
hsa-miR-125a-3p	1.27E-02	1.55E-01	1.59	33.37
hsa-miR-200b	2.31E-03	7.34E-02	1.59	28.83
hsa-miR-720	5.78E-03	1.03E-01	1.63	24.50
hsa-miR-93*	4.21E-02	3.31E-01	1.66	31.42
hsa-miR-34b*	5.62E-03	1.03E-01	1.68	30.38
hsa-miR-34a	1.67E-02	1.85E-01	1.70	27.84
hsa-miR-34c-3p	1.14E-03	5.96E-02	1.84	32.41
hsa-miR-28-3p	9.80E-03	1.30E-01	1.88	30.45
hsa-miR-940	5.91E-03	1.03E-01	1.92	28.64
hsa-miR-10a	1.45E-03	6.60E-02	1.95	33.75
hsa-miR-147b	5.27E-03	1.03E-01	2.06	33.18
hsa-miR-431	7.91E-03	1.20E-01	2.17	33.99
hsa-miR-26a	5.87E-04	3.90E-02	2.19	28.37
hsa-miR-181a*	5.28E-03	1.03E-01	2.23	33.04
hsa-miR-146a	7.46E-03	1.19E-01	2.52	34.32
hsa-miR-181a	2.82E-04	2.95E-02	2.55	27.03
hsa-miR-181b	1.97E-05	1.44E-02	2.56	29.44
hsa-miR-663	4.12E-03	1.02E-01	2.57	31.66
hsa-miR-34a*	1.40E-02	1.68E-01	2.88	32.94
hsa-miR-328	3.70E-03	1.00E-01	3.03	34.71
hsa-miR-181a-2*	2.66E-02	2.61E-01	3.53	31.67
hsa-miR-24-1*	6.81E-03	1.13E-01	3.86	35.23
hsa-miR-205	2.55E-02	2.58E-01	4.06	32.50
hsa-miR-665	9.39E-03	1.27E-01	4.13	31.60
hsa-miR-373*	3.24E-02	2.85E-01	5.95	35.40

Supplemental Table 4: miRNA comparison: HCC +/+ vs HCC -/+

miRNA ID	p-value	q-value	Fold change	Median Cp
hsa-miR-126	3.88E-03	2.70E-01	0.41	33.57
hsa-miR-25*	4.22E-02	5.10E-01	0.61	34.04
hsa-miR-181a	1.30E-02	3.30E-01	1.51	27.03
hsa-miR-361-3p	2.61E-02	4.18E-01	1.59	33.51
hsa-miR-34a	1.75E-02	3.82E-01	1.59	27.84
hsa-miR-495	1.17E-02	3.26E-01	1.61	34.55
hsa-miR-181a*	1.38E-03	1.87E-01	1.70	33.04
hsa-miR-663	4.58E-02	5.22E-01	1.89	31.66
hsa-miR-200b*	7.57E-03	3.00E-01	2.12	33.65
hsa-miR-1237	2.89E-02	4.23E-01	2.14	34.26
hsa-miR-940	2.01E-03	1.87E-01	2.32	28.64

Supplemental Table 5: miRNA comparison: HCC -/+ vs HCC -/-

miRNA ID	p-value	q-value	Fold change	Median Cp
hsa-miR-490-3p	1.23E-03	8.53E-02	0.15	35.72
hsa-miR-30c-1*	1.40E-02	3.74E-01	0.40	35.69
hsa-miR-891b	4.72E-02	5.30E-01	1.71	33.77

Supplemental Table 6: mRNA comparison: +/+ vs +/-

Probe Id	ILMN_Gene	HCC827			PC-9		
		FC	pVal	qVal	FC	pVal	qVal
Downregulated							
ILMN_1738578	*FILIP1L*	0.22	2.95E-05	5.83E-03	0.55	1.10E-03	1.02E-01
ILMN_1730906	*FILIP1L*	0.23	2.76E-05	5.83E-03	0.56	1.14E-03	1.03E-01
ILMN_1761425	*OLFML2A*	0.25	3.62E-05	5.95E-03	0.63	2.37E-03	1.26E-01
ILMN_2391150	*FILIP1L*	0.27	9.47E-05	8.46E-03	0.53	1.20E-03	1.03E-01
ILMN_1810420	*DYSF*	0.27	1.22E-06	3.15E-03	0.51	9.45E-04	9.88E-02
ILMN_2368530	*IL32*	0.28	6.31E-05	7.22E-03	0.38	1.90E-05	5.49E-02
ILMN_1682775	*EDN1*	0.28	2.20E-05	5.61E-03	1.58	5.79E-03	1.72E-01
ILMN_3307729	*CXXC5*	0.28	1.65E-04	1.07E-02	0.66	7.87E-03	1.91E-01
ILMN_1732296	*ID3*	0.28	7.23E-05	7.62E-03	0.30	1.25E-07	6.03E-03
ILMN_2121408	*HBEGF*	0.29	7.20E-05	7.62E-03	2.17	1.11E-03	1.02E-01
ILMN_1810836	*PDE5A*	0.32	3.77E-05	6.07E-03	0.63	6.14E-05	6.57E-02
ILMN_1778010	*IL32*	0.34	1.11E-04	9.01E-03	0.59	1.06E-02	2.15E-01
ILMN_2235851	*LINCR*	0.34	1.19E-04	9.27E-03	0.50	1.20E-04	6.80E-02
ILMN_2388547	*EPSTI1*	0.36	1.16E-04	9.16E-03	0.62	3.43E-04	7.91E-02
ILMN_1719986	*PIK3IP1*	0.36	5.81E-05	7.02E-03	0.60	1.57E-03	1.09E-01
ILMN_1815745	*SOX4*	0.36	4.74E-04	1.75E-02	0.61	1.36E-03	1.06E-01
ILMN_1744381	*SERPINE1*	0.37	8.49E-05	8.03E-03	0.48	2.29E-04	7.75E-02
ILMN_2376723	*CDKN2B*	0.37	3.03E-05	5.83E-03	0.54	6.66E-03	1.81E-01
ILMN_1806733	*COL18A1*	0.40	5.37E-06	3.94E-03	0.66	2.05E-05	5.49E-02
ILMN_1678671	*KLHL24*	0.40	4.70E-04	1.75E-02	0.63	6.11E-03	1.76E-01
ILMN_1663080	*LFNG*	0.41	3.55E-05	5.94E-03	0.55	9.91E-03	2.09E-01
ILMN_1806667	*FRAS1*	0.41	9.82E-06	4.50E-03	0.54	3.82E-04	8.06E-02
ILMN_1705144	*ULK1*	0.41	8.92E-05	8.19E-03	0.54	1.90E-04	7.47E-02
ILMN_1744949	*RHOBTB3*	0.41	1.79E-03	3.45E-02	0.58	3.42E-05	6.26E-02
ILMN_2371055	*EFNA1*	0.42	2.19E-05	5.61E-03	0.57	1.34E-05	5.30E-02
ILMN_1654696	*C15ORF48*	0.42	9.24E-04	2.40E-02	0.59	2.09E-03	1.20E-01

ILMN_1690040	*TM7SF2*	0.43	3.35E-05	5.91E-03	0.62	2.29E-03	1.24E-01
ILMN_1735052	*ULK1*	0.44	5.35E-05	6.83E-03	0.58	1.04E-03	1.02E-01
ILMN_1732071	*HIST2H2BE*	0.44	4.57E-04	1.73E-02	0.56	1.58E-03	1.09E-01
ILMN_1723198	*CDKN2B*	0.45	1.56E-03	3.21E-02	0.52	1.48E-04	7.00E-02
ILMN_1730670	*FSTL3*	0.45	4.39E-04	1.69E-02	0.65	3.76E-03	1.46E-01
ILMN_3307693	*WFDC2*	0.45	8.67E-06	4.44E-03	1.58	1.17E-03	1.03E-01
ILMN_1699631	*GATS*	0.46	9.91E-06	4.50E-03	0.65	5.68E-03	1.70E-01
ILMN_1721876	*TIMP2*	0.46	3.38E-04	1.51E-02	0.65	1.04E-03	1.02E-01
ILMN_2201678	*FSTL1*	0.46	1.43E-04	1.02E-02	0.61	1.16E-02	2.22E-01
ILMN_1711069	*YPEL5*	0.47	1.11E-03	2.63E-02	0.63	4.09E-03	1.52E-01
ILMN_2151281	*GABARAPL1*	0.47	2.21E-03	3.85E-02	0.58	3.06E-04	7.86E-02
ILMN_1704154	*TNFRSF19*	0.47	3.18E-04	1.47E-02	0.67	3.45E-03	1.43E-01
ILMN_1762561	*PLA2G10*	0.47	3.22E-05	5.83E-03	0.49	1.63E-04	7.15E-02
ILMN_2391861	*GSTM1*	0.47	4.90E-04	1.79E-02	0.59	1.60E-03	1.10E-01
ILMN_1792689	*HIST1H2AC*	0.47	7.10E-04	2.12E-02	0.63	9.11E-03	2.03E-01
ILMN_1721626	*ARID5B*	0.48	3.80E-04	1.60E-02	0.57	2.39E-03	1.26E-01
ILMN_1654398	*RGL1*	0.48	3.24E-04	1.48E-02	0.63	8.44E-04	9.76E-02
ILMN_2144426	*HIST2H2AA3*	0.50	2.34E-03	3.99E-02	0.57	2.08E-03	1.20E-01
ILMN_1691410	*BAMBI*	0.50	7.29E-05	7.62E-03	0.65	7.10E-04	9.31E-02
ILMN_1666845	*KRT17*	0.50	6.10E-04	1.97E-02	0.64	5.66E-04	8.92E-02
ILMN_1694432	*CRIP2*	0.50	5.00E-04	1.81E-02	0.54	7.48E-05	6.57E-02
ILMN_1778668	*TAGLN*	0.51	3.84E-04	1.61E-02	0.63	2.21E-03	1.23E-01
ILMN_1672605	*C7ORF41*	0.51	6.00E-04	1.95E-02	0.62	1.68E-03	1.11E-01
ILMN_1791280	*HSPB8*	0.51	1.40E-03	3.02E-02	0.58	1.98E-02	2.74E-01
ILMN_1657111	*C14ORF78*	0.52	3.25E-04	1.48E-02	0.42	2.50E-04	7.84E-02
ILMN_1737561	*LOC88523*	0.53	5.65E-05	6.97E-03	0.64	1.87E-04	7.47E-02
ILMN_1740772	*APBB3*	0.53	7.20E-05	7.62E-03	0.66	1.50E-03	1.08E-01
ILMN_3243156	*AHNAK2*	0.54	5.73E-05	6.99E-03	0.46	1.37E-03	1.06E-01
ILMN_1691884	*STC2*	0.54	1.98E-05	5.61E-03	1.52	5.15E-04	8.69E-02
ILMN_1676213	*SRPX2*	0.55	2.46E-04	1.31E-02	1.60	1.43E-03	1.07E-01
ILMN_1667295	*VASN*	0.55	3.19E-03	4.79E-02	0.65	7.26E-03	1.86E-01
ILMN_1717326	*SLC29A3*	0.56	1.09E-03	2.62E-02	0.48	1.38E-04	6.90E-02
ILMN_1778136	*ZMYND15*	0.56	2.05E-04	1.20E-02	0.66	1.22E-03	1.03E-01
ILMN_1706531	*ABCC5*	0.56	1.36E-03	2.96E-02	0.58	1.04E-02	2.14E-01
ILMN_1759792	*CLIP4*	0.56	6.30E-03	7.15E-02	0.60	1.46E-03	1.08E-01
ILMN_2306189	*MAGED1*	0.57	7.77E-04	2.20E-02	0.62	2.39E-03	1.26E-01
ILMN_1659047	*HIST2H2AA3*	0.57	1.10E-03	2.62E-02	0.53	1.09E-03	1.02E-01
ILMN_1703335	*LACTB*	0.57	3.12E-03	4.73E-02	0.65	6.38E-03	1.78E-01
ILMN_1800412	*BMP1*	0.58	1.11E-03	2.62E-02	0.65	5.98E-03	1.74E-01
ILMN_2315979	*LBH*	0.58	1.76E-03	3.44E-02	0.46	6.13E-05	6.57E-02
ILMN_2371458	*CXCR7*	0.58	3.89E-03	5.37E-02	0.63	4.69E-04	8.48E-02
ILMN_2192072	*MMP7*	0.59	2.21E-03	3.85E-02	1.78	4.76E-04	8.48E-02
ILMN_1739428	*IFIT2*	0.60	7.19E-03	7.77E-02	0.55	6.69E-03	1.81E-01
ILMN_1709683	*RASSF2*	0.60	7.56E-03	8.04E-02	0.56	1.81E-04	7.42E-02
ILMN_1685415	*HBP1*	0.60	5.84E-03	6.85E-02	0.61	2.24E-04	7.73E-02
ILMN_1791147	*YPEL3*	0.60	5.69E-04	1.92E-02	0.62	2.13E-03	1.21E-01
ILMN_2160764	*HBP1*	0.60	3.32E-03	4.90E-02	0.62	5.11E-03	1.65E-01
ILMN_1720865	*OSBPL7*	0.60	5.15E-04	1.84E-02	0.54	7.04E-05	6.57E-02
ILMN_2165354	*DCLK1*	0.61	1.09E-03	2.61E-02	0.63	1.02E-03	1.02E-01
ILMN_1811574	*MAPK8IP3*	0.61	7.31E-04	2.14E-02	0.58	3.17E-03	1.39E-01
ILMN_1812721	*LOC728014*	0.61	2.53E-04	1.32E-02	0.60	6.54E-04	9.21E-02
ILMN_1710209	*MFSD6*	0.62	9.47E-03	9.21E-02	0.64	1.44E-03	1.07E-01
ILMN_1757406	*HIST1H1C*	0.62	2.35E-03	3.99E-02	0.55	1.90E-04	7.47E-02
ILMN_3242900	*HIST2H2AA4*	0.62	1.13E-02	1.03E-01	0.52	8.37E-04	9.76E-02
ILMN_1651496	*HIST1H2BD*	0.63	1.62E-03	3.28E-02	0.56	2.97E-03	1.36E-01
ILMN_1800540	*CD55*	0.63	1.54E-02	1.25E-01	0.56	5.52E-04	8.77E-02
ILMN_2115218	*ANKRD10*	0.63	2.60E-04	1.34E-02	0.63	7.26E-05	6.57E-02
ILMN_2384745	*PSG4*	0.63	1.27E-03	2.87E-02	0.65	5.89E-04	8.92E-02
ILMN_1781386	*WIPI1*	0.63	1.79E-04	1.13E-02	0.61	5.80E-03	1.72E-01
ILMN_2371053	*EFNA1*	0.63	5.63E-04	1.91E-02	0.60	9.57E-06	5.30E-02
ILMN_1744937	*PTPRM*	0.64	1.52E-04	1.04E-02	0.66	1.63E-04	7.15E-02
ILMN_1685403	*MMP7*	0.64	5.32E-04	1.86E-02	1.51	4.16E-03	1.53E-01

ILMN_1801043	*GSN*	0.64	1.90E-03	3.57E-02	0.64	6.77E-03	1.82E-01
ILMN_1758719	*NEDD9*	0.64	1.91E-03	3.57E-02	0.62	9.64E-03	2.06E-01
ILMN_2184373	*IL8*	0.64	5.05E-04	1.82E-02	3.52	8.35E-06	5.30E-02
ILMN_1657760	*SYT17*	0.64	1.28E-03	2.88E-02	0.64	7.86E-03	1.91E-01
ILMN_1781285	*DUSP1*	0.64	2.92E-04	1.41E-02	1.69	2.47E-03	1.27E-01
ILMN_1810729	*UBL3*	0.65	9.50E-04	2.44E-02	0.60	4.20E-03	1.54E-01
ILMN_1763144	*NEU1*	0.66	1.64E-03	3.31E-02	0.67	8.99E-04	9.84E-02
ILMN_1682599	*GPRC5A*	0.66	4.75E-03	6.08E-02	0.52	2.88E-03	1.34E-01
ILMN_1654262	*ZMAT3*	0.66	3.47E-02	2.04E-01	0.66	8.56E-04	9.76E-02
ILMN_1804938	*GPR175*	0.66	1.85E-03	3.52E-02	0.58	3.21E-03	1.39E-01
ILMN_1764201	*MAP2*	0.66	2.45E-03	4.08E-02	0.64	3.64E-05	6.26E-02
ILMN_1810275	*SLC7A7*	0.66	1.42E-04	1.01E-02	0.47	2.03E-03	1.19E-01
ILMN_2376859	*PDGFD*	0.66	2.65E-03	4.28E-02	0.65	1.36E-02	2.35E-01

Upregulated

ILMN_1804277	*SPRED1*	1.50	1.36E-02	1.15E-01	2.05	1.16E-05	5.30E-02
ILMN_3307841	*AGR2*	1.53	5.57E-04	1.90E-02	2.27	6.86E-04	9.31E-02
ILMN_1682799	*STAMBPL1*	1.53	4.26E-04	1.67E-02	1.60	3.85E-03	1.47E-01
ILMN_1708936	*EXOSC3*	1.54	4.35E-04	1.69E-02	1.61	1.59E-03	1.10E-01
ILMN_1795930	*PTGER4*	1.54	9.69E-05	8.50E-03	1.58	2.18E-04	7.73E-02
ILMN_1672662	*SLC20A1*	1.54	1.10E-02	1.01E-01	1.80	1.62E-03	1.10E-01
ILMN_1815169	*MCM5*	1.55	1.23E-03	2.82E-02	1.63	8.92E-04	9.84E-02
ILMN_2143795	*MGC4677*	1.56	4.59E-04	1.73E-02	1.71	5.00E-04	8.61E-02
ILMN_1782488	*RNASEH2B*	1.58	4.91E-04	1.79E-02	1.55	3.98E-05	6.38E-02
ILMN_1736940	*HPRT1*	1.58	4.61E-03	5.96E-02	1.60	1.22E-02	2.26E-01
ILMN_1658607	*DLEU2*	1.59	7.58E-03	8.05E-02	1.54	9.10E-03	2.03E-01
ILMN_2056975	*HPRT1*	1.60	5.07E-05	6.71E-03	1.69	3.98E-04	8.12E-02
ILMN_1663575	*MGC87042*	1.60	4.41E-04	1.70E-02	1.89	4.58E-04	8.48E-02
ILMN_1791002	*SKP2*	1.60	9.27E-04	2.41E-02	1.58	8.25E-04	9.73E-02
ILMN_1674706	*MTHFD2*	1.62	4.03E-04	1.64E-02	1.57	2.76E-03	1.32E-01
ILMN_2224143	*MCM3*	1.63	6.76E-04	2.07E-02	1.51	6.45E-03	1.79E-01
ILMN_1653856	*STS-1*	1.63	6.22E-05	7.21E-03	2.10	2.88E-04	7.86E-02
ILMN_1798654	*MCM6*	1.63	1.63E-03	3.30E-02	1.84	9.22E-04	9.85E-02
ILMN_1721901	*CTNNAL1*	1.63	1.64E-02	1.30E-01	1.68	8.11E-04	9.73E-02
ILMN_2371700	*UCHL5IP*	1.64	1.88E-03	3.56E-02	1.60	9.51E-04	9.89E-02
ILMN_1669523	*FOS*	1.65	4.70E-04	1.75E-02	4.89	1.66E-05	5.49E-02
ILMN_2359287	*ITGA6*	1.65	1.49E-03	3.14E-02	1.76	5.17E-03	1.65E-01
ILMN_2053415	*LDLR*	1.66	2.61E-05	5.70E-03	1.70	9.49E-04	9.89E-02
ILMN_2048700	*ATAD2*	1.66	5.29E-03	6.46E-02	1.64	3.10E-04	7.86E-02
ILMN_2044832	*NOP56*	1.68	6.60E-06	4.29E-03	1.57	2.64E-04	7.86E-02
ILMN_1679267	*TGM2*	1.69	1.04E-03	2.57E-02	1.66	3.44E-04	7.91E-02
ILMN_2396020	*DUSP6*	1.70	6.55E-05	7.27E-03	1.79	5.33E-04	8.73E-02
ILMN_2364384	*PPARG*	1.70	3.43E-04	1.51E-02	1.61	2.77E-03	1.32E-01
ILMN_1776577	*DSCC1*	1.71	2.17E-03	3.81E-02	1.59	8.80E-03	1.99E-01
ILMN_1791232	*SPRED2*	1.72	1.66E-06	3.15E-03	1.64	3.09E-03	1.39E-01
ILMN_3253579	*HAUS8*	1.72	9.40E-05	8.46E-03	1.51	1.72E-02	2.59E-01
ILMN_1796074	*C18ORF56*	1.72	4.56E-04	1.73E-02	1.63	5.87E-03	1.73E-01
ILMN_2338038	*AK3L1*	1.73	1.23E-04	9.42E-03	1.71	1.96E-03	1.17E-01
ILMN_1779711	*DTL*	1.73	2.42E-03	4.06E-02	1.60	8.75E-03	1.99E-01
ILMN_1699354	*EPHA2*	1.74	1.84E-03	3.51E-02	2.41	2.75E-04	7.86E-02
ILMN_2108357	*RPL39L*	1.78	4.21E-03	5.65E-02	1.51	3.02E-03	1.37E-01
ILMN_1778890	*PPIL5*	1.79	3.36E-04	1.51E-02	1.51	1.83E-02	2.67E-01
ILMN_1809931	*NDRG1*	1.81	1.30E-04	9.73E-03	0.52	5.40E-04	8.73E-02
ILMN_1736441	*PDXP*	1.82	1.44E-05	5.01E-03	1.51	1.03E-02	2.13E-01
ILMN_1790537	*C16ORF75*	1.82	8.10E-04	2.24E-02	1.64	1.29E-03	1.04E-01
ILMN_1754272	*GINS3*	1.83	3.87E-04	1.62E-02	1.74	1.41E-03	1.07E-01
ILMN_1755834	*FEN1*	1.85	2.28E-05	5.61E-03	1.65	7.36E-03	1.86E-01
ILMN_1814282	*ISG20L1*	1.85	1.48E-03	3.13E-02	1.81	6.24E-05	6.57E-02
ILMN_2155172	*BRIX1*	1.85	2.33E-04	1.28E-02	1.66	7.16E-04	9.31E-02
ILMN_1721833	*IER5*	1.89	4.95E-04	1.80E-02	1.61	9.86E-05	6.80E-02
ILMN_1674231	*CHAF1B*	1.92	6.89E-06	4.30E-03	1.56	5.57E-03	1.70E-01

ILMN_1681503	*MCM2*	1.93	3.94E-05	6.17E-03	1.51	3.26E-03	1.40E-01
ILMN_2362545	*ZWINT*	1.93	1.56E-03	3.22E-02	1.50	1.26E-02	2.28E-01
ILMN_1712413	*RPL39L*	1.93	1.81E-03	3.47E-02	1.55	2.37E-03	1.26E-01
ILMN_1794501	*HAS3*	1.93	2.04E-05	5.61E-03	1.55	3.38E-04	7.91E-02
ILMN_2157240	*MNS1*	1.94	3.87E-04	1.62E-02	1.58	7.40E-03	1.86E-01
ILMN_1658027	*RAD54L*	1.94	7.55E-06	4.30E-03	1.58	3.20E-03	1.39E-01
ILMN_1716445	*LOC727761*	1.96	1.28E-03	2.87E-02	1.52	7.85E-03	1.91E-01
ILMN_2413898	*MCM10*	1.97	2.29E-03	3.92E-02	2.03	4.25E-04	8.38E-02
ILMN_2412384	*CCNE2*	1.97	2.20E-04	1.25E-02	1.71	1.38E-03	1.06E-01
ILMN_2146761	*FABP5*	1.98	1.97E-05	5.61E-03	1.55	5.85E-04	8.92E-02
ILMN_1724040	*ANKRD57*	2.00	4.35E-04	1.69E-02	1.58	7.61E-04	9.37E-02
ILMN_1665510	*ERRFI1*	2.01	1.97E-04	1.18E-02	1.99	1.23E-04	6.80E-02
ILMN_1711005	*CDC25A*	2.01	1.16E-04	9.16E-03	1.76	4.09E-04	8.19E-02
ILMN_1668814	*CENPM*	2.02	6.36E-04	2.01E-02	1.66	4.84E-03	1.63E-01
ILMN_1683120	*UNG*	2.03	4.82E-05	6.50E-03	1.61	5.25E-03	1.67E-01
ILMN_1800225	*PPARG*	2.06	2.32E-04	1.28E-02	1.67	3.06E-04	7.86E-02
ILMN_1738027	*BRCA1*	2.06	1.40E-03	3.03E-02	1.50	9.74E-04	1.00E-01
ILMN_3266606	*FABP5L2*	2.06	9.33E-06	4.50E-03	1.65	8.57E-03	1.99E-01
ILMN_2311089	*BRCA1*	2.07	4.53E-06	3.93E-03	1.57	3.41E-03	1.42E-01
ILMN_2370365	*RFC4*	2.07	3.05E-04	1.44E-02	1.56	5.32E-03	1.67E-01
ILMN_2160929	*FEN1*	2.11	2.71E-05	5.83E-03	1.80	6.31E-04	9.07E-02
ILMN_2148796	*MND1*	2.12	8.30E-04	2.27E-02	1.76	2.60E-03	1.30E-01
ILMN_1788462	*AMD1*	2.16	1.65E-03	3.32E-02	1.51	4.85E-03	1.63E-01
ILMN_1694502	*PRIM1*	2.19	9.79E-05	8.54E-03	1.60	4.18E-04	8.33E-02
ILMN_3176989	*HAUS8*	2.20	3.49E-06	3.57E-03	1.51	8.79E-04	9.77E-02
ILMN_3298716	*LOC729231*	2.22	1.25E-05	4.85E-03	1.97	3.99E-03	1.50E-01
ILMN_2043918	*DLEU1*	2.22	8.08E-05	7.93E-03	1.50	2.77E-03	1.32E-01
ILMN_1737184	*CDCA7*	2.23	1.98E-03	3.64E-02	2.45	2.69E-04	7.86E-02
ILMN_2235137	*FANCD2*	2.23	3.90E-04	1.62E-02	1.58	2.31E-03	1.24E-01
ILMN_1774336	*POLE2*	2.24	4.11E-04	1.66E-02	1.67	1.10E-03	1.02E-01
ILMN_1790100	*C11ORF82*	2.25	5.25E-04	1.84E-02	1.62	8.10E-03	1.94E-01
ILMN_1731184	*MELK*	2.26	1.56E-03	3.22E-02	1.60	1.13E-02	2.20E-01
ILMN_1704418	*FOXD1*	2.26	3.35E-05	5.91E-03	1.61	2.03E-02	2.76E-01
ILMN_3203196	*LOC100132240*	2.28	1.37E-04	9.95E-03	1.55	8.66E-03	1.99E-01
ILMN_2221564	*LYAR*	2.29	8.02E-06	4.30E-03	2.04	5.48E-04	8.77E-02
ILMN_2181432	*SPC24*	2.29	5.80E-04	1.94E-02	1.75	1.46E-03	1.08E-01
ILMN_1739222	*ETV5*	2.30	1.58E-04	1.06E-02	2.59	8.66E-04	9.77E-02
ILMN_2141807	*C15ORF23*	2.31	1.26E-04	9.54E-03	1.54	1.13E-02	2.20E-01
ILMN_1761486	*C13ORF34*	2.32	2.80E-04	1.38E-02	1.67	3.55E-04	7.91E-02
ILMN_1656501	*DUSP5*	2.34	3.37E-04	1.51E-02	3.19	2.43E-05	5.76E-02
ILMN_1715616	*PPIL5*	2.34	1.46E-04	1.02E-02	1.55	1.53E-03	1.09E-01
ILMN_1671906	*MND1*	2.35	1.62E-05	5.30E-03	1.66	3.63E-03	1.45E-01
ILMN_1678669	*RRM2*	2.36	2.94E-05	5.83E-03	1.54	1.67E-04	7.15E-02
ILMN_1705407	*NOP56*	2.40	1.51E-03	3.15E-02	1.51	3.93E-02	3.65E-01
ILMN_1784860	*RFC3*	2.40	1.85E-04	1.15E-02	1.69	8.71E-04	9.77E-02
ILMN_2215545	*C3ORF26*	2.41	4.18E-04	1.66E-02	1.50	7.44E-03	1.87E-01
ILMN_2210129	*PRIM1*	2.43	2.91E-05	5.83E-03	1.74	1.17E-02	2.23E-01
ILMN_1697220	*NT5E*	2.46	2.20E-04	1.25E-02	1.71	1.44E-03	1.07E-01
ILMN_1794875	*AGPAT9*	2.46	1.96E-03	3.62E-02	1.53	2.54E-02	3.04E-01
ILMN_1737195	*CENPK*	2.49	5.73E-04	1.93E-02	1.63	5.61E-03	1.70E-01
ILMN_1729115	*LOC651816*	2.51	1.86E-05	5.61E-03	1.53	3.38E-02	3.44E-01
ILMN_1764362	*LYAR*	2.54	1.64E-04	1.07E-02	1.93	2.80E-04	7.86E-02
ILMN_2212909	*MELK*	2.54	2.51E-05	5.67E-03	1.67	5.56E-03	1.69E-01
ILMN_1654268	*HMGB2*	2.58	1.55E-05	5.24E-03	1.59	1.36E-03	1.06E-01
ILMN_1711470	*UBE2T*	2.60	1.92E-04	1.17E-02	1.81	1.17E-03	1.03E-01
ILMN_2362549	*ZWINT*	2.61	1.13E-04	9.05E-03	1.62	1.33E-03	1.05E-01
ILMN_1719749	*PTGES3*	2.61	4.56E-04	1.73E-02	1.67	8.12E-03	1.94E-01
ILMN_1695414	*ASF1B*	2.61	4.09E-06	3.86E-03	1.66	1.24E-03	1.03E-01
ILMN_1786065	*UHRF1*	2.69	3.98E-05	6.17E-03	1.86	5.73E-03	1.71E-01
ILMN_1673673	*PBK*	2.75	9.68E-06	4.50E-03	1.64	4.40E-03	1.56E-01
ILMN_1720114	*GMNN*	2.81	1.11E-05	4.80E-03	1.95	2.67E-03	1.30E-01
ILMN_3219455	*LOC644745*	2.81	1.04E-04	8.70E-03	1.50	3.00E-04	7.86E-02

ILMN_1703946	*ADORA2B*	2.88	1.46E-05	5.05E-03	2.11	8.06E-04	9.73E-02
ILMN_1710428	*CDC2*	2.88	1.94E-05	5.61E-03	1.84	3.78E-03	1.47E-01
ILMN_1719256	*CKS1B*	2.89	2.43E-05	5.66E-03	1.59	7.69E-04	9.41E-02
ILMN_1796589	*TRIP13*	2.91	4.26E-05	6.29E-03	1.65	7.59E-04	9.37E-02
ILMN_2041046	*CKS1B*	2.93	9.89E-06	4.50E-03	1.51	1.35E-03	1.06E-01
ILMN_3275936	*LOC100133277*	3.00	7.53E-05	7.76E-03	1.50	3.04E-02	3.31E-01
ILMN_1670353	*RAD51AP1*	3.03	2.60E-04	1.34E-02	1.77	9.85E-04	1.00E-01
ILMN_1651237	*CDT1*	3.05	5.41E-05	6.83E-03	1.69	2.41E-03	1.26E-01
ILMN_1771841	*FOSL1*	3.06	9.02E-05	8.25E-03	3.18	1.69E-04	7.15E-02
ILMN_1806040	*TYMS*	3.13	2.16E-05	5.61E-03	1.79	5.51E-04	8.77E-02
ILMN_1694177	*PCNA*	3.13	1.44E-05	5.01E-03	1.77	1.19E-03	1.03E-01
ILMN_1777564	*MAD2L1*	3.15	3.43E-05	5.92E-03	1.96	6.45E-04	9.15E-02
ILMN_2368718	*CENPM*	3.16	5.33E-05	6.82E-03	1.85	3.00E-03	1.37E-01
ILMN_3220769	*LOC729964*	3.19	8.02E-04	2.23E-02	1.70	3.01E-04	7.86E-02
ILMN_1728972	*FAM64A*	3.23	1.20E-06	3.15E-03	1.52	6.58E-06	5.30E-02
ILMN_2215640	*TUBA3D*	3.27	5.33E-05	6.82E-03	1.59	1.09E-02	2.18E-01
ILMN_1763907	*C6ORF173*	3.28	6.15E-05	7.21E-03	1.73	9.28E-03	2.03E-01
ILMN_1670238	*CDC45L*	3.28	3.54E-05	5.94E-03	1.78	3.89E-04	8.06E-02
ILMN_2357438	*AURKA*	3.30	5.42E-05	6.83E-03	1.57	8.56E-04	9.76E-02
ILMN_1806037	*TK1*	3.40	1.17E-06	3.15E-03	1.54	4.40E-04	8.42E-02
ILMN_1705750	*TGM2*	3.40	9.28E-06	4.50E-03	4.73	4.67E-05	6.57E-02
ILMN_1809590	*GINS2*	3.42	4.62E-06	3.93E-03	2.00	5.01E-04	8.61E-02
ILMN_1683450	*CDCA5*	3.46	5.41E-06	3.94E-03	1.64	1.41E-03	1.07E-01
ILMN_1686097	*TOP2A*	3.49	8.44E-05	8.03E-03	1.55	3.00E-03	1.37E-01
ILMN_1687978	*PHLDA1*	3.53	6.79E-05	7.39E-03	4.09	3.58E-05	6.26E-02
ILMN_1728934	*PRC1*	3.54	3.11E-05	5.83E-03	1.50	4.83E-04	8.48E-02
ILMN_1714730	*UBE2C*	3.54	2.34E-06	3.15E-03	1.68	2.06E-03	1.20E-01
ILMN_2285996	*KIAA0101*	3.55	1.27E-05	4.85E-03	1.64	1.05E-02	2.15E-01
ILMN_1781943	*FAM83D*	3.59	3.87E-06	3.79E-03	1.50	4.85E-04	8.48E-02
ILMN_2063168	*MALL*	3.72	1.27E-05	4.85E-03	3.22	1.39E-04	6.90E-02
ILMN_1684217	*AURKB*	3.78	1.75E-05	5.48E-03	1.55	3.54E-03	1.44E-01
ILMN_1747911	*CDC2*	3.86	2.82E-05	5.83E-03	1.57	7.55E-04	9.37E-02
ILMN_3205271	*LOC100132863*	3.87	1.38E-04	9.97E-03	1.81	2.40E-03	1.26E-01
ILMN_2219712	*HMGB2*	4.04	9.56E-06	4.50E-03	1.51	1.11E-02	2.19E-01
ILMN_2202948	*BUB1*	4.17	6.05E-07	3.15E-03	1.52	6.68E-05	6.57E-02
ILMN_1786125	*CCNA2*	4.35	4.29E-05	6.30E-03	1.58	3.48E-05	6.26E-02
ILMN_2051373	*NEK2*	5.81	8.87E-07	3.15E-03	1.60	5.06E-05	6.57E-02
ILMN_1762899	*EGR1*	8.54	2.76E-06	3.24E-03	8.36	9.98E-07	1.60E-02

7 Acknowledgements